ELECTROLUMINESCENCE BY HOT ELECTRONS IN DOPED AND UNDOPED ZnS

A thesis presented by

Nicole Elizabeth Rigby B.Sc.

to the University of St. Andrews in application for the Degree of Doctor of Philosophy

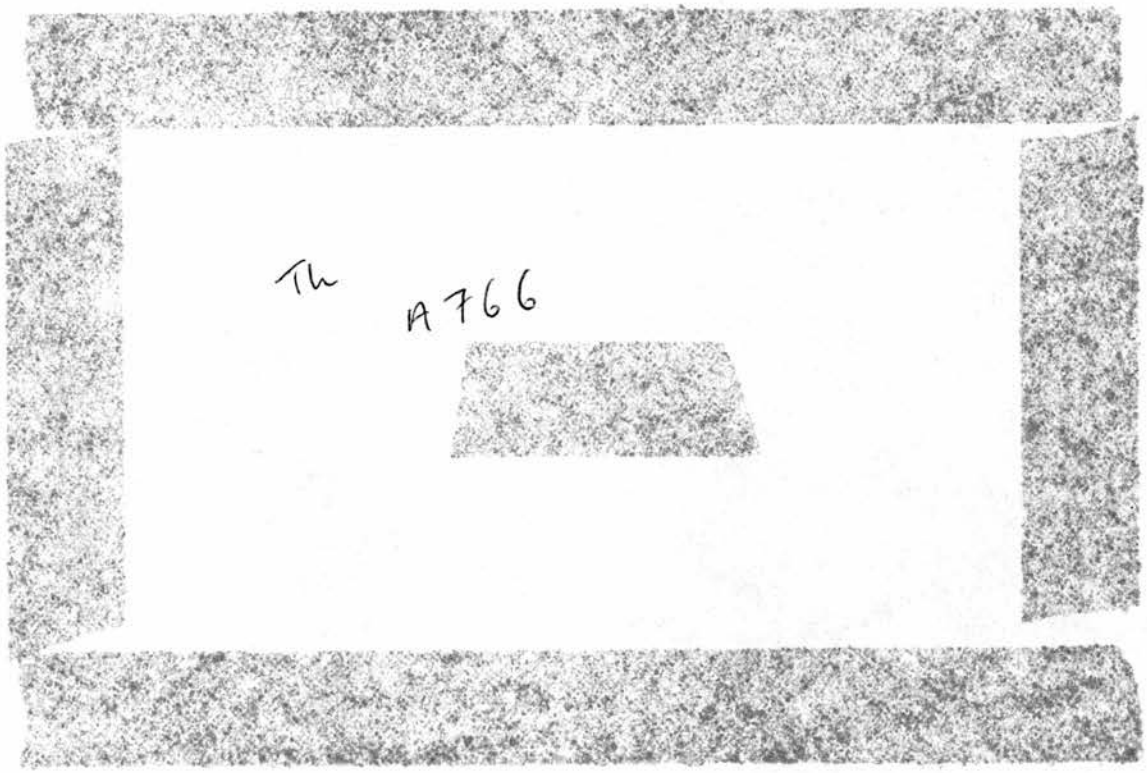
Th
A766

DECLARATION

I hereby certify that this thesis has been composed by me, and is a record of work done by me, and has not previously been presented for a higher degree.

The research was carried out in the Wolfson Institute of Luminescence, within the School of Physical Sciences in the University of St. Andrews, under the supervision of Professor J.W. Allen.

Nicole E. Rigby.

CERTIFICATE

I certify that Nicole Elizabeth Rigby has spent nine terms at research work in the Wolfson Institute of Luminescence within the School of Physical Sciences in the University of St. Andrews under my direction, that she has fulfilled the conditions of the Resolution of the University Court, 1967, No.1, and that she is qualified to submit the accompanying thesis in application for the Degree of Doctor of Philosophy.

Research Supervisor.

CAREER

I first matriculated in the University of St. Andrews in October 1980. In 1984 I obtained the Degree of Bachelor of Science with First Class Honours in Physics and the first Neil Arnott prize.

In October 1984, following the award of an SERC Scholarship, I enrolled as a research student under the Resolution of the University Court, 1967, No.1, as a candidate for the degree of Doctor of Philosophy.

ACKNOWLEDGEMENTS

Firstly, I would like to thank my supervisor, Professor J.W.Allen, for his invaluable enthusiasm, help and guidance throughout the last three years.

I would also like to thank Dr. D.Hommel for supplying the ZnS:RE samples and for his enthusiasm during the rare-earth work.

Financial support for the research was provided by SERC.

ABSTRACT

The physical processes involved in the electroluminescence of ZnS Schottky diodes have been studied separately.

The excitation of the manganese centre in ZnS:Mn diodes has been studied. The excitation mechanism in one diode was found to be an energy transfer process. The subsequent decay of the manganese centre was found to be governed by energy transfer out of the manganese to non-radiative centres. It was shown that these two energy transfer processes could be treated independently. The proportion of the depletion region over which the excitation of the manganese takes place has been estimated. This was found to be a small region slightly larger than the depletion width for zero bias.

The electroluminescence of ZnS:RE diodes has been studied. It was shown that the excitation of the rare-earth is most likely to be an energy transfer process. Direct evidence was found for the presence of hot electrons in the ZnS:RE diodes. It was shown that the simultaneous presence of these hot electrons and luminescent rare-earth centres was insufficient to guarantee rare-earth emission.

Light emission due to intervalley transitions of hot electrons in the conduction band of undoped ZnS has been observed. Consequently, more information was obtained on the distribution of the hot electrons in ZnS.

CONTENTS

CHAPTER 1:Introduction 1

CHAPTER 2:Energy transfer in ZnS:Mn and ZnSe:Mn

INTRODUCTION 6

BACKGROUND THEORY

2.1 Kinetics of energy transfer 7

2.2 Theory of spatially dependent energy transfer after Theodor Forster 11

EXPERIMENTAL METHODS

2.3 The sample 16

2.4 Experimental procedure 17

RESULTS AND DISCUSSION

2.5 Evidence that energy is being transferred into the manganese 19

2.6 Analysis of the shape of the decay curves 20

2.7 Implications of the ZnS:Mn results 21

2.8 Energy transfer in ZnSe:Mn 24

2.9 Implications of the ZnSe:Mn results 24

CONCLUDING REMARKS 30

CHAPTER 3:Estimation of the emitting region in a reverse biased ZnS:Mn Schottky diode

INTRODUCTION 32

BACKGROUND THEORY 34

EXPERIMENTAL METHODS

3.1 Measurement of the decay time 38

3.2 Electrical characteristics 39

3.3 Measurement of the relative quantum efficiency 39

RESULTS

3.4 Zero d.c. bias 40

3.5 1V d.c. forward bias 40

3.6 Electrical characteristics 41

3.7 Relative quantum efficiency 41

DISCUSSION 43

CONCLUDING REMARKS 50

CHAPTER 4:Electroluminescence of ZnS:RE Schottky diodes

INTRODUCTION 52

EXPERIMENTAL METHODS

4.1 Growth and preparation of the samples 54

4.2 Measurement of the emission spectra 55

4.3 Calibration of the system for measuring spectra 56

4.4 Measurement of the decay time 57

4.5 Measurement of the quantum efficiency 59

RESULTS

4.6 Calibration of the system 60

4.7 The emission spectra 61

4.8 Decay times of the ZnS:Re samples 62

4.8.1 Decay of the ZnS:Sm,Li sample 62

4.8.2 Decay of ZnS:Tb sample E 65

4.9 The relative quantum efficiency results 67

DISCUSSION 69

CONCLUDING REMARKS 74

CHAPTER 5:Light emission from hot electrons in ZnS

INTRODUCTION 76

EXPERIMENTAL METHODS

5.1 The samples 79

5.2 Measurement of the emission spectra 79

5.2.1 In the visible region 79

5.2.2 In the near i-r region 80

5.3 Measurement of the decay time 85

5.4 Measurement of the relative quantum efficiency 85

RESULTS

5.5 The emission spectra 87

5.6 Decay times of the samples 90

5.7 The relative quantum efficiency results 91

DISCUSSION 94

CONCLUDING REMARKS 103

CHAPTER 6:Conclusions 105

APPENDIX I 109

REFERENCES 111

CHAPTER 1

INTRODUCTION.

The electroluminescence of zinc sulphide was first reported by Destriau in 1936 [1]. He discovered that a suspension of phosphor particles in a liquid between plane-parallel electrodes emitted light when an a.c. voltage was applied. This effect was thought to be due to the recombination of excess carriers generated by impact ionization in high field regions. The work suggested the possibility of large area displays. However, no immediate positive effort was put into developing the phenomenon into a practical device. This may be attributed to the immaturity of the fabrication techniques of electrically conductive films. The transparent conductive film SnO_2 was developed ten years later. During the 1950's an extensive effort was made in preparing electroluminescent phosphors and incorporating the powders in solid insulators. A typical electroluminescent cell is shown in fig.(1.1). The powder devices were however, very inhomogeneous and this hindered scientific work on the material. Nevertheless, a large volume of experimental data was published in this period and several reviews of the data were made [2], [3]. By the late 1950's many companies were making displays based on this type of device but within a few years most of them had withdrawn. This was because the powder devices were unreliable, had a short lifetime and were insufficiently bright to give good contrast in moderate ambient light levels. At this time single crystals of ZnS had been grown [4], [5], and thin films of ZnS had been made [6], [7], but both these technologies were at a primitive stage of development. Work on the powder panels continued on a smaller scale during the 1960's and early 1970's, an example being the DCEL (DC electroluminescent) powder panels produced by Vecht [8]. In 1973

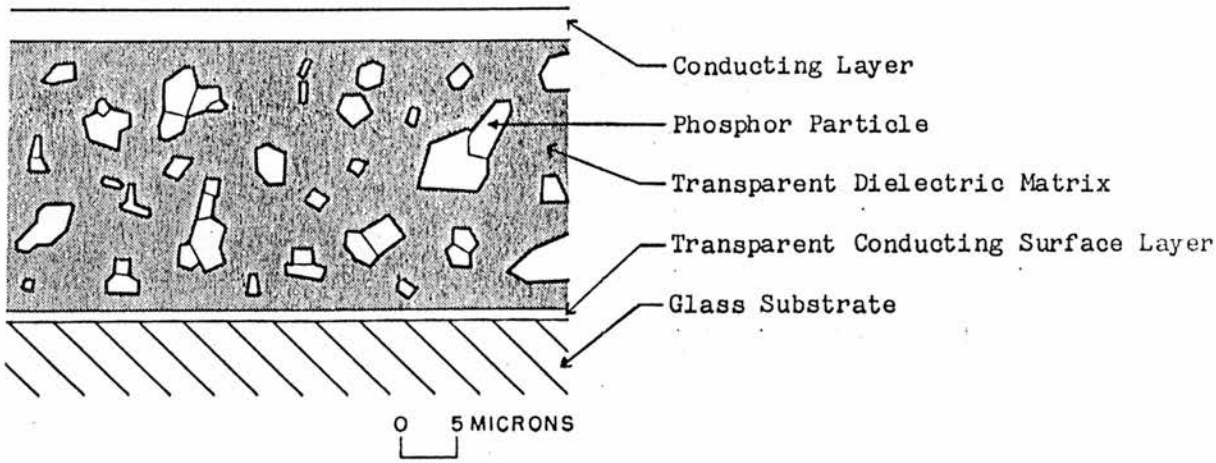

Fig.(1.1)

A typical EL powder cell.

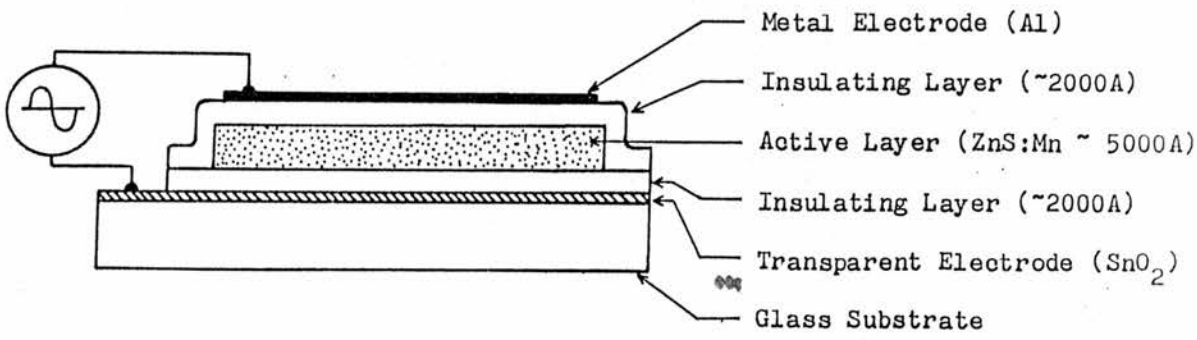

Fig.(1.2)

Structure of an ACEL thin film device.

Vecht et al. reviewed the state of the art of the DCEL ZnS devices with emphasis on the properties of the devices which were relevant to their application in a wide range of displays [9]. It was concluded that DCEL zinc sulphide showed promise as a low cost solid-state display medium. It was apparent however, that for this type of device high brightness and long lifetimes were mutually exclusive. The electroluminescence of single crystals [10], [11], and thin films [12], [13] was also investigated during this period. A major breakthrough came in 1974 when Inoguchi et al. reported an extremely long lifetime and high brightness in an ACEL (AC electroluminescent) thin film ZnS:Mn device [14]. The fundamental structure of this device is shown in fig.(1.2). The device consists of a triple layer structure, namely, an active layer sandwiched between two insulating layers. This double insulating sandwich structure prevents any undesirable leakage current from flowing through the device. Consequently, the device can keep an electric field which is sufficiently high for electroluminescence across the active layer witnout breakdown. The triple layer is sandwiched between a glass substrate with a transparent conducting coating and a metal electrode which can be shaped into the characters of a display. The device usually has an outer insulating layer to protect it from humidity. This type of EL device was found to have a number of advantages over the DCEL powder devices described in [9]. Contrast in the thin film devices is good as they consist of a few layers of transparent films and a metal electrode. The powder devices have a poor contrast caused by the scattering of light by the coarse phosphor particles. Apart from this, the thin film devices also have high brightness and excellent stability. An inherent memory function has also been found in

this type of device [15]. These features encouraged several manufacturers to enter the field, most notably Lohja, who have made displays for Helsinki airport using a new growth technique [16], and Sharp who have made displays for lapheld computers. These devices which are based on evaporated or sputtered thin films are much more homogeneous than the powder devices which were previously available. As well as enabling the production of the commercial displays mentioned above, this has also led to improvements in the quality of scientific work which can be performed on ZnS devices [17-23]. However, more controlled experiments can be performed on single crystals of conducting ZnS. These are now available. For this reason, the work here was performed on ZnS single crystals which were fabricated into Schottky diodes. This enabled the study of the physical processes involved in electroluminescence.

High field electroluminescence involves electron production and acceleration, excitation of the luminescent centre and photon emission. After more than fifty years of effort a great deal is known about the final step in the light emission process, but little is known about the earlier ones. This is largely because the final step can be isolated by using photoluminescence, whilst the preceding steps are more difficult to separate. In particular, a lot of work has been done on the manganese emission in ZnS:Mn [24]. In this thesis, the processes involved in the electroluminescence of reverse bias ZnS Schottky diodes have been studied separately.

When a reverse bias is applied to the metal-semiconductor junction of a large band gap material such as ZnS, the metal-semiconductor barrier is so high that there is negligible electron flow from the metal over the barrier into the semiconductor. Tunnelling through the edge of the depletion region is the dominant mechanism of electron flow. For Schottky diode devices therefore, it is known how the electrons are produced and that they are injected into the conduction band from the metal contact. The electrons are then accelerated in the high field of the depletion region of the junction. The magnitude of this field can be determined from capacitance-voltage measurements. The hot electrons then excite the luminescent centres by impact excitation or energy transfer processes. It can be seen therefore that Schottky diodes provide a well-defined system in which the mechanisms of electroluminescence can be studied.

The proportion of the depletion region over which the excitation of the luminescent centres takes place has been determined in a ZnS:Mn diode. The method follows that of Langer [38], but with some modifications as some of the assumptions made in his treatment are inappropriate. The dominant excitation mechanism in ZnS:Mn is believed to be direct impact excitation. It has been shown here that under some conditions the excitation mechanism can be an energy transfer process. In fact, two energy transfer processes were found to occur simultaneously. Firstly, at short applied pulse widths energy was found to be transferred to the manganese centre from another centre which was excited more efficiently by the electric field. Secondly, the decay of the

manganese emission showed that energy was also transferred out of the manganese to non-radiative centres. It was found that these two energy transfer processes could be treated independently.

The electroluminescence of ZnS:RE diodes was studied. Impact excitation was previously thought to be the dominant excitation mechanism of the rare-earth centres in ZnS as was shown by Krupka [25]. There is however some controversy about the evidence as for example Marrello et al. were unable to repeat Krupka`s results. It has been shown here that his data could be interpreted in terms of an energy transfer mechanism. It is concluded that the excitation of the rare-earth is likely to be by the impact of hot electrons for some conditions and by energy transfer for others. Direct evidence has been found for the presence of hot electrons in ZnS:RE diodes. It has been shown that the simultaneous presence of these hot electrons and luminescent rare-earth centres is insufficient to guarantee rare-earth emission.

The properties of the hot electrons in ZnS were studied in undoped material. Light emission due to the transitions of the hot electrons in the conduction band of ZnS was observed. This type of light emission has previously been observed in ZnSe diodes by Turvey and Allen [42]. Skolnick [66] claimed to have seen this type of emission in ZnS:Mn,Cu powder devices. However when his spectra were corrected for the system response [26], the emission appeared to be one of the many blue emissions caused by impurities in ZnS. From the experimental results obtained here more information was obtained on the distribution of the hot electrons in ZnS at high fields.

CHAPTER 2

ENERGY TRANSFER IN ZnS:Mn and ZnSe:Mn.

INTRODUCTION.

In this chapter energy transfer processes in single crystal Schottky diode devices of ZnS:Mn and ZnSe:Mn will be discussed. Electroluminescence experiments were performed on these materials. Chimczak observed energy transfer into the manganese in ZnS:Mn [26] and ZnSe:Mn (priv. comm.) single crystals. The non-exponentiality of the manganese decay in ZnS:Mn thin film structures has been analysed in terms of energy transfer from copper centres to the manganese centres by Chimczak et al. [27]. In contrast Goede et al. [28] observed a non-exponential decay in ZnS:Mn and interpreted this in terms of energy transfer out of the manganese to non-radiating centres. It will be shown here that both these energy transfer processes can occur simultaneously and that in ZnS:Mn the two processes can be treated independently.

The results are contrasted with the work of other authors [18,29,30] who discussed the non-exponential decay of manganese in ZnS:Mn in terms of the presence of manganese pairs and triplets. The decay was then analysed as a sum of exponential decays each with a decay time corresponding to a single manganese centre or a pair or a triplet.

For ZnSe:Mn diodes it will be shown that both energy transfer processes affect the shape of the decay curve and therefore they can no longer be treated independently. A theory is devised which combines the theories of energy transfer into and out of the manganese to aid the interpretation of the results.

BACKGROUND THEORY.

2.1 Kinetics of energy transfer.

Firstly, consider the case where there is no energy transfer. Let A be the concentration of centres in the ground state and A^* be the concentration in the excited state. The excitation rate is r_a and the lifetime of the excited centres is τ. It is assumed that only a small fraction of A is excited so that r_a is independent of A^*. An excitation pulse of length T_p is applied.

(a) During the Pulse.

The dynamic equation is

$$\frac{dA^*}{dt} = r_a - \frac{A^*}{\tau} . \qquad (2.1)$$

This gives

$$A^*(t) = r_a \tau [1 - \exp(-t/\tau)] . \qquad (2.2)$$

At the end of the pulse we have

$$A^*(T_p) = r_a \tau [1 - \exp(-T_p/\tau)] \qquad (2.3)$$

(b) After the Pulse.

The dynamic equation is now

$$\frac{dA^*}{dt} = \frac{-A^*}{\tau} \qquad (2.4)$$

If the concentration at time T_p is $A^*(T_p)$ then

$$A^*(t) = A^*(T_p)\exp\frac{-(t - T_p)}{\tau}. \qquad (2.5)$$

Using equation (2.3) gives us

$$A^*(t) = r_a\tau[1 - \exp(-T_p/\tau)]\exp\left[\frac{-(t - T_p)}{\tau}\right] \qquad (2.6)$$

The intensity of the emitted light is proportional to A^*/τ, so the total light emission is proportional to $\int A^* dt$. The total light emitted from one pulse is proportional to,

$$\int_0^\infty A^* dt = \int_0^{T_p} r_a\tau[1-\exp(-t/\tau)]dt + \int_{T_p}^\infty r_a\tau[1-\exp(-T_p/\tau)]\exp\left[\frac{-(t-T_p)}{\tau}\right]dt \qquad (2.7)$$

$$\int_0^{T_p} r_a\tau[1 - \exp(-t/\tau)]dt = r_a\tau T_p + r_a\tau^2\exp(-T_p/\tau) - r_a\tau^2 \qquad (2.8)$$

$$\int_{T_p}^\infty r_a\tau[1 - \exp(-T_p/\tau)]\exp\left[\frac{-(t - T_p)}{\tau}\right]dt = r_a\tau^2 - r_a\tau^2\exp(-T_p/\tau) \qquad (2.9)$$

i.e.

$$\int_0^\infty A^* dt = r_a\tau T_p \qquad (2.10)$$

The total light emitted from one pulse is thus proportional to the excitation pulse length.

Secondly, consider what happens when energy transfer into the luminescent centre A takes place. Suppose that the B centres are excited at a rate r_b and energy is transferred to the A centres at a transfer rate ζ. The luminescent A centres then decay with lifetime τ.

Assumptions

a)Only a small proportion of A and B are excited so that the ground state concentrations A, B can be taken as constant.

b)Only B is excited by the applied excitation process, i.e. A is only excited by energy transfer.

c)There is no back transfer from A to B.

d)Excited states of B only lose energy by transfer, i.e. the B centres are not luminescent.

The concentrations of the excited centres are given by A^* and B^* respectively, and the ground state concentrations are given by A, B. The dynamic equations are then

$$\frac{dB^*}{dt} = r_b - \zeta AB^* \qquad (2.11)$$

$$\frac{dA^*}{dt} = \zeta AB^* - \frac{A^*}{\tau} \qquad (2.12)$$

Consider what happens at the end of an exciting pulse. i.e.

$$\frac{dB}{dt} = -\zeta AB^* . \qquad (2.13)$$

Then,

$$B^*(t) = B^*(0)\exp(-\zeta At) \qquad (2.14)$$

i.e. the number of excited energy transfer centres decreases with

time as the energy is transferred to A centres.

$$\frac{dA^*}{dt} = \zeta A B^*(t) - \frac{A^*}{\tau} \qquad (2.15)$$

$$= \zeta A B^*(0) \exp(-\zeta A t) - \frac{A^*}{\tau} \qquad (2.16)$$

This is a linear ordinary differential equation which has a solution:-

$$A^*(t) = \zeta \frac{A\tau B^*(0)}{1 - \zeta A \tau} \exp(-\zeta A t) + c\exp(-t/\tau) \qquad (2.17)$$

where c is a constant of the integration which at short pulse widths can determined by the condition $A^*(0) = 0$, which gives

$$A^*(t) = \frac{B^*(0)\tau}{1/\zeta A - \tau} [\exp(-\zeta A t) - \exp(-t/\tau)] \qquad (2.18)$$

The luminescent intensity L is proportional to A^*/τ i.e.

$$L \propto \frac{B^*(0)}{1/\zeta A - \tau} [\exp(-\zeta A t) - \exp(-t/\tau)]. \qquad (2.20)$$

This analysis also predicts that the intensity of the emitted light will continue to increase after the end of the applied pulse. The delay time of the electroluminescence maximum after the end of the pulse can be obtained by determining the time t_m when dL/dt=0. This gives

$$t_m = \frac{\ln(\zeta A \tau)}{\zeta A - 1/\tau} . \qquad (2.21)$$

2.2 Theory of spatially dependent energy transfer after Theodor Forster [31].

In the above treatment the energy transfer rate has simply been taken as proportional to the product AB^*. We now consider the effect of the spatial distribution of the centres. A distribution of A and B centres is considered in which some of the A centres are excited.

Assumptions.

a)Excited A centres transfer energy to the B centres.

b)There is no back transfer from B to A.

c)There is no diffusion of energy among the A centres.

The transfer probability from an A^* centre to a B centre is given by

$$P_{AB} = \frac{1}{\tau_o}\left(\frac{R_o}{R}\right)^6 \qquad (2.22)$$

where R is the A^*B distance, τ_o is the lifetime of an isolated A^* centre and R_o is the distance where the transfer probability is $1/\tau_o$.

If ρ is the probability of an A centre being in an excited state then the decay rate of one A^* centre is given by

$$-\frac{d\rho}{dt} = \frac{1}{\tau_o} + \sum_{k=1}^{N} \frac{1}{\tau_o}\left(\frac{R_o}{R_k}\right)^6 \qquad (2.23)$$

where N is the total number of B centres in the volume considered and R_k is the distance of the k^{th} centre. On integration we have that

$$\rho(t) = \exp-\left[1 + \sum_{k=1}^{N}\left(\frac{R_o}{R_k}\right)^6 \frac{t}{\tau_o}\right] \qquad (2.24)$$

i.e. each single decay centre has a pure exponential decay, but the decay constant is different for different centres. The above equation can be rewritten as

$$\overline{\rho(t)} = \exp(-t/\tau_o) \prod_{k=1}^{N} \left[\exp - \left(\frac{R_o}{R_k}\right)^6 \frac{t}{\tau_o} \right] . \qquad (2.25)$$

Take $w(R)dR$ as the probability of a B centre being within $R \rightarrow R + dR$, then

$$\overline{\rho(t)} = \exp(-t/\tau_o) \prod_{k=1}^{N} \int_0^{R_G} \exp\left[-\left(\frac{R_o}{R_k}\right)^6 \frac{t}{\tau_o} \right] w(R_k) dR_k \qquad (2.26)$$

where the volume of the specimen is

$$V = \frac{4}{3} \pi R_G^3 . \qquad (2.27)$$

Define an integral

$$J(t) = \int_0^{R_G} \exp\left[-\left(\frac{R_o}{R_k}\right)^6 \frac{t}{\tau_o} \right] w(R) dR \qquad (2.28)$$

therefore

$$\rho(t) = \exp(-t/\tau_o)[J(t)]^N . \qquad (2.29)$$

If it is a simple case of a random distribution of centres, then $w(R) = \frac{4\pi R^2 dR}{V}$

so we have that

$$J(t) = \frac{4\pi}{V} \int_0^{R_G} \exp\left[-\left(\frac{R_o}{R}\right)^6 \frac{t}{\tau_o} \right] R^2 dR . \qquad (2.30)$$

Here we have made an approximation in assuming that R_k is a continuous distribution. This is valid if R_o >> lattice spacing (i.e. $R_o \sim 20$ A or greater). The integral can be determined using reduced variables. Take

$$\xi = \left(\frac{R_o}{R}\right)^6 \frac{t}{\tau_o} \quad \text{and} \quad \xi_G = \left(\frac{R_o}{R_G}\right)^6 \frac{t}{\tau_o}$$

$$\xi_G << 1 \text{ as } R_G >> R_o .$$

We then have that

$$J(t) = \frac{1}{2} (\xi_G)^{1/2} \int_{\xi_G}^{\infty} \exp(-\xi)\, \xi^{-3/2}\, d\xi . \qquad (2.31)$$

The integral may be expanded as a power series :-

$$\int_{\xi_G}^{\infty} \exp(-\xi)\, \xi^{-3/2}\, d\xi = 2(\xi_G)^{-1/2} - 2(\pi)^{1/2} - 6(\xi_G)^{1/2} + \ldots \qquad (2.32)$$

therefore,

$$J(t) \approx 1 - (\pi \xi_G)^{1/2} . \qquad (2.33)$$

Only the first two terms of the series are required as $\xi_G << 1$.

This expression for J(t) gives us

$$\overline{\rho(t)} = \exp(-t/\tau_o)[\, 1 - (\pi \xi_G)^{1/2}\,]^N \qquad (2.34)$$

$$= \exp(-t/\tau_o) \lim_{N \to \infty} \left[1 - \frac{1}{N} . N(\pi \xi_G)^{1/2} \right]^N \qquad (2.35)$$

$$= \exp(-t/\tau_o - N(\pi \xi_G)^{1/2}). \qquad (2.36)$$

Using the definition of e as

$$e = \left[1 + \frac{1}{N}\right]^N \qquad (2.37)$$

and substituting back for ξ_G gives

$$\overline{\rho(t)} = \exp\left[\frac{-t}{\tau_o} - \frac{\sqrt{\pi} N R_o^3}{R_G^3} \sqrt{\frac{t}{\tau_o}}\right]. \qquad (2.38)$$

This type of treatment leads to a non-exponential decay. Initially energy is transferred from A^* centres to the nearest B centres which results in a fast decay, then energy is transferred to B centres which are slightly further away which results in a slower decay and so on until $R > R_o$ when there is just the A decay.

The total amount of light out can be obtained by integrating over the decay curve. The luminescent efficiency is given by

$$\eta = c \int_0^\infty \overline{\rho(t)}\, dt \qquad (2.39)$$

where c is a constant. With no energy transfer we have

$$\eta_o = c \int_0^\infty \exp(-t/\tau_o)dt = c\tau_o \qquad (2.40)$$

so the relative luminescent intensity is given by

$$\frac{\eta}{\eta_o} = \frac{1}{\tau_o} \int_0^\infty \overline{\rho(t)}dt \qquad (2.41)$$

$$= \frac{1}{\tau_o} \int_0^\infty \exp\left[\frac{-t}{\tau_o} - \frac{\sqrt{\pi} N R_o^3}{R_G^3}\sqrt{\frac{t}{\tau_o}}\right]dt \quad . \qquad (2.42)$$

Define $s = t/\tau_o$ and $q = \frac{\sqrt{\pi}}{2}\frac{NR_o^3}{R_G^3}$

then,

$$\frac{\eta}{\eta_o} = \int_0^\infty \exp(-s - 2q(s)^{1/2})ds \quad . \qquad (2.43)$$

This is a standard integral

$$\frac{\eta}{\eta_o} = 1 - \sqrt{\pi} q e^{q^2} \bar{\Phi}(q) \qquad (2.44)$$

where

$$\bar{\Phi}(q) = \frac{2}{\sqrt{\pi}} \int_q^\infty \exp(-x^2)dx. \qquad (2.45)$$

The effects of diffusion upon the energy transfer process were considered by Yokota and Tanimoto [32]. They used the Pade approximant method to take into account the diffusion among the A centres. This treatment gave the following result :-

$$\rho(t) = \exp\left[\frac{-t}{\tau_o} - \frac{\sqrt{\pi}c_n}{c_o}\left(\frac{t}{\tau_o}\right)^{1/2}\left(\frac{1 + 10{\cdot}87\frac{D}{D_o}\left(\frac{t}{\tau_o}\right)^{2/3} + 15{\cdot}5\left(\frac{D}{D_o}\right)^2\left(\frac{t}{\tau_o}\right)^{4/3}}{1 + 8{\cdot}743\frac{D}{D_o}\left(\frac{t}{\tau_o}\right)^{2/3}}\right)^{3/4}\right] \quad (2{\cdot}47)$$

where τ_o is the lifetime of an A centre, c_n is the concentration of B centres, $c_o = [(4\pi/3)R_o^3)]^{-1}$ and $D = R_o^2/\tau_o$. D is a diffusion constant which depends upon the concentration of the A centres and the temperature.

If the concentration of A centres is very low then the diffusion constant can be taken to be zero, which gives the following expression.

$$\rho(t) = \exp\left[-\frac{t}{\tau_o} - \frac{\sqrt{\pi}c_n}{c_o}\left(\frac{t}{\tau_o}\right)^{1/2}\right] \qquad (2.47)$$

This is equivalent to the expression obtained by Forster where the concentration of the B centres is given by,

$$c_n = \frac{N}{(4\pi/3)R_G^3} \qquad (2.48)$$

EXPERIMENTAL METHODS.

2.3 The sample

The sample used throughout the work was a ZnS:Mn single crystal of dimensions 3mmx2mmx1mm. Four small indium contacts were made on one side of the sample. A single metal contact was made on the other side of the sample. The sample was therefore fabricated as a Schottky diode.

Procedure for making indium contacts.

The surface of the sample was examined under a microscope to ensure that it was smooth and clean. If necessary the sample was polished with jeweller`s rouge and etched. The etch was performed in pure bromine for about 30 seconds. The bromine was then removed by rinsing in methanol and the sample was left in carbon disulphide for about twenty minutes to remove any etch products.

Once the sample surface was satisfactory, the indium wire was shaved with a clean scalpel blade to remove the surface oxidaton layer. Small sections of the indium were then cut off and squashed onto the sample. The sample was then heated in a nitrogen/hydrogen atmosphere to 420 °C until the contacts `wetted` the surface of the sample.

2.4 Experimental procedure.

The total integrated light output per pulse from a reverse-biassed ZnS:Mn Schottky diode was determined as a function of applied pulse width at several temperatures.

The sample was mounted in a cryostat to enable temperature control. Pulses of 50V were applied from an Advance 55A pulse generator with widths varying from 10^{-7} s to a few ms. The light emitted from the diode was detected with an EMI 9558B photomultiplier with an S20 response. The photomultiplier tube was placed directly in front of the cryostat window. Aluminium foil and dark cloth were used to keep out as much of the stray light as possible. Time-resolved measurements were made using a Brookdeal 415/425A boxcar connected to a chart recorder.

Initially results were taken at room temperature. The cryostat was pumped down to minimize temperature fluctuations. It was found that if a pulse frequency of 20 or 30 Hz was used, then at large pulse widths (greater than 1 ms) the light output for a given pulse width decreased with time. This appeared to be a localised heating effect which was eliminated by reducing the frequency to 6 Hz. This of course reduced the number of pulses the boxcar sampled, so for smaller pulse widths (less than 0.5 ms) the frequency was increased to 40 Hz.

A trace of light intensity against time was recorded for several pulse widths ranging from 4ms to 0.1μs. For each trace the area under the curve was evaluated to give the total integrated light output. Once suitably scaled a graph was plotted of log(total integrated light output) against log(pulse width).

The temperature was increased using a heater which was made by wrapping insulated constantan resistance wire around a varnish coated copper bobbin above the sample holder as shown in fig.(2.1). The wirewound bobbin was again coated in GE varnish. The ends of the heater wire were soldered to circuit pins so a good contact could be made with the heater supply wires. The temperature was controlled and monitored using a Control and Readout Limited 405 temperature controller and a copper/constantan thermocouple. The heater current was supplied from a variable tap transformer. An a.c. supply was necessary as the temperature controller used a triac switching mechanism.

The experiment was performed at several temperatures up to 360K. This upper limit was set by the indium contacts.

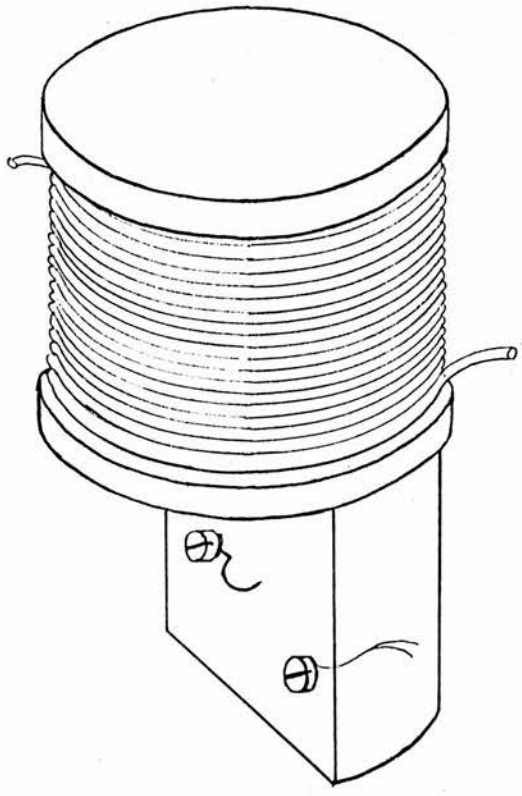

Fig.(2.1)

The sample holder and heater.

RESULTS AND DISCUSSION.

2.5 Evidence that energy is being transferred into the manganese.

Fig.(2.2) is a plot of the total integrated light output per pulse against the applied pulse width. It shows that for applied pulses of width 500μs or greater the total integrated light output is proportional to the applied pulse width at room temperature. This was the result obtained in section (2.1) for a system with no energy transfer. As the time for the manganese centres to become fully excited is about the same as the decay time then negligible energy transfer would be expected at pulse widths greater than 1 ms. At pulse widths less than 500 μs the light output is very much greater than the amount expected by extrapolation of the linear region. This is taken as evidence for energy transfer into the manganese from another centre which is excited more efficiently by the electric field.

If the results taken at different temperatures are suitably scaled and plotted on the same graph then the effect is seen in fig.(2.3). This shows that the energy transfer process is not strongly temperature dependent, which implies that the effect is not due to a complex centre involving a shallow donor or acceptor.

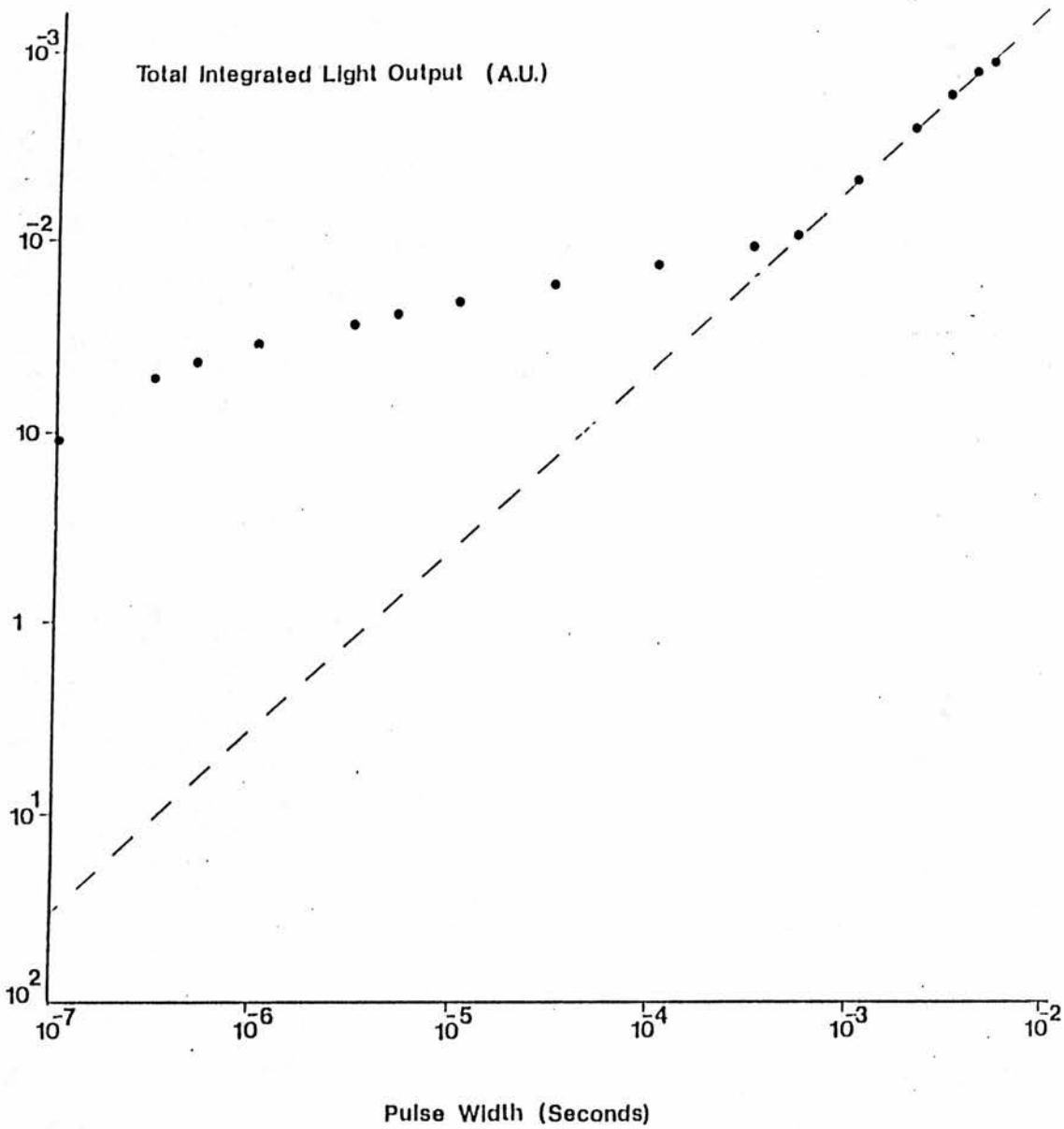

Fig.(2.2)

Variation of the total integrated light output with applied pulse width at 292K for a ZnS:Mn diode.

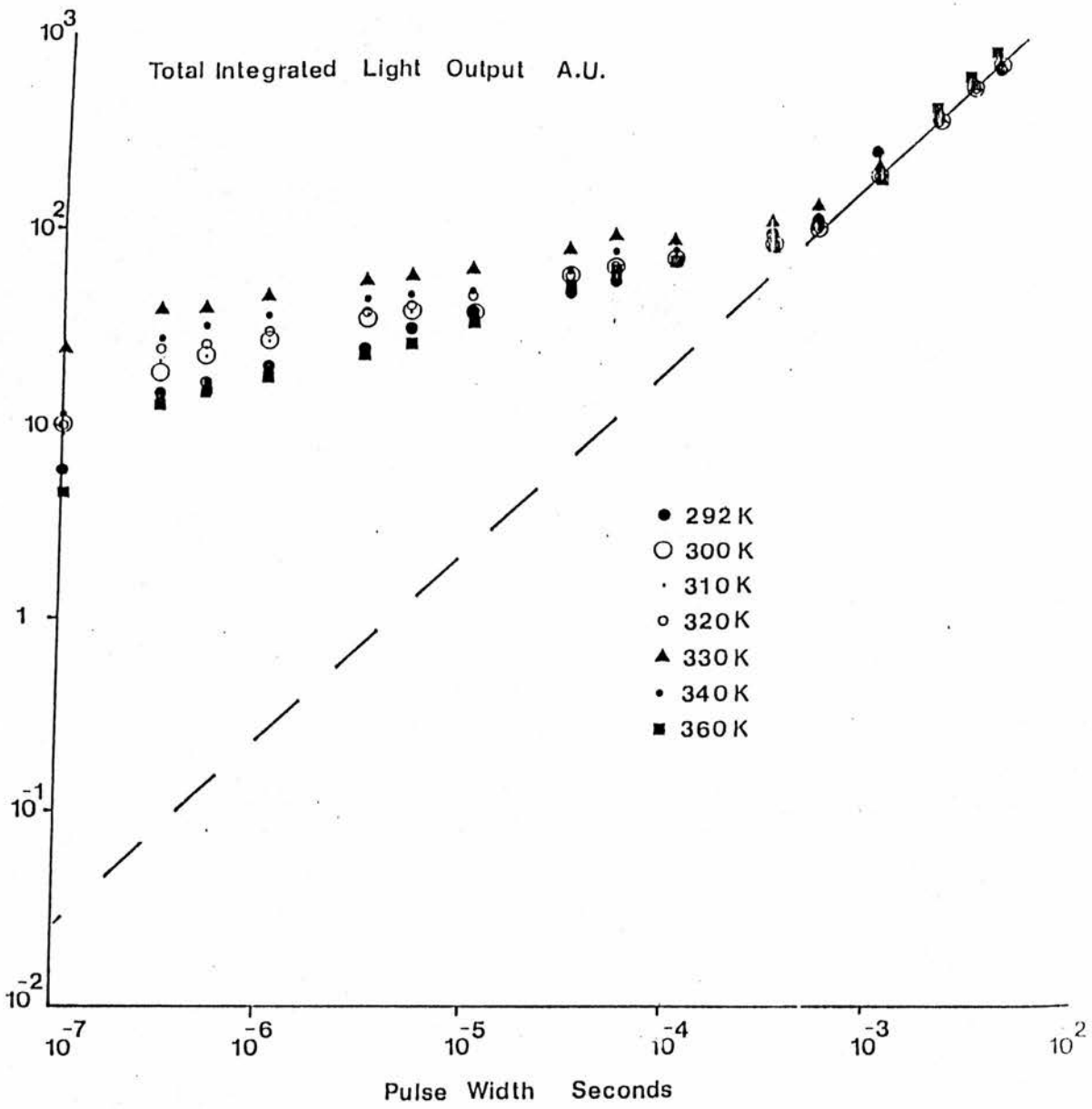

Fig.(2.3)

Variation of the total integrated light output with applied pulse width at different temperatures.

2.6 Analysis of the shape of the decay curves.

At each temperature the decay curves for four different pulse widths were superimposed. In each case the shapes of the decays were the same with some random variation as shown in figs.(2.4) to (2.10). In particular, there was no difference between the shapes of the decays for widths of 3ms where there is negligible energy transfer into the manganese and smaller pulse widths where there is strong transfer into the manganese.

The theory in section (2.2) was considered where the A centres represented the manganese centres and the B centres represented non-radiative centres. Equation (2.47) could be well-fitted to the decay curves [see ▲ in figs.(2.4) to (2.10)]. For each temperature the value of τ_o which gave the best fit was 2.0 ms $\pm$ 0.1 ms which is a reasonable value for the isolated manganese decay time [33]. The value of c_n/c_o varied with temperature as follows:-

temperature K	c_n/c_o
291	0.762 ± 0.033
300	0.677 ± 0.033
310	$0.621 \pm 0/033$
320	0.621 ± 0.035
330	0.677 ± 0.035
340	0.762 ± 0.046
360	0.790 ± 0.035.

It can be seen from this that c_n/c_o does not have a strong temperature dependence.

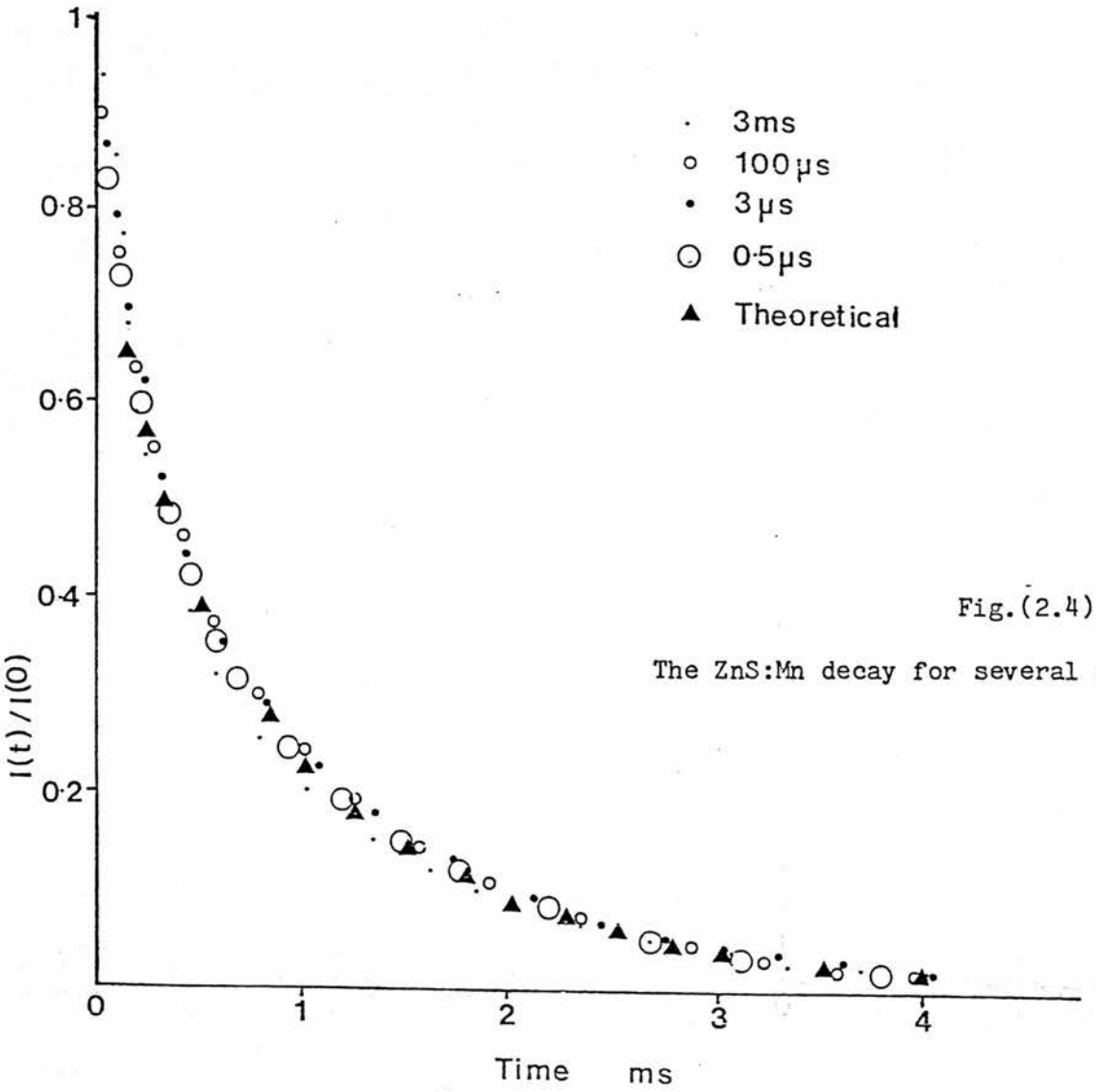

Fig.(2.4)

The ZnS:Mn decay for several pulse widths at 292K.

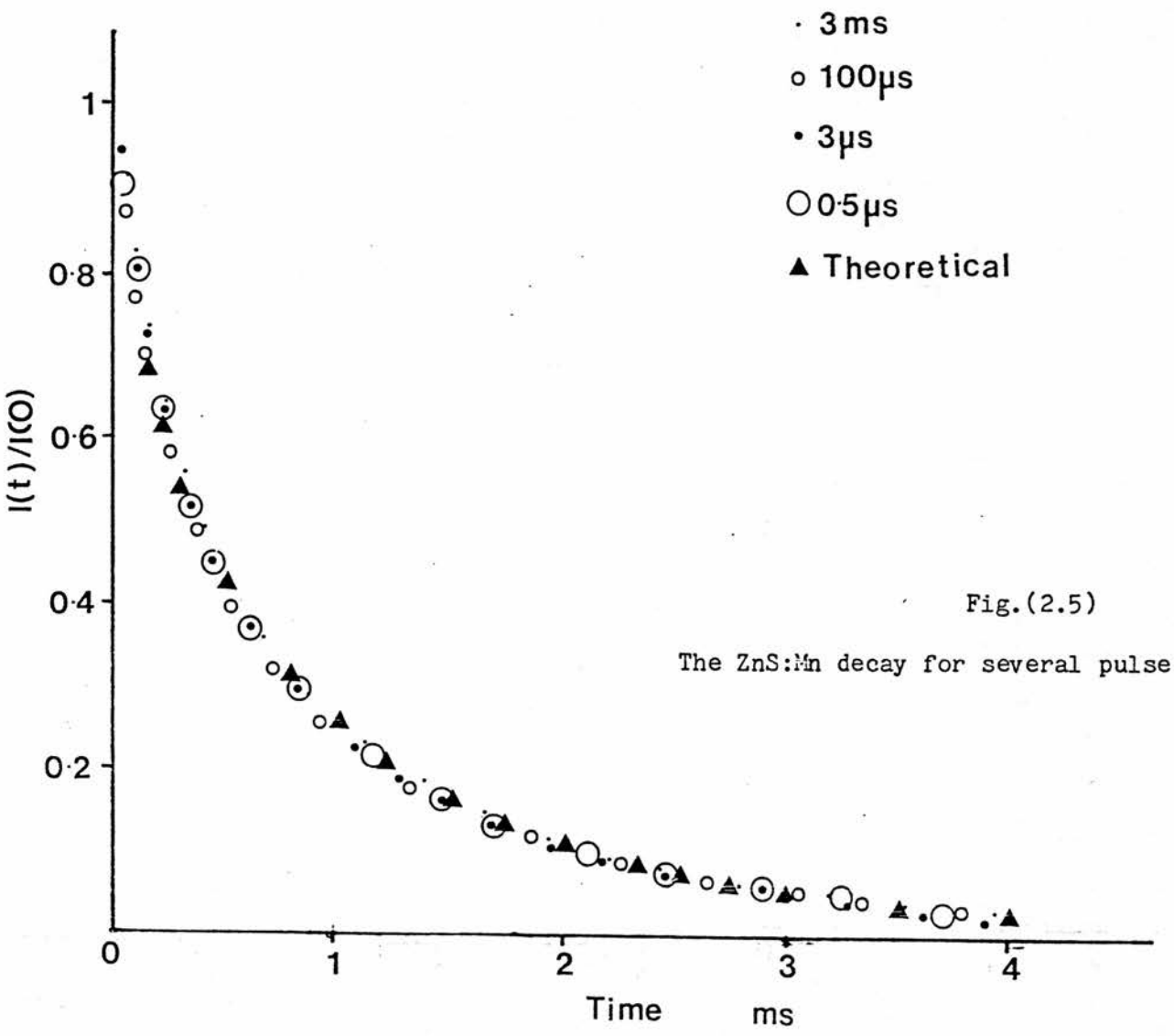

Fig.(2.5)

The ZnS:Mn decay for several pulse widths at 300K.

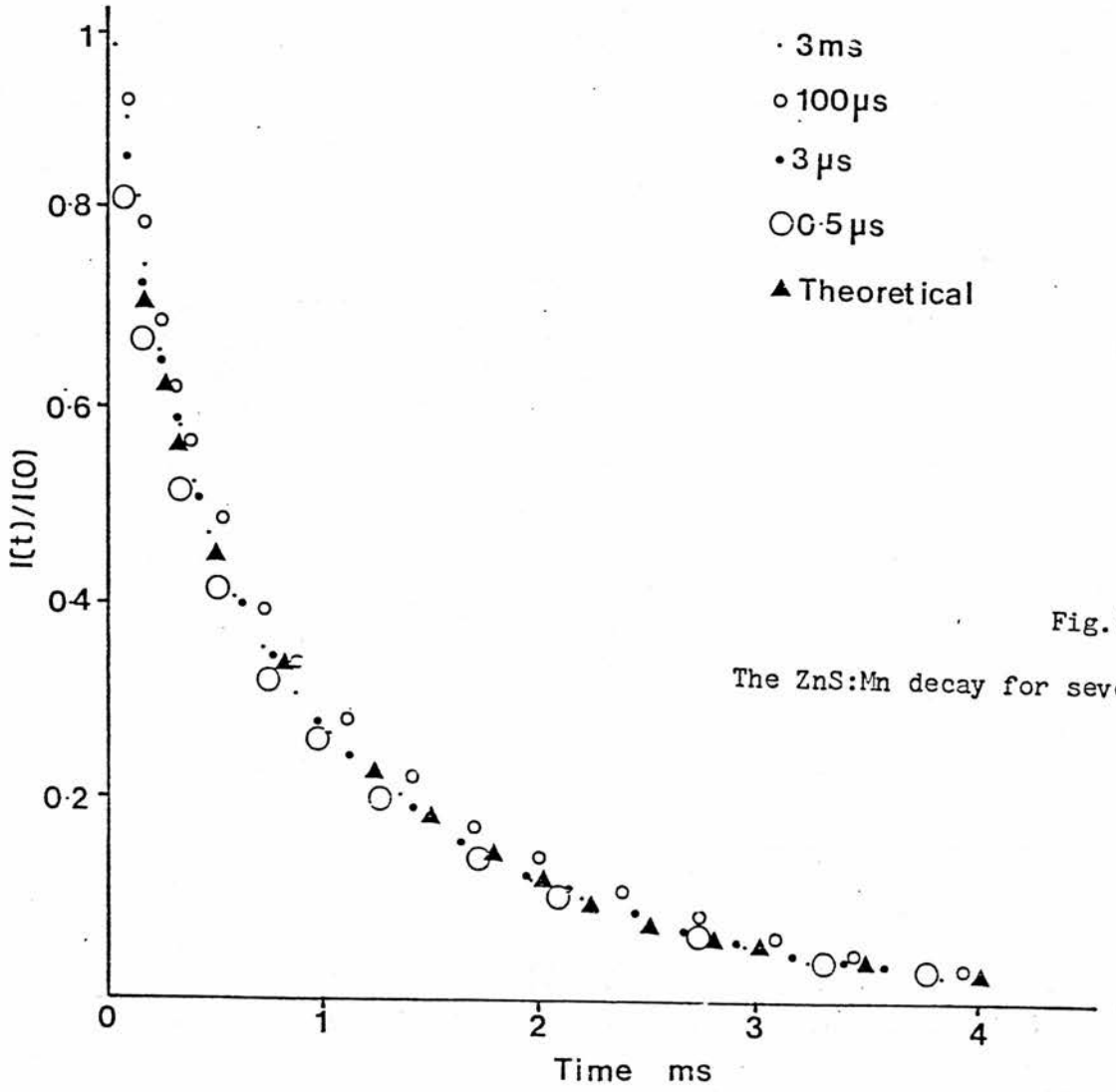

Fig.(2.6)

The ZnS:Mn decay for several pulse widths at 310K.

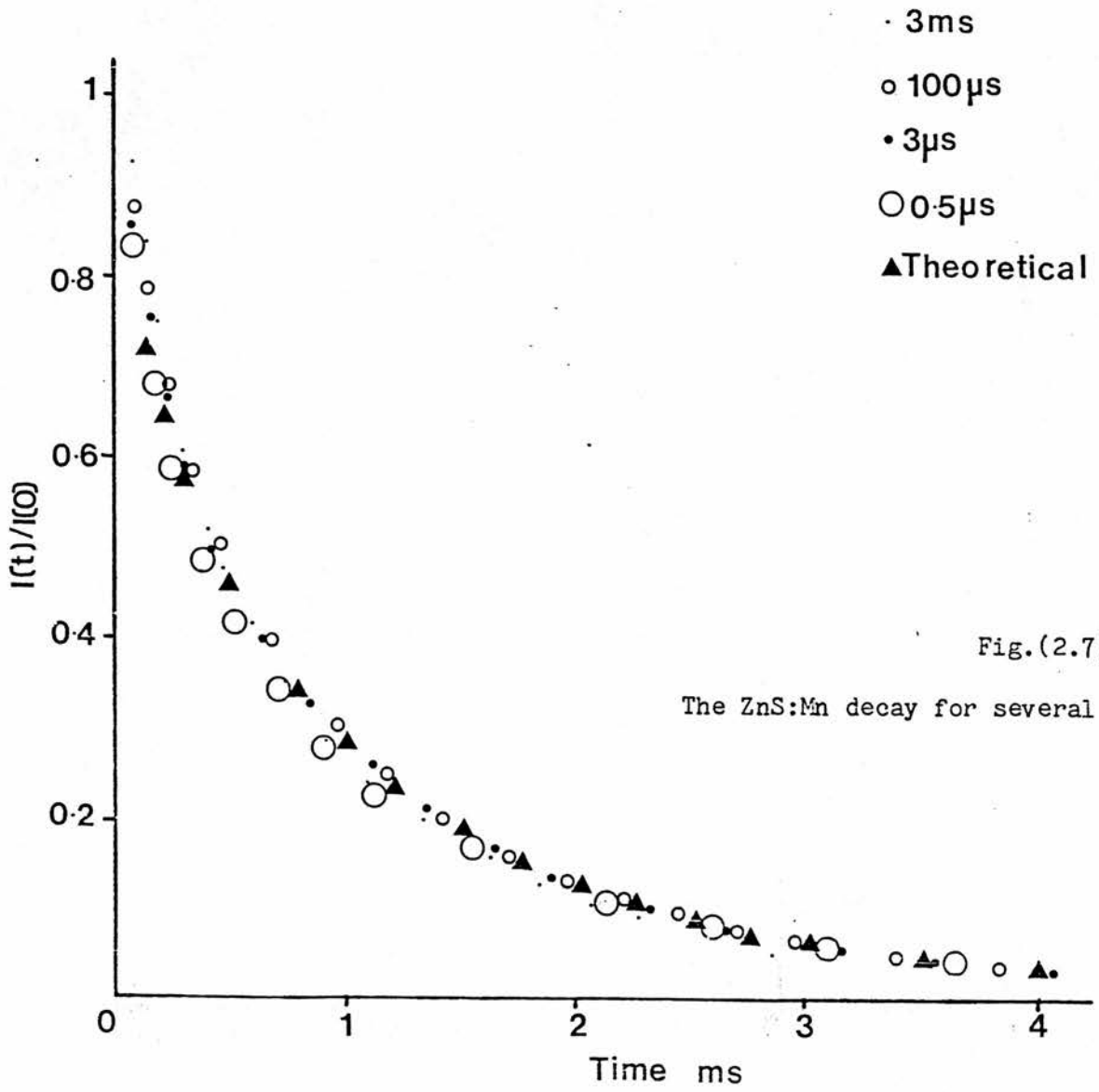

Fig.(2.7)

The ZnS:Mn decay for several pulse widths at 320K.

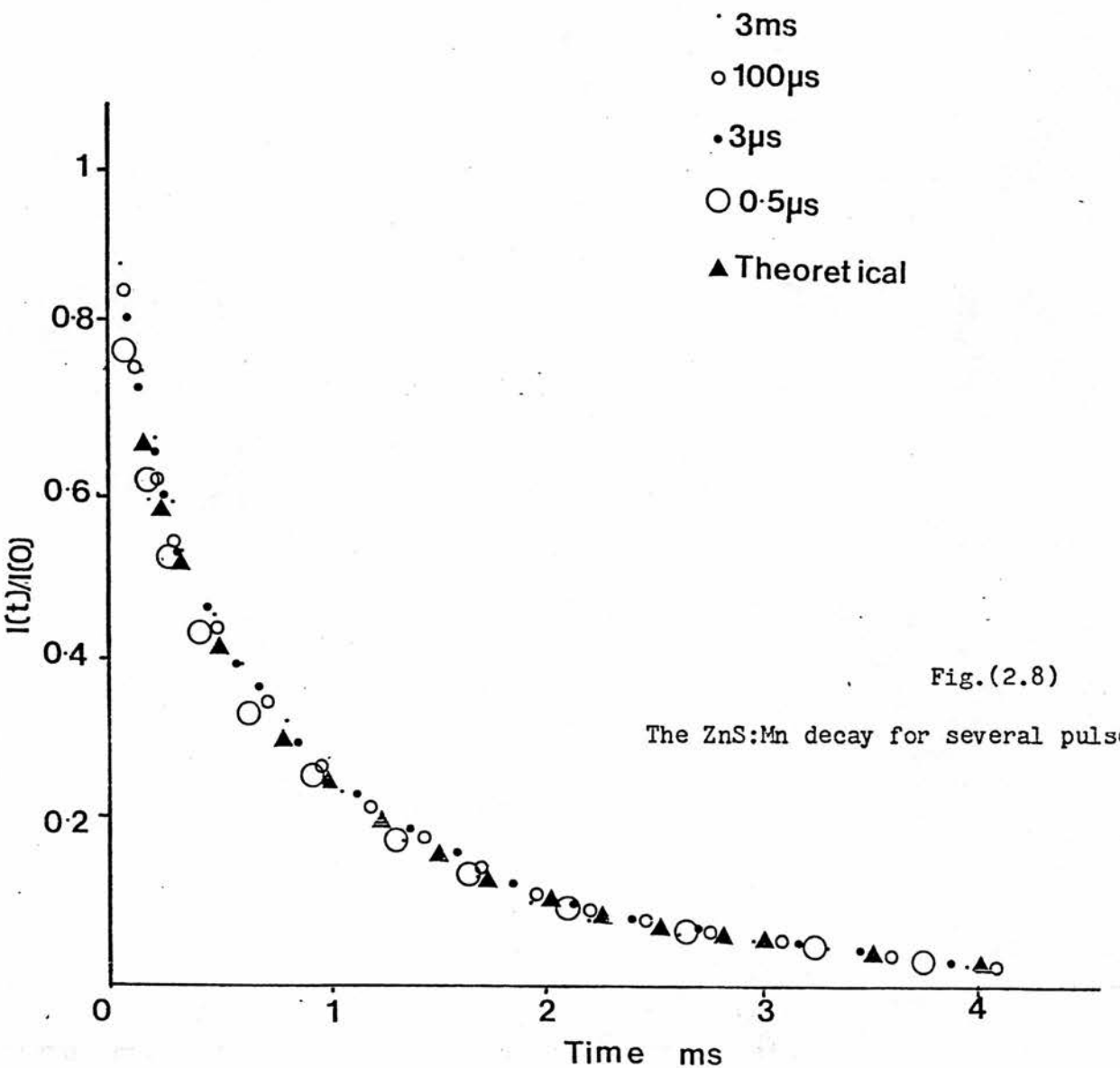

Fig.(2.8)

The ZnS:Mn decay for several pulse widths at 330K.

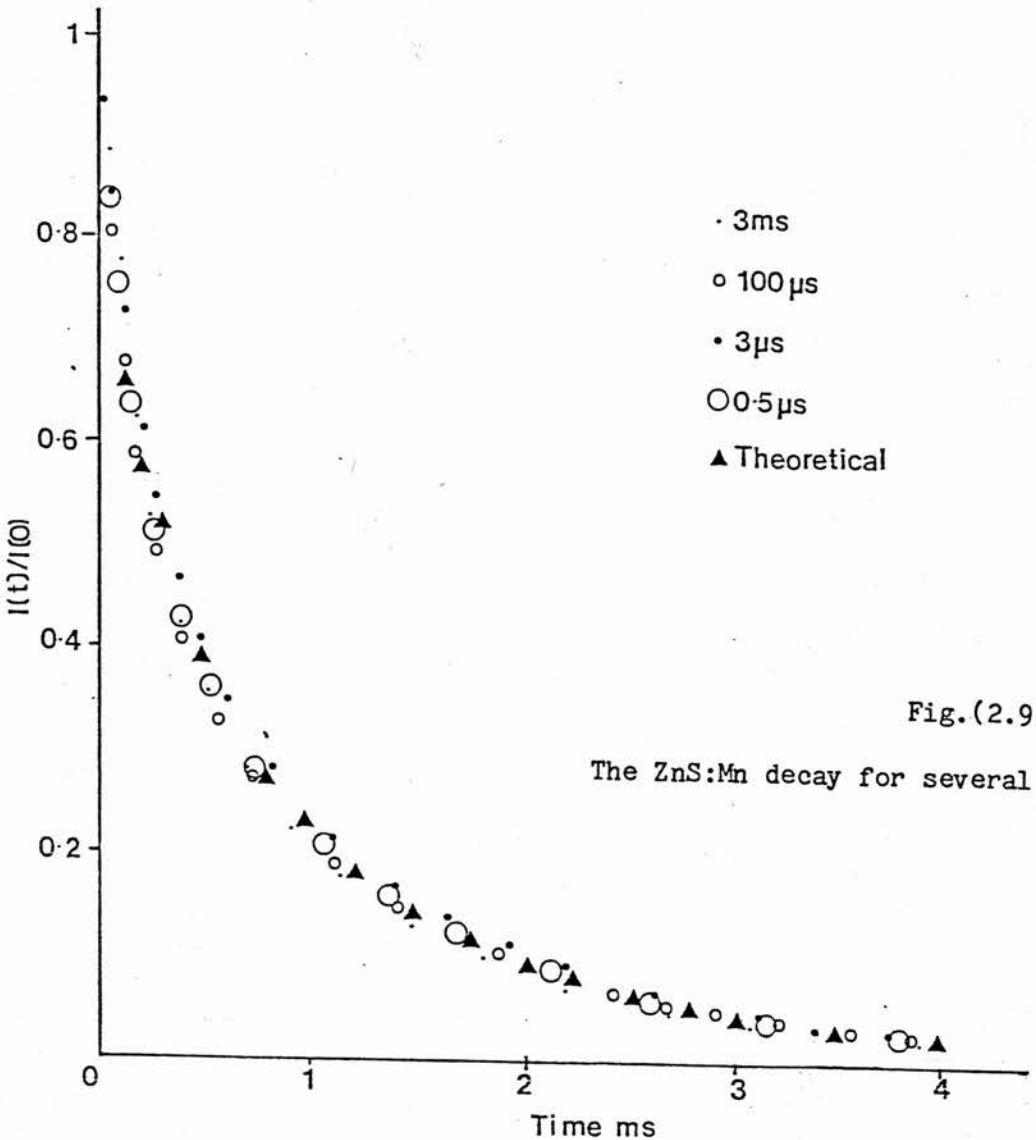

Fig.(2.9)

The ZnS:Mn decay for several pulse widths at 340K.

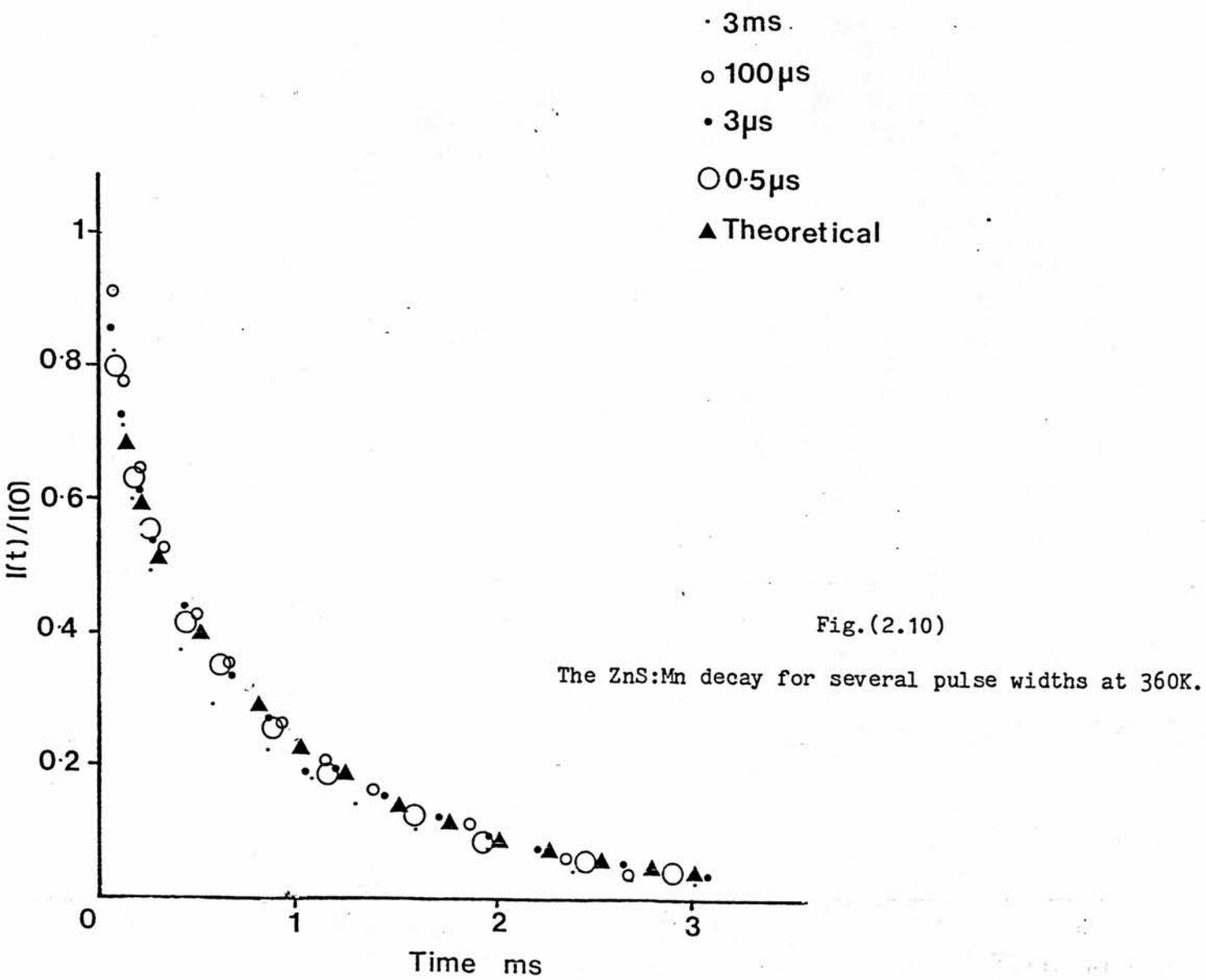

Fig.(2.10)

The ZnS:Mn decay for several pulse widths at 360K.

The results show that there are two energy transfer processes occurring in the sample simultaneously. Firstly, there is energy transfer into the manganese from another centre which is excited more efficiently by the electric field at short pulse widths as was observed by Chimczak [26]. Secondly, there is energy transfer out of the manganese to nearby non-radiative centres as was observed by Goede et al. [28].

The non-exponential nature of the manganese decay is due to energy transfer out of the manganese. Energy transfer into the manganese does not affect the shape of the decay as can be seen from figs.(2.4) to (2.10) where the decays for 3ms applied pulses have the same shape as the decays for shorter pulse widths where strong energy transfer into the manganese is taking place. This implies that in this sample the two energy transfer processes can be treated independently.

2.7 Implications of the ZnS:Mn results.

For ZnS:Mn Schottky diodes the theory of spatially dependent energy transfer given in section (2.2) fits the decay curves very well. This implies that the non-exponential nature of the decay is due to energy transfer out of the manganese and that the energy transfer into the manganese is homogeneous.

Previously, the non-exponential decay of the manganese emission in ZnS:Mn measured in photo- or electroluminescence has been discussed in terms of the occurrence of manganese pairs and triplets at higher manganese concentrations. The existence of

manganese pairs in cubic ZnS:MnS was shown by McClure [34]. Busse et al. [29] studied the photoluminescence of ZnS:Mn and showed that at sufficiently high concentrations, manganese ions in ZnS can form pairs which can also act as luminescent centres. This resulted in a non-exponential decay. Compared with single manganese ions the pairs are characterised by shorter lifetimes ~ 0.15ms. They also found that there was little energy exchange between singles and pairs and the energy absorbed in pairs was mainly emitted by pairs.

The same type of non-exponential decay was observed by Walentynowicz et al. [18] when they performed electroluminescence experiments on ZnS:Mn thin films. Here the lifetime of the pairs was found to be 0.2 ms. The electroluminescent decay of ZnS:Mn thin films was also studied by Vlasenko et al. [30]. The decay was found to be mainly due three manganese centres, singles, pairs and triplets. The pairs were found to have a decay time of 0.2 ± 0.02 ms and the triplets had a decay time of 30 ± 5 μs. In all the above cases the decay though non-exponential, could easily be split into a sum of exponentials each with the decay time of the different manganese centres.

The non-exponential decay of the ZnS:Mn sample observed in this experiment cannot be due to the presence of manganese pairs and triplets as it has been shown that the energy transfer into the manganese is homogeneous and one would not expect homogeneous energy transfer into centres which have different decay times.

Selle [35] performed photoluminescence experiments on ZnS:Mn and observed a non-exponential decay for samples with low manganese concentrations (10^{-3} - 10^{-4} % wt.) when the excitation wavelength was 400 nm. Under these excitation conditions the excitation is through impurity absorption which leads to there being electrons in the conduction band which recombine and transfer their energy to the manganese centres. Selle also observed a long afterglow which is due to electrons in the conduction band being trapped in trap centres for a long time before recombination. He fitted his data to a non-exponential decay which differed from an exponential decay by a positive term which depended upon the ratio between direct absorption in the manganese and the impurity absorption. This is an example of energy transfer into the manganese where the decay is not governed by an equation which has the form of eq.(2.20).

The constant term c_n/c_o in equation (2.47) is the number of non-radiative transfer centres in the transfer region. The value of c_n/c_o for this sample was found to be of the order of unity. This is to be expected for the following reasons. If $c_n/c_o \ll 1$ then there would be such a low concentration of non-radiative centres in the transfer region that energy transfer out of the manganese would be negligible and the decay would be almost exponential. On the other hand, if $c_n/c_o \gg 1$ then the efficiency of the manganese emission would be very low and it would not be practical to use such a sample for an experiment. From this reasoning it can be seen that if the effect of energy transfer out of the manganese to non-radiative centres is to be observed experimentally, then the value of c_n/c_o will be of the

order of unity. Goede [28] also used an equation of the form of (2.47) to fit his data. The values which gave a good fit to his data were τ_o = 3.3 ms and c_n/c_o = 1.2, 2.0, 2.4 which are also of the order of unity.

2.8 Energy transfer in ZnSe:Mn

Energy transfer was also observed by E. Chimczak in a ZnSe:Mn Schottky diode (priv. comm.). One of his decay curves is shown in fig.(2.11). It can be seen from this figure that equation (2.47) provides a good fit at the lower end of the decay (i.e. when energy is being transferred out of the manganese to far away non-radiative centres), but at short times this is no longer so. The value of τ_o used in the fitting was 48μs and the value of c_n/c_o was 0.733. The difference in the manganese emission lifetime in ZnS and ZnSe is due to the overlap of the manganese wave functions with the nearest neighbour wave functions i.e. S, Se. The selenium atom is much larger than the sulphur atom therefore it has a much stronger spin-orbit coupling. The value of c_n/c_o was again of the order of unity.

2.9 Implications of the ZnSe:Mn results.

Chimczak analysed the curve in terms of energy transfer into single manganese ions pairs and triplets as these had been shown to be present in ZnS:Mn [18,29,30]. He used an expanded form of equation (2.20), namely (2.49).

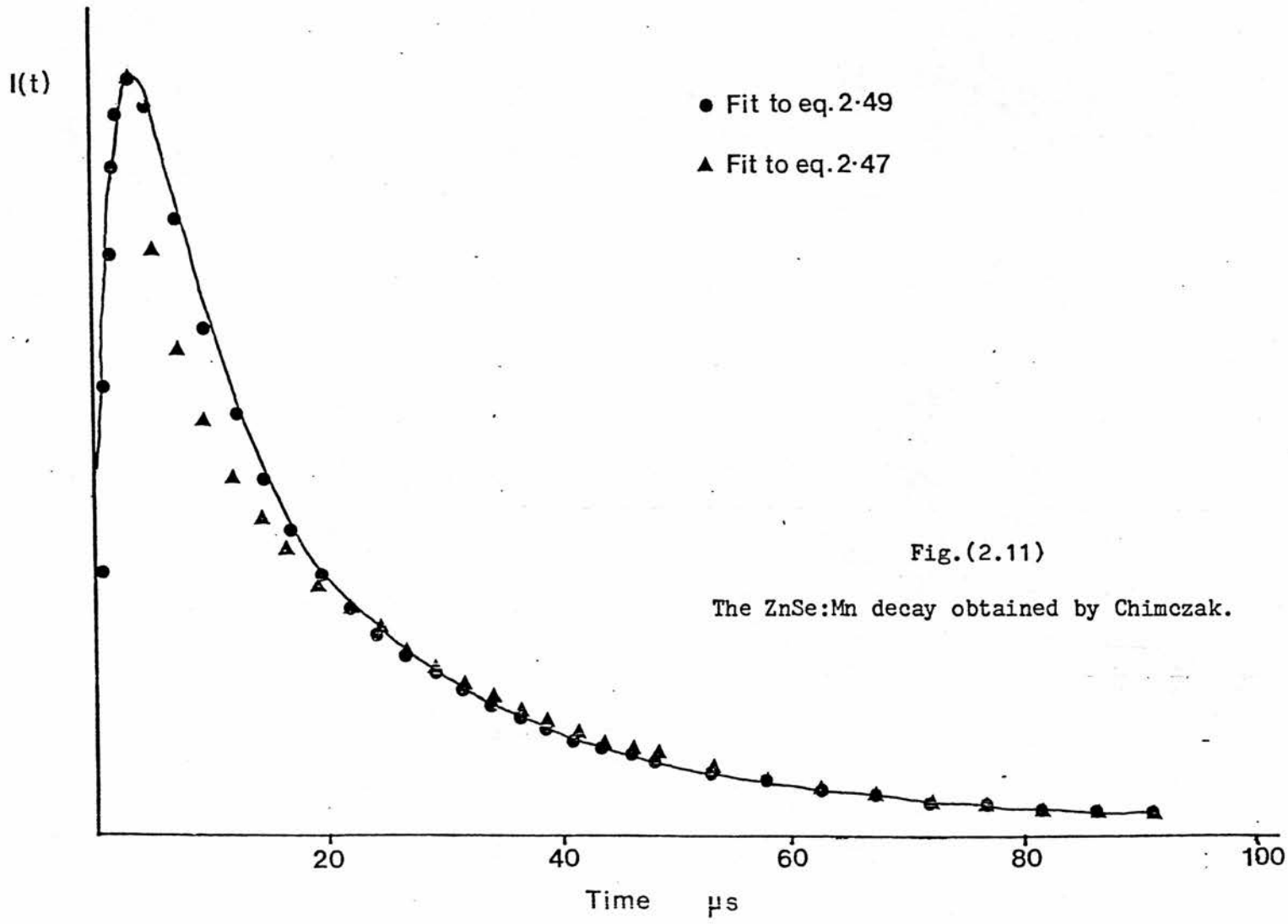

Fig.(2.11)

The ZnSe:Mn decay obtained by Chimczak.

$$L(t) = \frac{N_{s1}}{1/\zeta_1 A_1 - \tau_1}\left[\exp(-\zeta_1 A_1 t) - \exp(-t/\tau_1)\right]$$

$$+ \frac{N_{s2}}{1/\zeta_2 A_2 - \tau_2}\left[\exp(-\zeta_2 A_2 t) - \exp(-t/\tau_2)\right]$$

$$+ \frac{N_{s3}}{1/\zeta_3 A_3 - \tau_3}\left[\exp(-\zeta_3 A_3 t) - \exp(-t/\tau_3\right] \quad . \quad (2.49)$$

In this expression N_{sn} (n = 1,2,3) is proportional to the concentration of transferring centres which transfer their energy to the manganese centres (n=1 denoting single manganese centres, n=2 denoting pairs and n=3 denoting triplets). ζ_n is the transfer rate from the transferring centre to the manganese, A_n is the concentration of the manganese centres, $\zeta_n A_n$ is the probability of transfer to the manganese centres and τ_n is the lifetime of the manganese emission.

A good fit to the decay curve was found with the following values:-

$$N_{s1} = 341 \qquad \tau_1 = 36.7\mu s$$
$$N_{s2} = 195 \qquad \tau_2 = 10.3\mu s$$
$$N_{s3} = 54 \qquad \tau_3 = 3.8\mu s$$

$$1/\zeta_1 A_1 = 1/\zeta_2 A_2 = 1/\zeta_3 A_3 = 1.78\mu s$$

This implies that energy is transferred into single manganese, pairs or triplets with the same probability. The single manganese ions, pairs and triplets in ZnS:Mn have been shown to have decay times differing by about an order of magnitude [18,29,30]. The same is likely to be true in ZnSe:Mn. It is

unlikely therefore, for energy transfer into single manganese ions, pairs and triplets to be at the same rate. This shows that the non-exponentiality of the decay is unlikely to be due to manganese pairs and triplets. The value of the decay time for the single manganese centres (36.7 μs) is somewhat lower than the expected value of 220 μs [36]. This is possibly due to energy transfer out of the manganese.

Different methods of interpreting the results will now be considered. The non-exponentiality of the decay may be due to inhomogeneous transfer into the manganese i.e. the transfer into the manganese depends upon the distance between the manganese centre and the non-radiating centre. This theory can also be fitted using equation (2.49) with $A_1 = A_2 = A_3$, where τ_n is the lifetime of the manganese emission dependent upon the manganese-non-radiative centre distance. Similarly, ζ_n is the transfer rate into the manganese. However, the values of ζ_n which give a good fit to the decay curve again imply that the energy transfer rate into the manganese is the same for each n, i.e. the energy transfer into the manganese is homogeneous.

A third possibility is that the non-exponentiality of the decay is due to energy transfer out of the manganese, as was found for the ZnS:Mn diode, but the non-radiative centres may not be randomly distributed as was assumed in the derivation of equation (2.38). Some evidence for this is given by Roppischer and Jacobs [37] who noted that the manganese ions in ZnSe:Mn have associated neighbouring point defects on the selenium site.

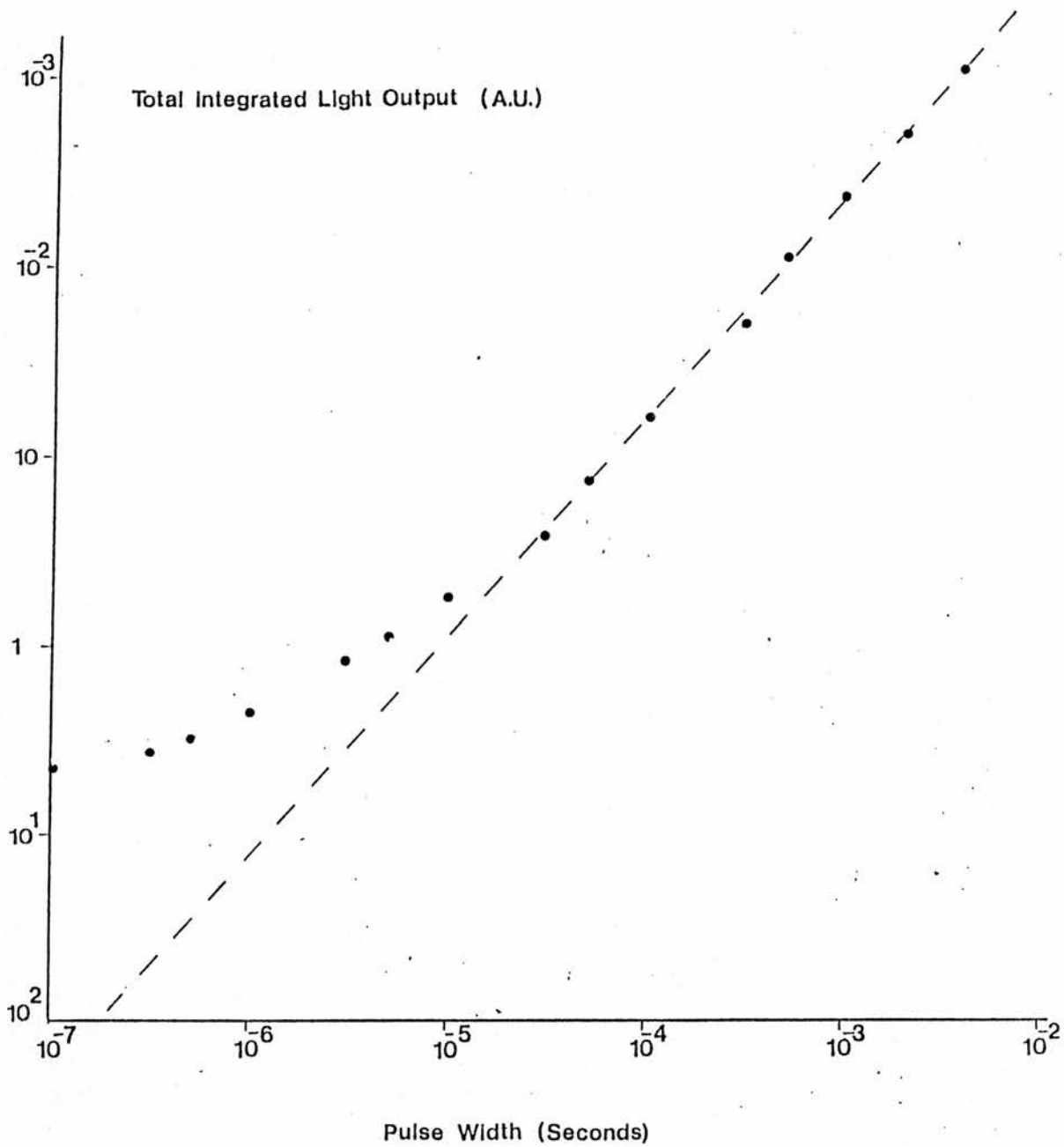

Fig.(2.12)

Variation of the total integrated light output with applied pulse width for a ZnSe:Mn diode.

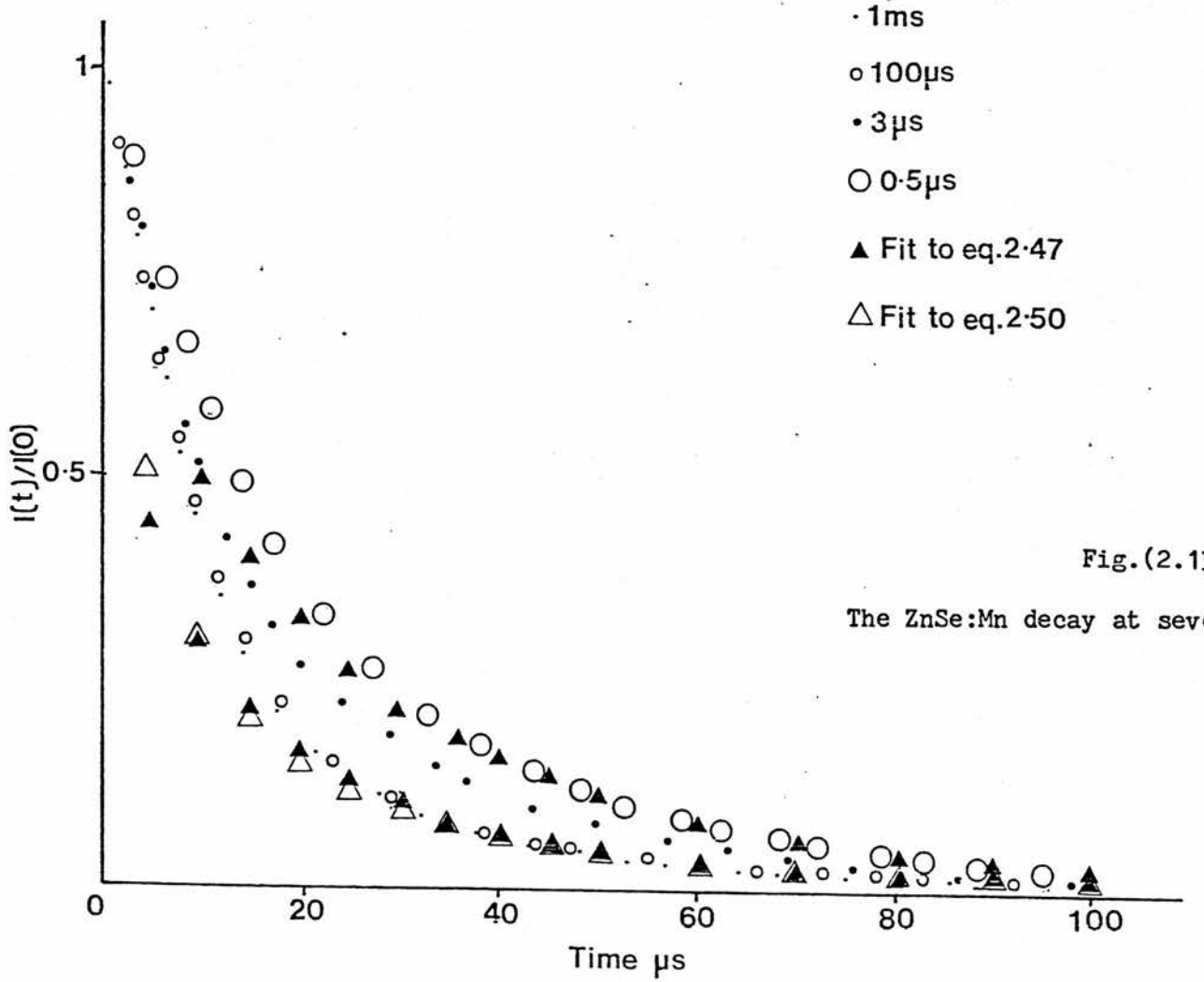

Fig.(2.13)

The ZnSe:Mn decay at several pulse widths.

It seems unlikely that the non-exponential nature of the decay is due to either manganese pairs and triplets or inhomogeneous transfer into the manganese. However, there is insufficient evidence to show that the cause is energy transfer out of the manganese with non-randomly distributed non-radiating centres.

As only one plot was available from the work of E. Chimczak, the experiment was repeated at room temperature using one of his samples. This was a ZnSe:Mn Schottky diode of dimensions 2mmx2mmx1mm and with an evaporated gold Schottky contact. The plot of the total integrated light output against applied pulse width is shown in fig.(2.12). From this it can be seen that energy is transferred into the manganese when the applied pulse width is less tham 30 μs (the lower value of the pulse width in ZnSe:Mn a consequence of the shorter decay time of the Mn in ZnSe).

The decay curves for several applied pulse widths were superimposed as shown in fig.(2.13). When there is negligible energy transfer into the manganese (i.e. pulse widths 1ms and 100μs) the decay curves have the same shape. However, for pulse widths less than 30μs the rate of decay decreases with decreasing pulse width. This shows that energy transfer into the manganese affects the shape of the manganese decay curve (unlike the ZnS:Mn results).

Equation (2.47) was again fitted to the decay curves (▲ in fig.(2.13)). Values of τ_o = 60μs and c_n/c_o = 1.410 gave a good fit to the decay curve with negligible energy transfer into the manganese at the end of the decay but deviated from the decay curve at the start of the decay, i.e. when energy is being transferred to nearby non-radiating centres. The same was true of the 0.5μs decay curve but with values τ_o = 45μs and c_n/c_o = 0.564. Again the values of c_n/c_o in both cases are of the order of unity. The possibility that the non-exponential decay is due to inhomogeneous transfer into the manganese is ruled out as this would not explain the 1ms and 100μs decay curves where negligible energy transfer into the manganese takes place.

If the non-exponential decay is due to manganese pairs and triplets then the decay when there is negligible energy transfer into the manganese should be fitted by an equation of the form of (2.50) as was found by previous authors [18,29,30].

$$\rho(t) = A_1\exp(-t/\tau_1) + A_2\exp(-t/\tau_2) + A_3\exp(-t/\tau_3) \qquad (2.50)$$

If the values of τ used are those which gave a good fit in fig.(2.11) and the values of A are A_1 = 0.17, A_2 = 0.39 and A_3 = 0.44, then the resulting expression is shown by △ in fig.(2.13). Again this gives a reasonable fit at the end of the decay but deviates from the decay curve at the start of the decay. A good fit could not be found using different values of τ and A. It is unlikely therefore that the non-exponentiality of the decay is due to manganese pairs and triplets.

There are two processes occurring in this sample of ZnSe:Mn. Firstly, there is energy transfer into the manganese from another centre which leads to more efficient emission at short pulse widths. As the amount of energy transfer into the manganese increases the rate of decay decreases. Energy transfer into the manganese therefore affects the shape of the decay. Secondly, the decay curves for pulse widths of 30 μs or greater are still strongly non-exponential even though there is negligible energy transfer into the manganese. This implies that there is another process occurring in the sample which gives a non-exponential decay. This could be energy transfer out of the manganese. For this sample the two energy transfer processes are not independent as was the case for the ZnS:Mn sample.

As the two energy transfer processes are not independent a theory was devised which combined the theories given previously for energy transfer into and out of the manganese. In the derivation of of equation (2.18) it was assumed that the decay of the A centres (or manganese centres in this case) was purely exponential with a single lifetime τ. The ZnS:Mn results show that the decay of the manganese is non-exponential due to energy transfer out of the manganese into non-radiating centres. If the decay of the manganese centres is assumed to take the form of equation (2.47) then the resulting expression is derived in Appendix I.

Unfortunately, due to the number of variables in this equation it was not possible to find the values of c_n/c_o and τ_o and fit the expression to the decay curves in figs.(2.11) and (2.13) as previously. If it had been possible it would have been interesting to see if a good fit was found with a single lifetime and transfer rate, or whether two or three terms were necessary as in equation (2.49). If the latter was so it could have been seen if the transfer rate into the manganese was the same in each term.

CONCLUDING REMARKS.

There are two energy transfer processes occurring simultaneously in the samples of ZnS:Mn and ZnSe:Mn studied. Energy is transferred into the manganese at short pulse widths from centres which are more efficiently excited than the manganese. At larger pulse widths these centres saturate. Also, energy is transferred out of the manganese to non-radiative centres. In ZnS:Mn these two processes can be treated independently and the manganese decay can be well-fitted by the theory of spatially dependent energy transfer [31] where the energy is transferred out of the manganese.

In ZnSe:Mn both energy transfer processes affect the shape of the decay curve. The decay was discussed in terms of the presence of manganese pairs and triplets in the material, but these were not thought to be the cause of the non-exponential nature decay. As the two energy transfer processes occurring in

this sample could not be treated independently a new theory was devised which combined the theories of energy transfer in and out of the manganese. Unfortunately, there were too many variables in the resulting expression to fit this to the data. This expression would still not explain however, the decay when there is negligible energy transfer into the manganese. The possibility of energy transfer out of the manganese with the far away centres being randomly distributed and the nearby centres not was also discussed. This theory however would not explain why the decay curve is affected by energy transfer into the the manganese. It is possible that the results could be fitted by a combination of the latter two theories, i.e. a theory which considered energy transfer into the manganese where the manganese is assumed to have a decay which is governed by energy transfer out of the manganese, the far away non-radiative centres being randomly distributed and the nearby centres not. This theory however could not be tested out.

CHAPTER 3

ESTIMATION OF THE EMITTING REGION IN A REVERSE BIASED ZnS:Mn SCHOTTKY DIODE.

INTRODUCTION.

When a reverse bias excitation pulse is applied to a metal-semiconductor junction the centres in the depletion region of the junction are excited. When the excitation pulse ends the width of the depletion region is reduced and any excited centres now outside the depletion region will return to the ground states non-radiatively, giving their energy to nearby electrons in the conduction band - the Auger quenching effect. Efficient luminescence is therefore a consequence of the fact that emission is generated in the depletion region of the junction. In the bulk of the crystal the lifetime of the emitting centre is very short due to Auger quenching. Within a depletion region however, it is limited only by the radiative lifetime if other non-radiative processes can be neglected.

J.M. Langer [38] developed a method of profiling the emission in a metal-semiconductor junction based on this Auger quenching effect. He illustrated this method by looking at the non-exponential decay of CdF_2:Mn,Y crystals. The success of this method depends upon the emitting region being sufficiently large such that when the applied reverse bias is reduced part of the emitting region will be outside the new depletion region. N.Gordon tried this method with ZnSe:Mn Schottky diodes but found negligible effect (unpublished). This is because most of the light is produced near the metal contact.

In contrast however, Hu Xiao-peng et al. [39] observed this effect with ZnSe:Mn diodes and with ZnS:Er and ZnS:Sm thin films. Both J.M. Langer and Hu Xiao-peng found that the ratio of the intensity of the slow component to the total intensity increased with decreasing voltage step.

Gordon and Allen [40] have shown that in conducting ZnS:Mn the Mn^{2+} luminescence is quenched with a large Auger coefficient ~ 2×10^{-9} $cm^3 s^{-1}$. It seemed possible therefore, to determine the emitting region in a sample of conducting ZnS:Mn.

In this chapter a non-exponential decay was observed from a reverse bias Schottky diode device of ZnS:Mn which included a very fast initial decay. The fast proportion of the decay changed with the applied reverse bias voltage pulse. The results were used to estimate the size of the emitting region. In order to get a more accurate estimate of the emitting region the separation of the fast decay from the non-exponential decay was attempted by comparing the experimental results with the theoretical non-exponential decay. The emitting region was also determined theoretically by calculating the fraction of electrons above the threshold energy at different points along the depletion region and this region was compared with the experimental results.

BACKGROUND THEORY.

If a reverse bias voltage of V is applied to a metal semiconductor junction, the width of the depletion region is proportional to $(V + V_{bi})^{1/2}$, where V_{bi} is the built-in potential of the junction. At the end of the pulse the width of the depletion region will be rapidly reduced from a value W due to the reverse bias voltage to a smaller value W_o which is the width for zero bias. This means that at the end of the pulse part of the emitting region may now be outside the depletion region and therefore Auger quenching will take place. This leads to a non-exponential decay, a fast part due to Auger quenching in the bulk material and a slower part due to the radiative decay in the depletion region of the junction. If the width of the emitting region is proportional to the width of the depletion region, then when a smaller reverse bias voltage is applied, the fast part of the decay will be reduced compared with the slow part. This is because for a smaller voltage less of the emitting region will be in the bulk material when the voltage is dropped to zero. This is shown schematically in fig.(3.1).

The division of the recombination processes in Schottky diode devices into fast and slow processes is too simple to develop a more accurate quantitative theory. In reality the lifetime of the excited centres changes gradually from the bulk value τ_q to the radiative lifetime τ_r inside the depletion region away from the edge. This leads to strongly non-exponential electroluminescence kinetics. The form of the

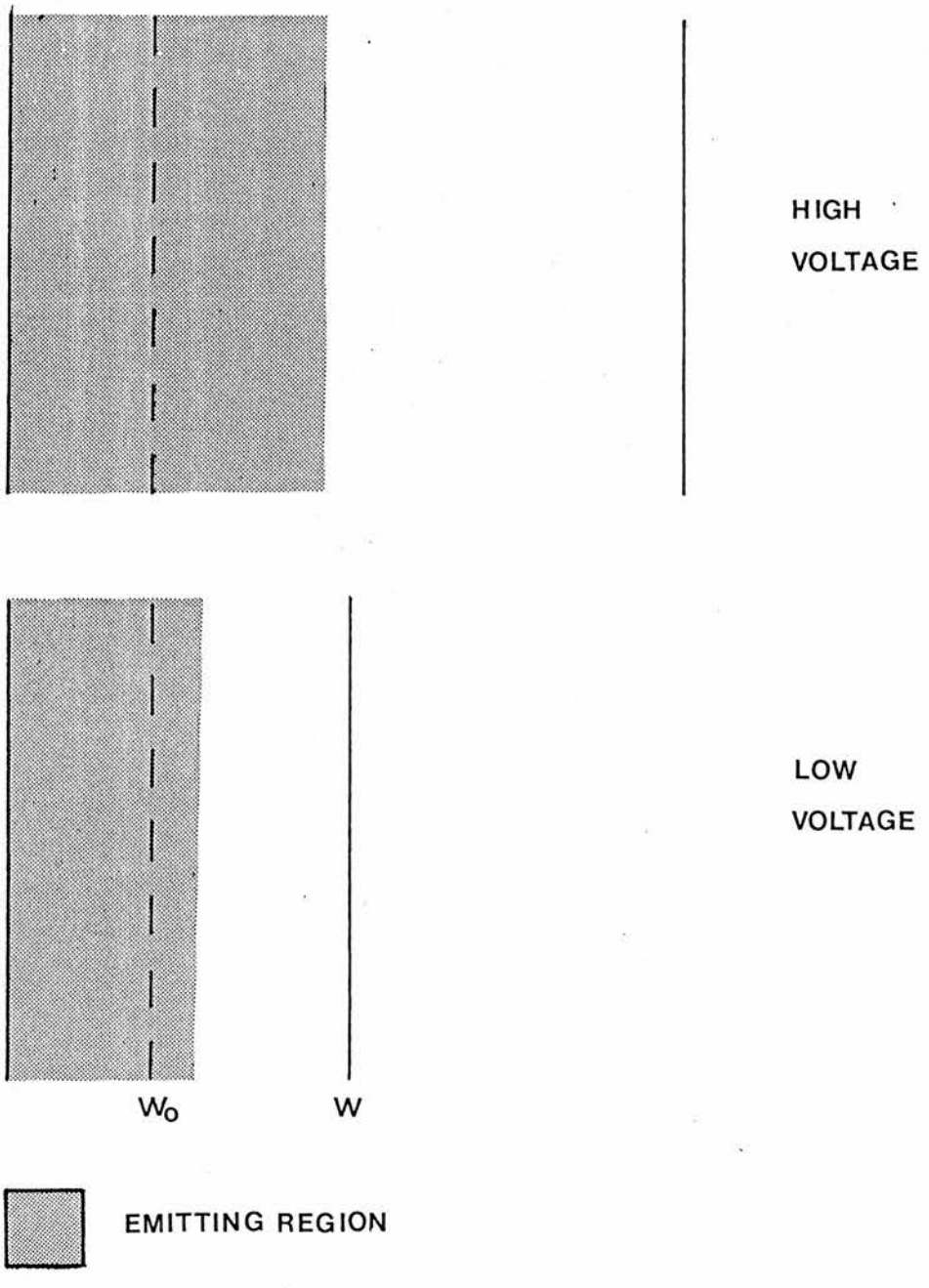

Fig.(3.1)

Schematic representation of the variation of the emitting region with applied reverse bias.

decay will be considered in the following. The treatment follows that of Langer, with some simplifications.

The intensity of the light output is given by

$$I(t) = \int \tau_r^{-1} N^*(x,t)\, dx. \qquad (3.1)$$

At time t=0 we have $N^*(x) = N_o^*(x)$ and so,

$$N^*(x) = N_o^*(x)\exp(-t/\tau) \qquad (3.2)$$

so

$$I(t) = \tau_r^{-1} \int N_o^*(x)\exp(-t/\tau)dx. \qquad (3.3)$$

If the decay time τ is a combination of the radiative decay time τ_r and the decay time due to the Auger quenching process $\tau_q(x)$ then

$$\frac{1}{\tau} = \frac{1}{\tau_r} + \frac{1}{\tau_q(x)} \qquad (3.4)$$

so

$$I(t) = \exp(-t/\tau_r)\ \tau_r^{-1} \int_0^W N_o^*(x)\exp(-t/\tau_q(x))dx \qquad (3.5)$$

where W is the depletion width.

It is useful to consider the quantity $Y(t) = I(t)\exp(t/\tau_r)$ i.e.

$$Y(t) = \tau_r^{-1} \int_0^W N_o^*(x)\exp(-t/\tau_q(x))dx. \qquad (3.6)$$

If a voltage is applied which produces a depletion region of

width W and the voltage is then dropped to zero which gives a depletion region of width W_o then the field, $N_o^*(x)$ and the decay time in the region vary as shown in fig.(3.2). In region A the decay time is the decay time due to the Auger quenching τ_q. In region C the decay time is that of the radiative centre τ_r. In region B of width Δ the decay is non-exponential due to the fact that the depletion region does not have an abrupt edge and the value of τ changes gradually from τ_q to τ_r. The above integration is done over the three regions separately, so we have

$$Y(t) \propto \int_0^{W_o-\Delta} N_o^*(x)dx + \int_{W_o-\Delta}^{W_o} N_o^*(x)\exp(-t/\tau_q(x)dx + 0 \qquad (3.7)$$

This describes a decay which consists of three parts, a fast part corresponding to the portion of the emitting region crossed by the depletion layer edge, a slow part corresponding to the non-crossed region and a non-exponential part inbetween.

The non-exponential region will now be considered in more detail. The decay time due to the Auger quenching is given by

$$\frac{1}{\tau_q(x)} = \gamma n(x) = \gamma n_o \exp(-eV/kT) \qquad (3.8)$$

where n(x) is the concentration of free electrons in the depletion region and n_o is the concentration in the bulk material. The potential V in the depletion region varies with distance across the depletion region starting with x=0 at the depletion region edge as

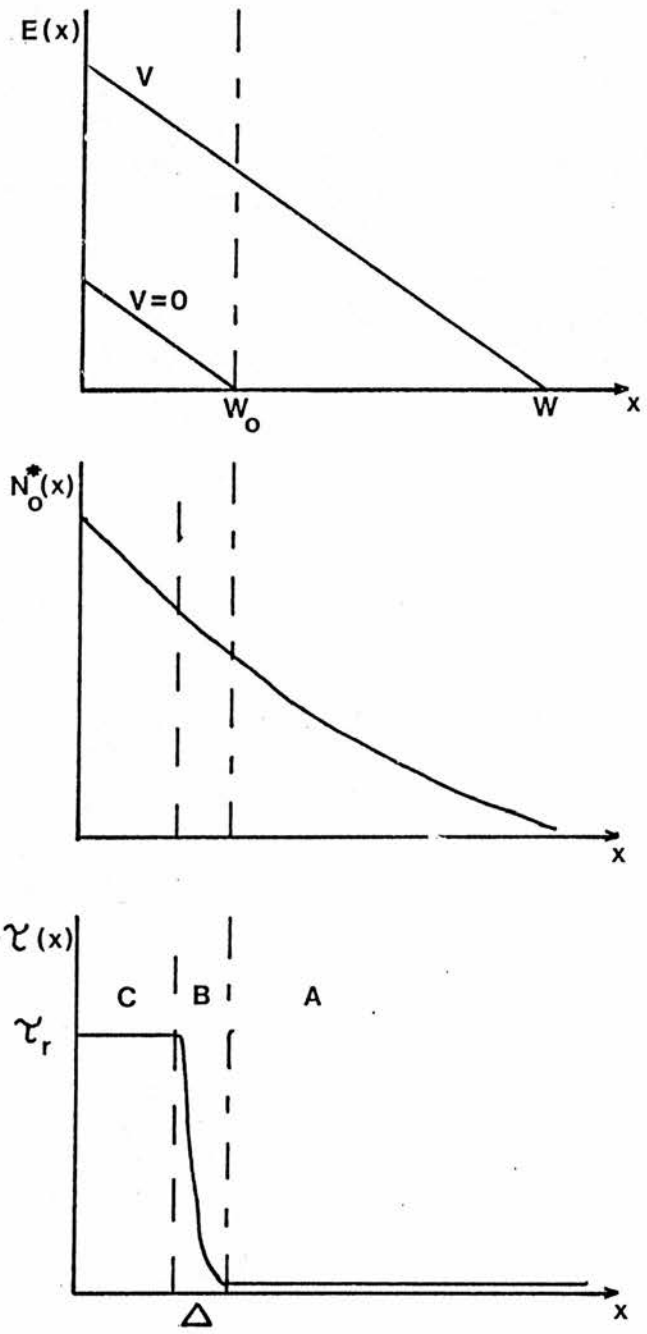

Fig.(3.2)

Variation of field, $N_o^*(x)$ and decay time along the depletion region.

$$V = \frac{eN_d x^2}{2\varepsilon_r \varepsilon_o} . \qquad (3.9)$$

If we define W_o as x=0 and assume that over the small region Δ $N_o^*(x)$ is constant and is given by $\overline{N}_o^*(x)$ then for the non-exponential region we have that

$$Y(t) \propto \overline{N}_o^*(x) \int_0^{\Delta} \exp\left[- \gamma n_o t \exp\left(\frac{-e^2 N_d x^2}{2\varepsilon_r \varepsilon_o kT} \right) \right] dx. \qquad (3.10)$$

EXPERIMENTAL METHODS.

3.1 Measurement of the decay time.

Reverse bias voltage pulses from an Advance PG55A pulse generator with a baseline at zero volts were applied to a ZnS:Mn Schottky diode. The light output was detected with an EMI 9558B photomultiplier tube and time-resolved measurements were made using a Brookdeal 415/425A boxcar system.

The decay curves were recorded for a variety of reverse bias pulses ranging between 30V and 50V.

In order to observe a bigger effect a forward bias was applied to the diode with the reverse bias pulses superimposed. This was achieved using the circuit shown in fig.(3.3). A 330 ohm resistor was used to protect the pulse generator in place of a diode as the diode introduced a reflection effect to the applied pulse. The other resistors were chosen so as to optimise the voltage drop across the diode and to minimise the time constant introduced because of the Schottky diode's depletion region capacitance.

Decay curves were recorded as previously for a variety of reverse bias voltage pulses keeping the forward bias constant.

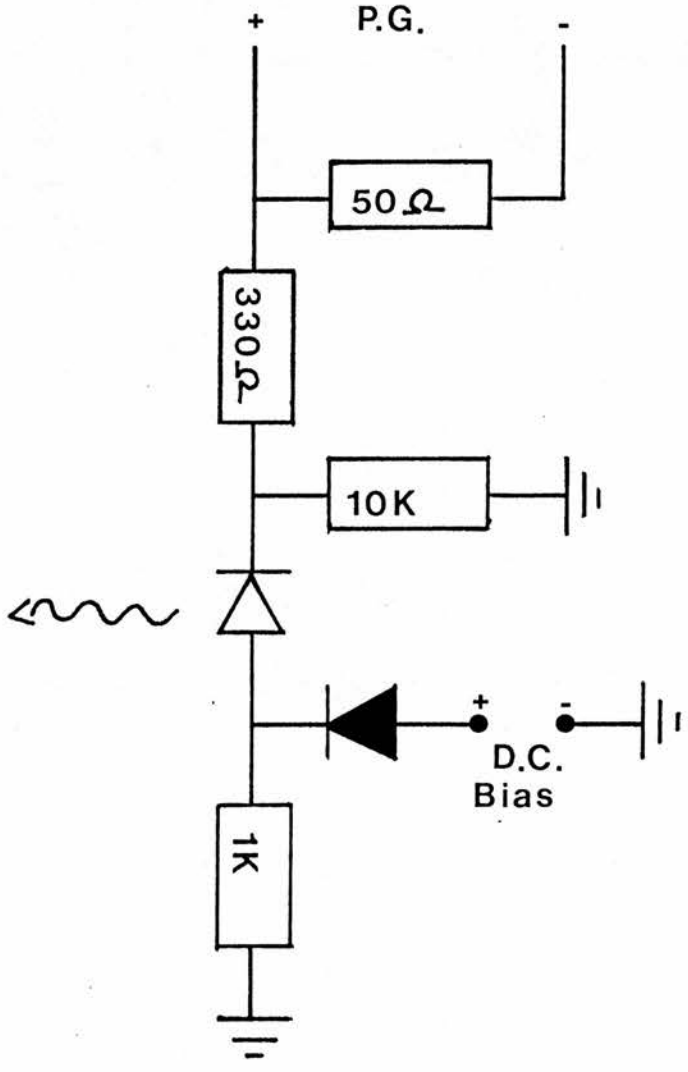

Fig.(3.3)

Circuit which superimposes a DC forward bias onto a reverse bias pulse.

3.2 Electrical characteristics.

Measurements of the differential capacitance (C) of the sample were made to determine the donor density (N_d). The capacitance measurements were made using a Wayne Kerr B601 RF bridge operating at 1MHz. If a graph is plotted of C^{-2} against voltage (V) then for an ideal Schottky barrier on n-type semiconductor the slope of the graph is given by

$$\frac{dC^{-2}}{dV} = \frac{2}{eN_d A^2 \varepsilon_r \varepsilon_o} \quad (3.11)$$

where ε_r is the permittivity of the semiconductor, e is the electronic charge and A is the area of the rectifying contact.

The current/voltage characteristics of the sample were determined using a high impedance Keithley 602 electrometer to measure the voltage.

3.3 Measurement of the relative quantum efficiency.

The relative quantum efficiency of the ZnS:Mn sample was measured by recording the light output per unit current through the sample. The sample was placed directly in front of an EMI 9558B photomultiplier tube and the light output of the diode was determined by measuring the output current of the tube and subtracting the dark current.

RESULTS.

3.4 Zero d.c bias .

The decay curves for a variety of reverse bias voltage pulses are shown in fig.(3.4). The decay curves consist of a fast decay (time constant < 50μs) followed by a non-exponential region, followed by a slower exponential decay. It can be seen from the figure that the decay does vary with the reverse bias voltage, though not to a great extent. There seems to be a bigger difference between the 50V, 46V and 42V results and a smaller difference between the results for lower voltages. The fast proportion of the decay increases with increasing voltage and the exponential time constant for the slow part of the decay decreases from 0.60ms at 30V to 0.49ms at 50V.

3.5 1V d.c. forward bias.

The decay times for a variety of reverse bias voltage pulses with 1V forward bias superimposed are shown in fig.(3.5). These do not differ greatly from those obtained with zero d.c. bias, with the fast proportion of the decay increasing with increasing reverse bias voltage, but not being any greater than for the zero d.c. bias results. The exponential time constant for the slow part of the decay varies from 0.55ms at 30V to 0.52ms at 46V.

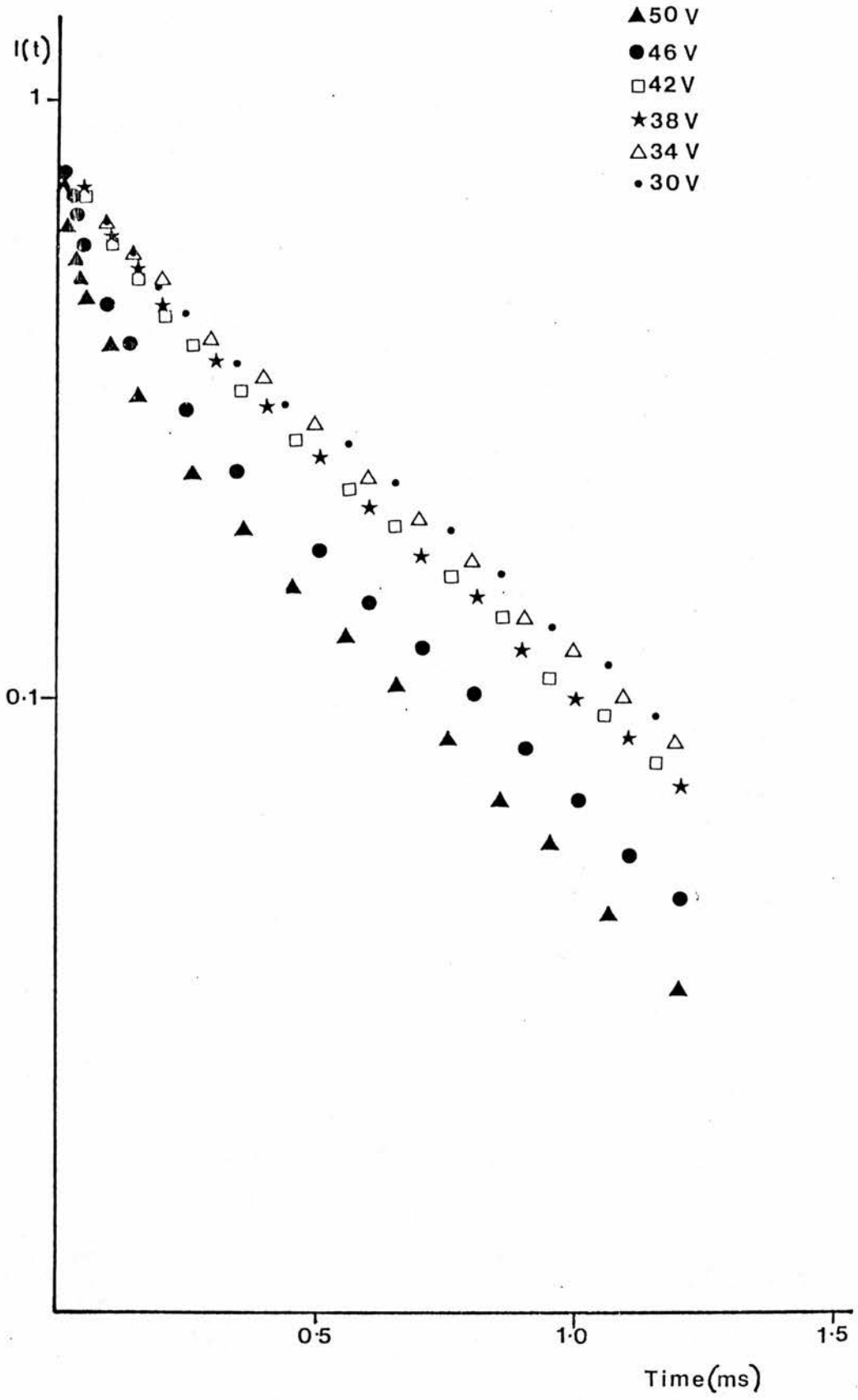

Fig.(3.4)

Decay kinetics of the ZnS:Mn sample for several reverse bias pulses.

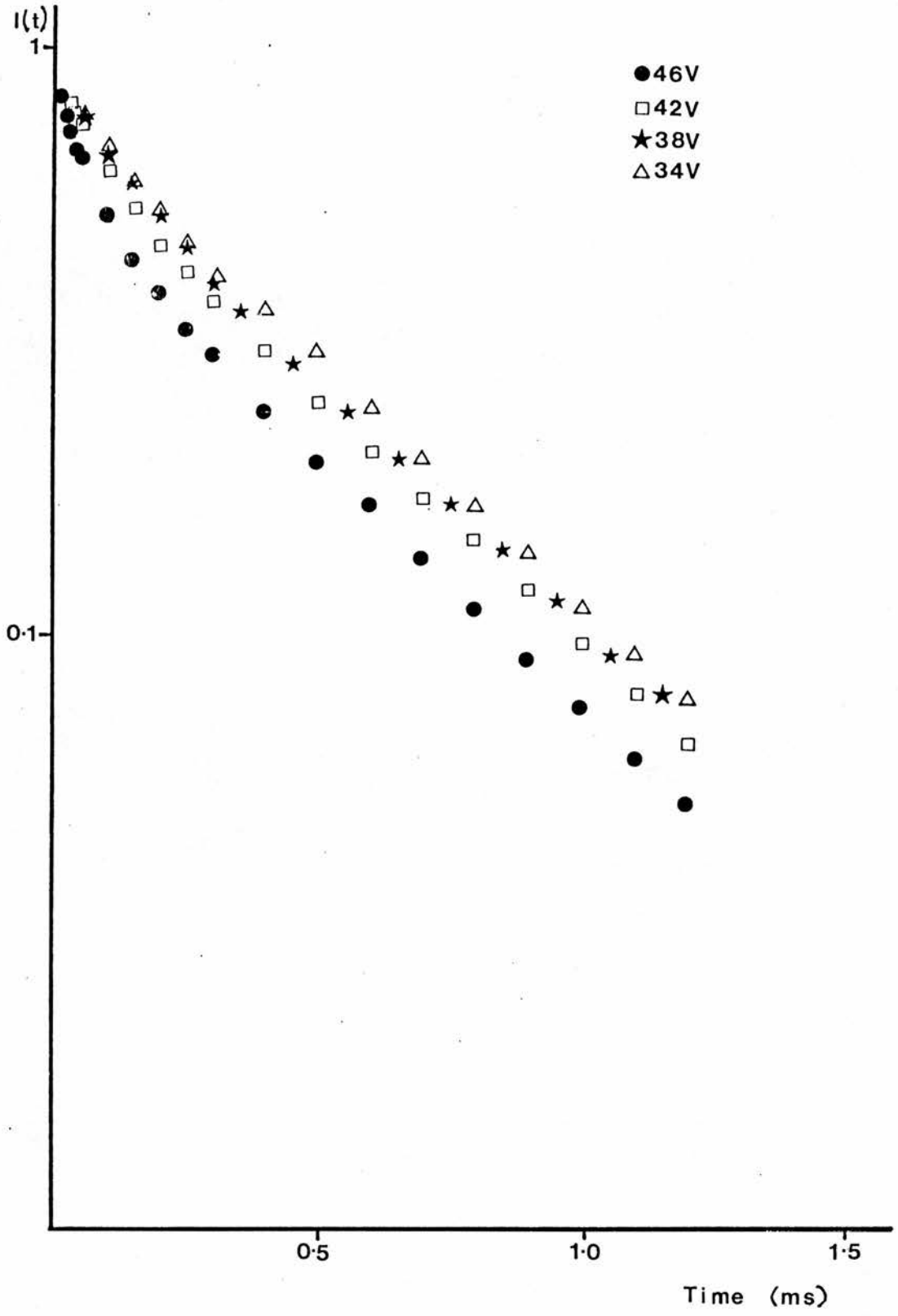

Fig.(3.5)

Decay kinetics of the ZnS:Mn sample for several reverse bias pulses with a 1V forward bias superimposed.

3.6 Electrical characteristics.

The gradient of the C-V plot was determined using a least squares analysis on a computer. This gave a donor density of 3.4×10^{15} cm^{-3}.

Once the donor density was known the depletion width W and the maximum electric field in the depletion region E_{max} could be found using the following expressions:-

$$W = \left[\frac{2\varepsilon_r (V_{bi} + V - kT/e)}{eN_d} \right]^{1/2} \qquad (3.12)$$

$$E_{max} = \left[\frac{2eN_d (V_{bi} + V - kT/e)}{\varepsilon_r} \right]^{1/2} \qquad (3.13)$$

where V_{bi} is the built-in potential of the junction and V is the applied reverse bias. At room temperature kT/e ~ 0.025eV, thus this term could be ignored whilst applied voltages of the order of 50V were being considered.

The current voltage characteristics are shown in fig.(3.6).

3.7 Relative quantum efficiency.

The quantum efficiency is given by

$$\eta = \eta_{rad} W N_{Mn} \sigma \qquad (3.14)$$

where η_{rad} is the probability that an excited manganese atom

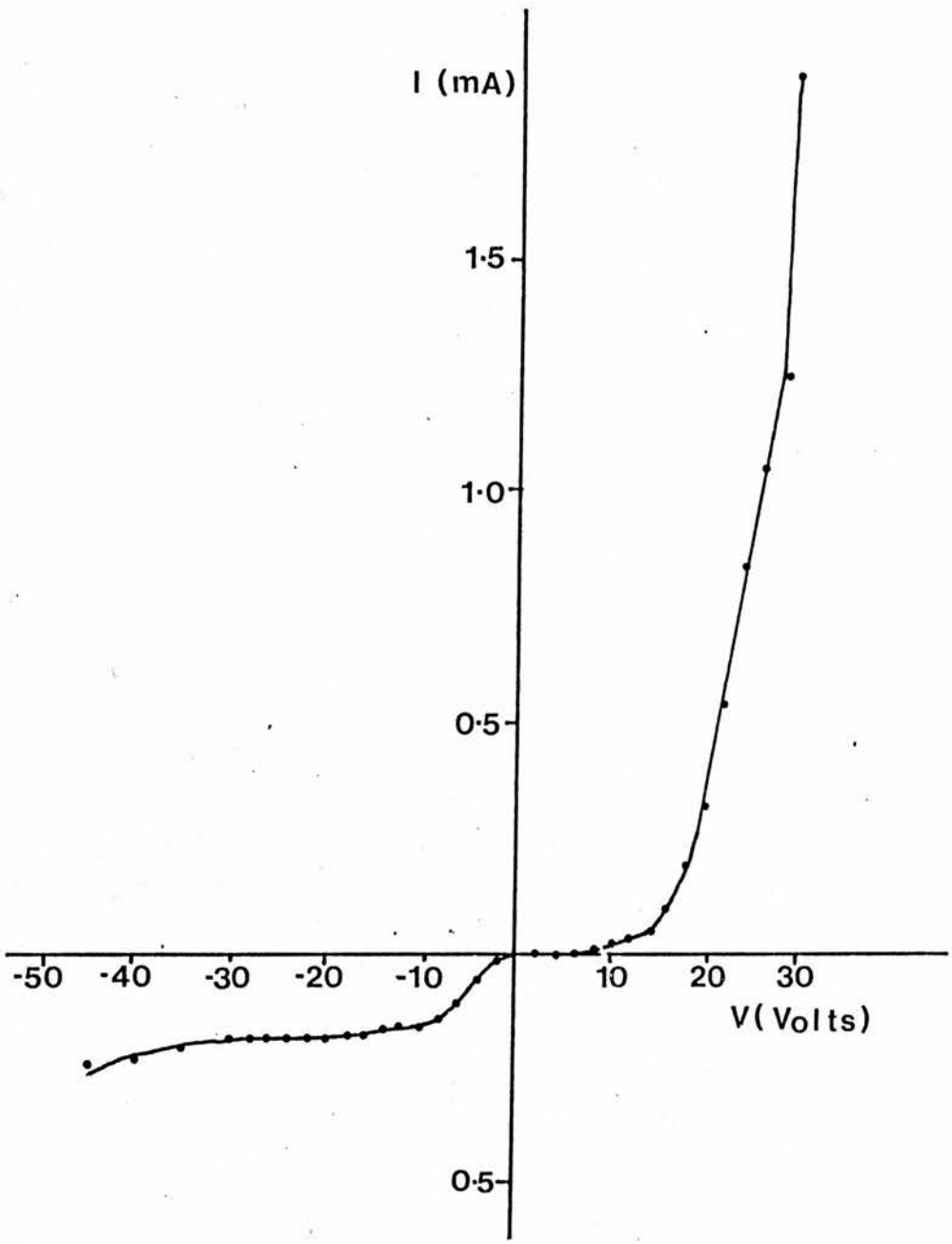

Fig.(3.6)

Current/voltage characteristics of the sample.

will decay radiatively (usually about 1), W is the depletion region width, N_{Mn} is the concentration of the manganese atoms and σ is the impact excitation cross-section. It can be shown that the cross-section can be approximated to

$$\sigma = \sigma_o \exp-(E_o/E)^2 \qquad (3.15)$$

where E_o is called the characteristic field [41]. The quantum efficiency is then

$$\eta = \eta_{rad} W N_{Mn} \sigma_o \exp-(E_o/E)^2. \qquad (3.16)$$

The value of E_o was required in order to find the density of excited states $N_o^*(x)$ across the depletion region, so a graph was plotted of $\ln\eta$ against E_{av}^2 where the average field is taken as the field in the depletion region and is given by $E_{max}/2$. A typical set of results is shown in fig.(3.7). The value of E_o was determined from the gradient of the graph. Several runs of the experiment were made and the average value was found to be 2.49×10^5 V cm^{-1} with a standard deviation of 1.2%.

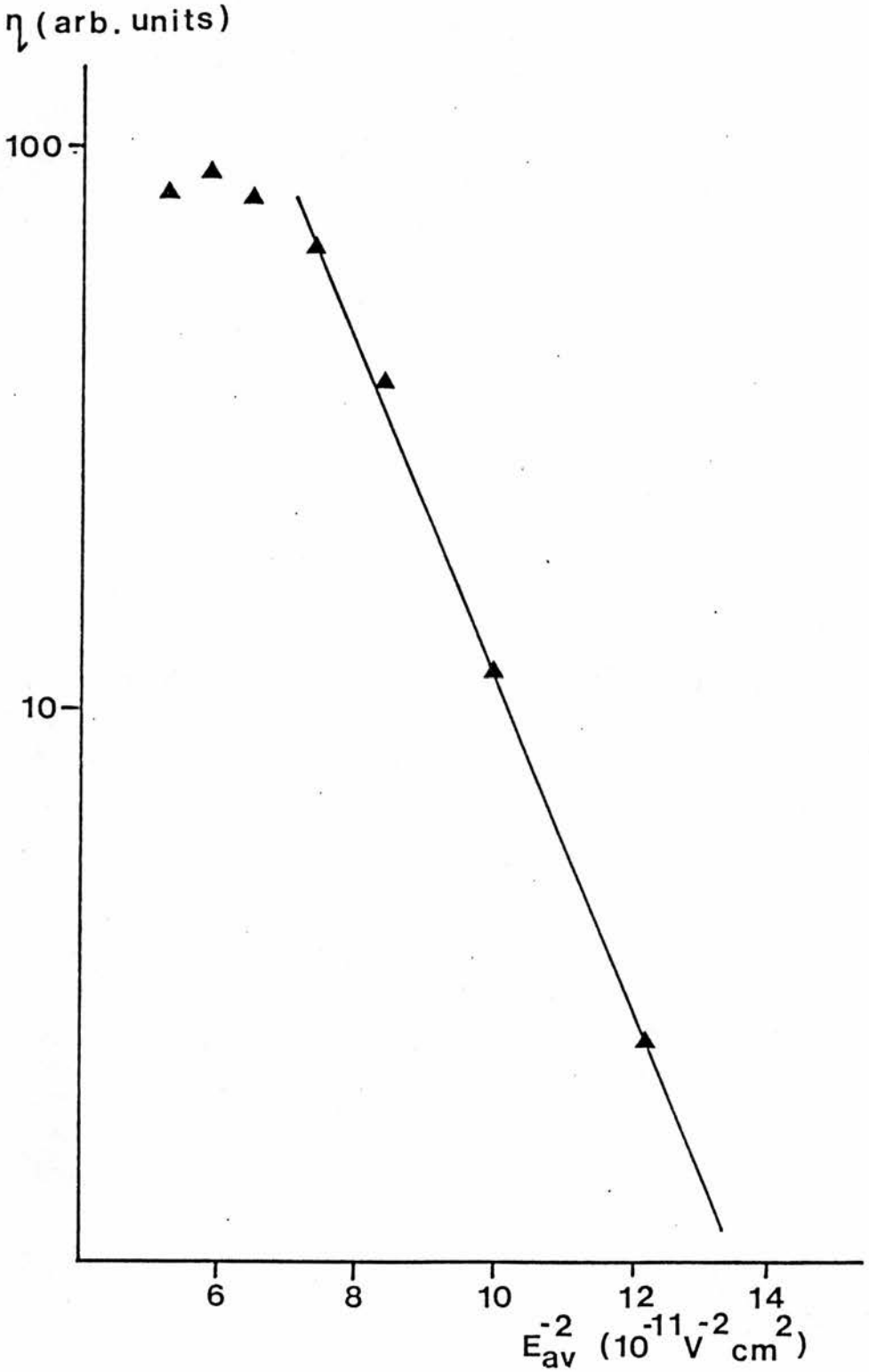

Fig.(3.7)

Variation of the quantum efficiency with field.

DISCUSSION.

The decay curves depended on the reverse bias pulse voltage to a limited extent. The fast decay only formed a small proportion of the total decay. This implies that the manganese emission region is predominantly over a small region similar to that of the depletion region for zero bias. This is also shown by the small change of the decay curves with the reverse bias pulse voltage for lower voltages.

When a forward bias is applied to the diode it is expected that the depletion region width will decrease substantially, which means that the fast proportion of the decay should be increased. This was not observed, and there are two possible reasons for this. Firstly, the manganese emission could occur over a small region similar to that of the depletion region width at a forward bias voltage of 1V. This is not likely as a small effect is seen for higher voltages when the voltage is dropped to zero, so an increase in this effect would be expected when the voltage is dropped from a high reverse bias to 1V forward bias. The most likely explanation can be seen by examining the current/voltage characteristics of the Schottky diode shown in fig.(3.6). The forward bias current increases very slowly with voltage until about 20V is applied. This is due to the presence of an oxide layer on the surface of the sample which could not be avoided. In forward bias therefore, some of the voltage will be dropped across the oxide layer and so the voltage dropped across the depletion region will not be the applied forward bias voltage. This means that the depletion region is not

significantly reduced by the application of a forward bias, which explains the results obtained in fig.(3.5).

The emitting region width can be determined theoretically by finding the fraction of excited manganese centres along the depletion region. In the straight line region of fig.(3.7) the fraction of excited manganese centres is given by f(E) where

$$f(E) \sim \exp-(E_o/E)^2 \qquad (3.17)$$

where E is the electric field at a given point in the depletion region and E_o is the characteristic field of the diode which determines the variation of quantum efficiency with applied field for the diode.

N. Gordon [41] noted that the electric field in the active region of a Schottky diode is not uniform, but varies linearly across the depletion region. He obtained an expression for the impact cross section which took account of the non-uniform field. For the range of E_o/E_{max} encountered experimentally in ZnS:Mn diodes this expression could be written as

$$\langle \sigma \rangle = 0.23 \exp-1.20(E_o/E_{max})^2. \qquad (3.18)$$

The experimental results in section 3.7 were fitted to the expression

$$\langle \sigma \rangle = \sigma_o' \exp-(E_o'/E_{max})^2. \qquad (3.19)$$

Comparison of equations (3.18) and (3.19) shows that if we are to

take account of the non-uniform field in our analysis, then the value of E_o' which we obtained in section 3.7 must be modified according to

$$E_o = 1.82E_o'. \qquad (3.20)$$

Substituting in this corrected value of E_o and as the field in the depletion region is linear, f(E) is given by

$$f(E) \sim \exp - \left[\frac{4.56 \times 10^5 \ W}{(W-x)E_{max}} \right]^2 \qquad (3.21)$$

where E_{max} is in Vcm^{-1} and x is the distance along the depletion region from the Schottky contact.

A plot of f(E) against fractions of the depletion width is shown for various reverse voltages between 30V and 50V in fig.(3.8). W_o marked on the graphs is the depletion width for an applied voltage of zero. If we consider applying a reverse bias pulse, then from the graph it can be seen that when the applied voltage is dropped to zero some of the excited manganese centres are outside the depletion region of the diode. It can also be seen that the proportion of excited manganese centres which are outside the depletion region when the applied voltage is dropped to zero decreases with decreasing applied voltage. This is also shown in the following table.

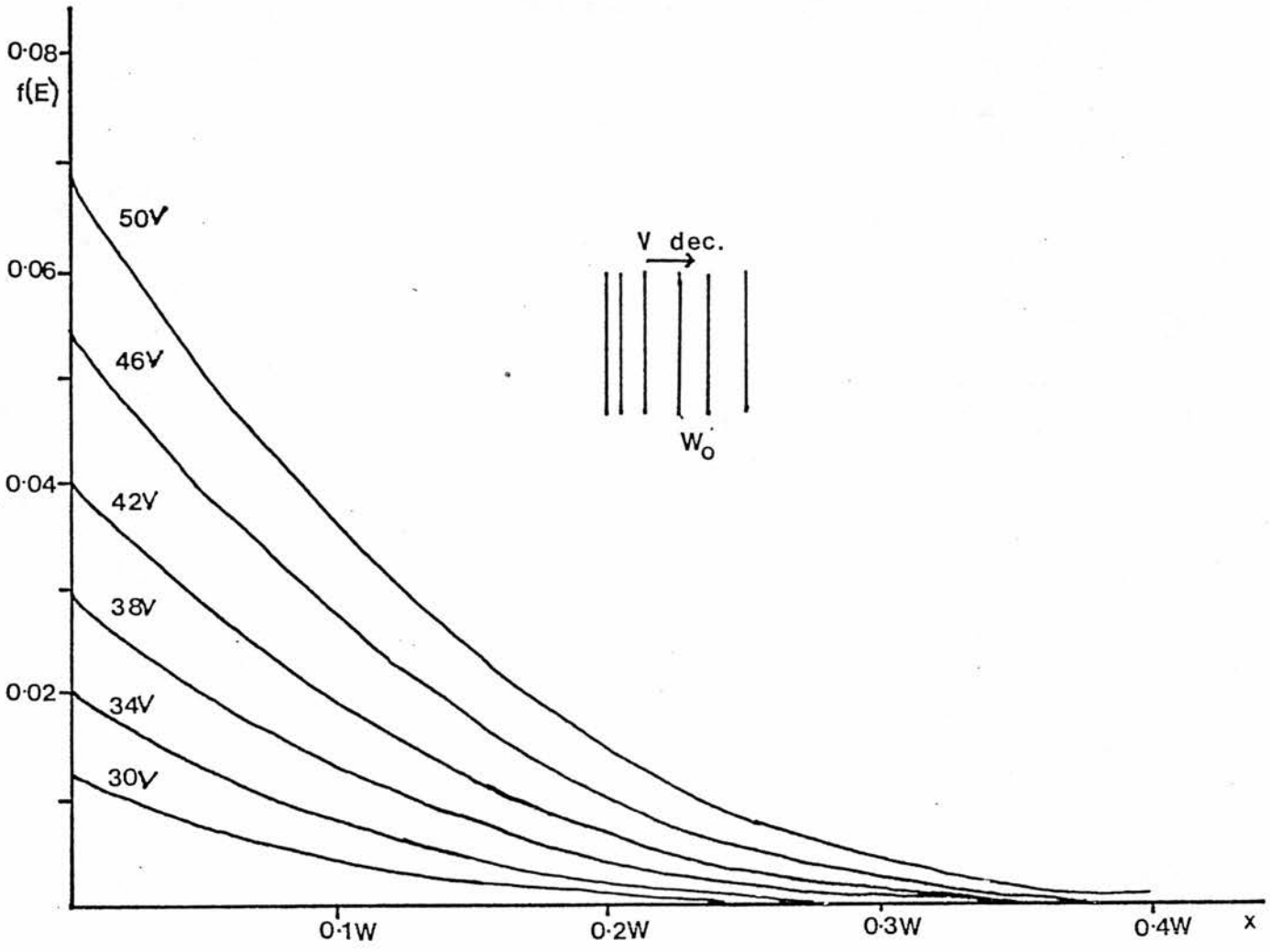

Fig.(3.8)

Variation of f(E) along the depletion region.

Applied voltage	% of emitting region outside the depletion region when the voltage is dropped to zero.
50V	12.4%
46V	10.2%
42V	7.0%
38V	4.7%
34V	2.1%
30V	0.9%

Fig.(3.8) shows that the emitting region does not spread over the whole of the depletion region, and in fact the fraction of excited manganese centres drops to almost zero about one third of the way along the depletion region. The above table shows that only a small proportion of the emitting region is outside the depletion region when the applied voltage is dropped to zero. This is in agreement with the qualitative estimate of the emitting region made from the results in fig.(3.4).

There are however, two features of the experimental results which this theoretical treatment does not explain. Firstly, the above table does not explain why there are larger differences in the shape of the decay for the higher voltage results compared with the lower voltage results. Secondly, the shape of the decay for a 30V applied pulse seems to deviate more from a true exponential decay than would be expected if only 1% of the emitting region is outside the depletion region when the applied voltage is dropped to zero. These discrepancies may be resolved

if we could find the exact proportion of the total decay which the fast decay constitutes. It could be that the shape of the decay for the lower voltage pulses is due mainly to regions B and C and is due only slightly to region A. This would explain why there is little difference in the shape of the decays for lower voltage pulses and why the decay deviates from an exponential form for a 30V applied pulse. This is quite probable as for the lower voltages pulses it is predicted theoretically that only a small proportion of the emitting region is outside the depletion region when the applied voltage is dropped to zero.

In order to test this theory it is necessary to take the results in fig.(3.4) and resolve them into the three regions, A the region where the decay is due to the Auger quenching, B the region where the decay is non-exponential and C the region where the decay is the radiative manganese decay. This can be done by fitting the form of the non-exponential region of the decay given by equation (3.10) to our results, and so separate the three regions. This is also expected to give a more accurate decay time for the fast part of the decay.

Firstly, our results were plotted in the form of $Y(t) = I(t)\exp(t/ \tau_r)$ against time. This is shown in fig.(3.9). The slow decay was now given by a straight line and if this was subtracted from the rest of the plot then the result was the decay in regions A and B as is shown in fig.(3.10).

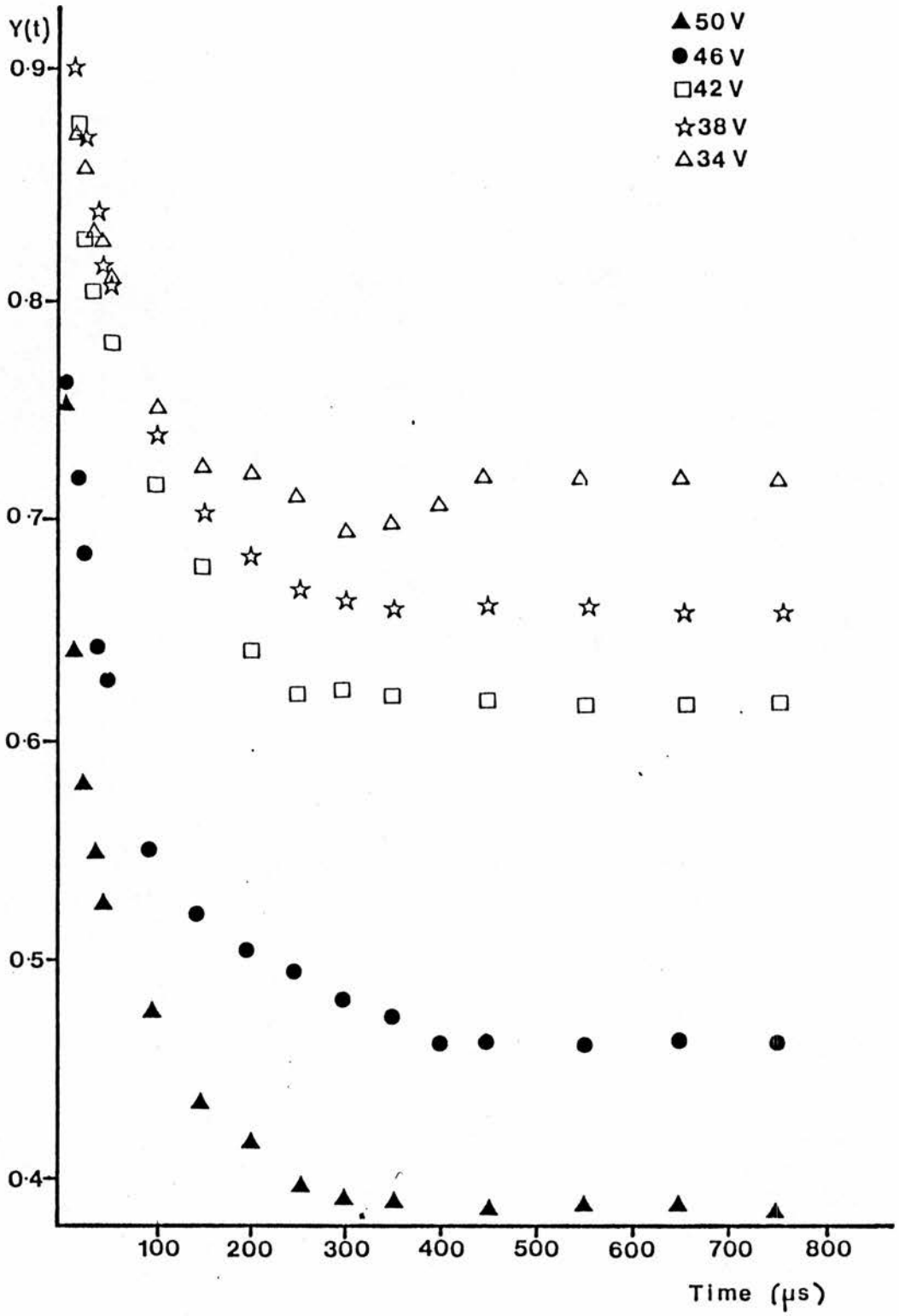

Fig.(3.9)

Modified decay kinetics of the sample where

$Y(t) = I(t)\exp(t/\tau)$.

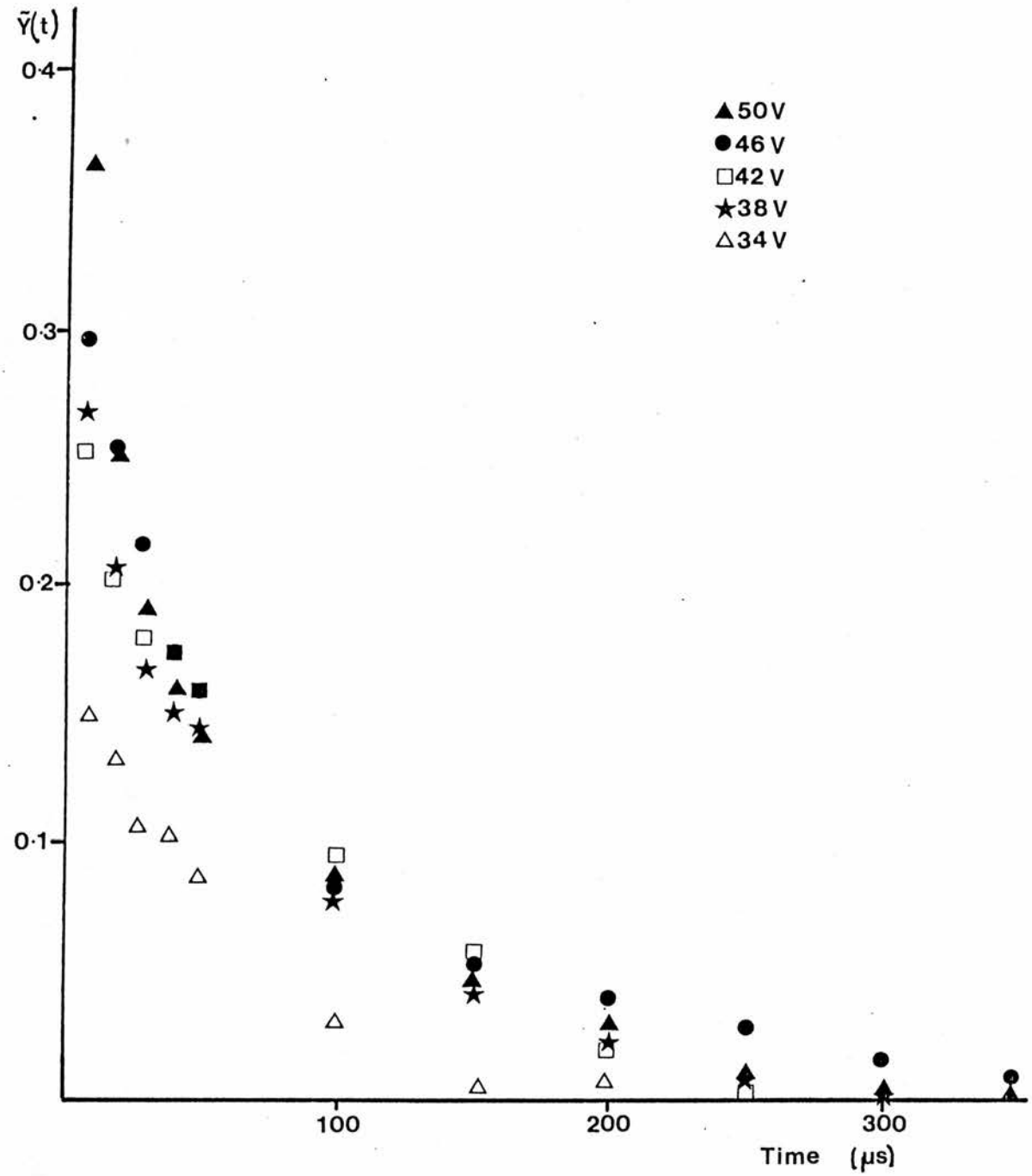

Fig.(3.10)

Modified decay kinetics of the sample

with the slow decay removed.

The non-exponential region of the decay was determined theoretically using equation (3.10). The value of $\overline{N_o}^*(x)$ was assumed to be constant over the small region Δ of the depletion region. The value of the donor density N_d was known from the C-V measurements and the value of the Auger coefficient γ in ZnS:Mn was found by Gordon and Allen [40] to be 2×10^{-9} $cm^3 s^{-1}$. The value of n_o was estimated assuming an activation energy of 0.05 eV. The value of Δ was estimated as follows. Equation (3.10) was evaluated numerically using the above values of γ, n_o and N_d for different values of Δ. The integral was evaluated for fixed values of t, the values chosen being 50 μs, 200 μs and 900 μs. The value of the integral was then plotted against Δ and this can be seen in fig.(3.11). The plot became linear in region C (the radiative decay region) as then the value of τ was constant and so from the graph Δ was estimated to be $\sim 2 \times 10^{-7}$ m.

The integral was then determined numerically using this value of Δ for different values of t. The resulting plot in fig.(3.12) gives the theoretical decay in the non-exponential region B. This plot was normalised at 100 μs to the 50V plot in fig.(3.4) and the two plots were superimposed in fig.(3.13). It can be seen from this that the two curves do not have the same shape even in the lower part of the curve. It is therefore not possible to separate regions A and B in this way. The most probable reason for this is that the assumption that $N_o^*(x)$ was constant over the region was inapplicable for this sample. As $\Delta \sim 0.27 W_o$ then this region is of appreciable size compared to the width of the depletion region at zero bias so it does seem

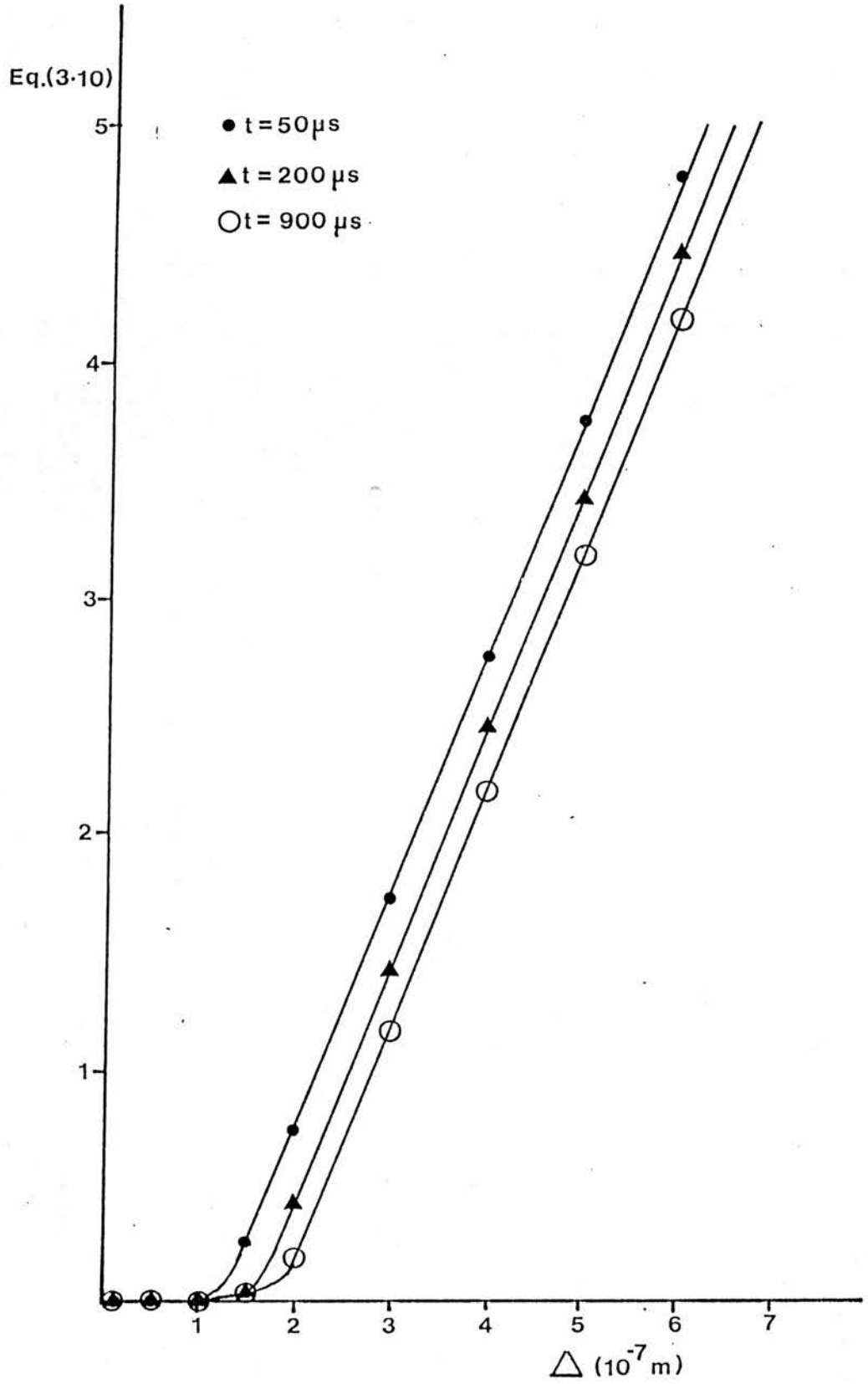

Fig.(3.11)

Variation of equation (3.10) with Δ for several values of t.

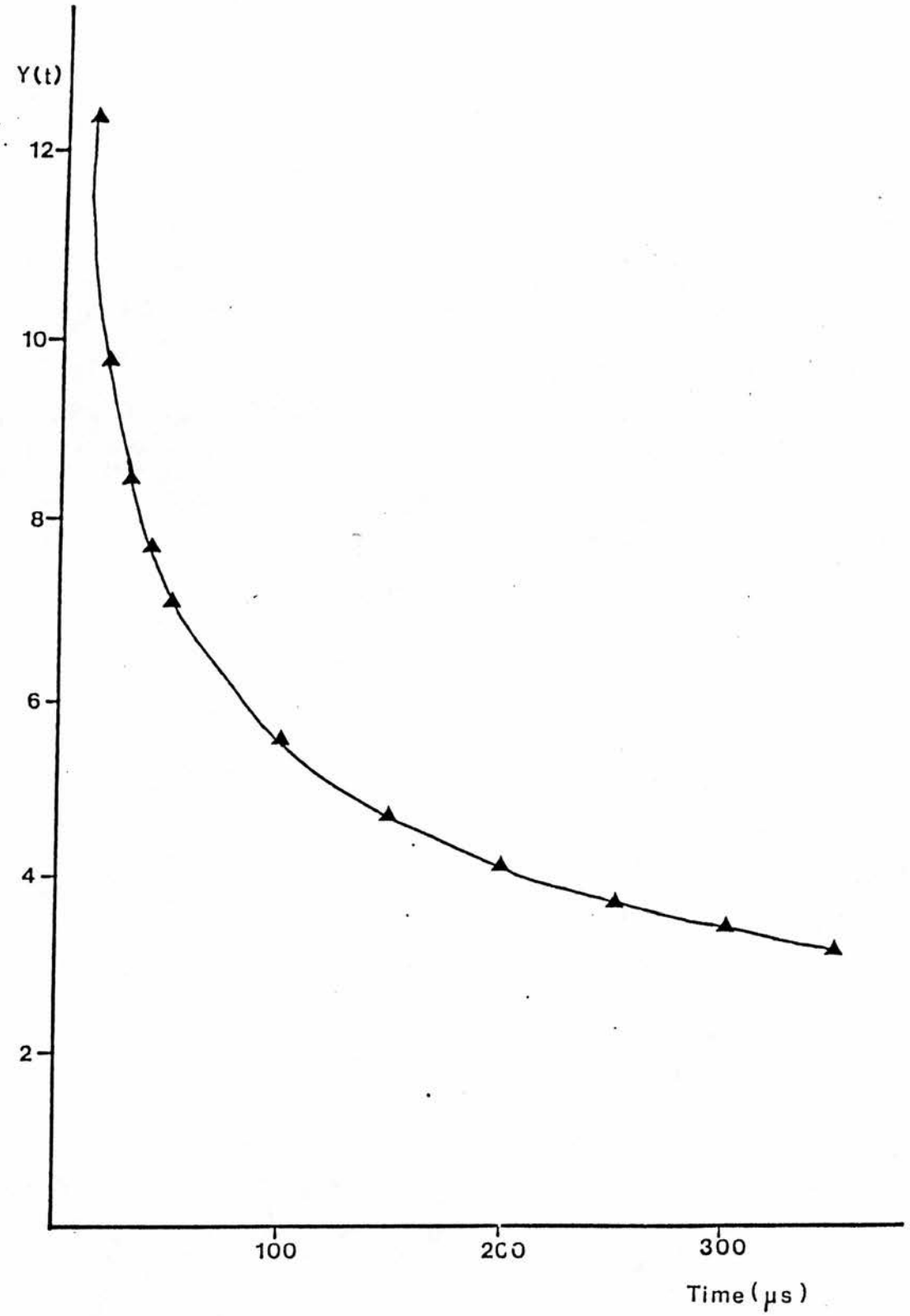

Fig.(3.12)

Theoretical form of the non-exponential region of the decay.

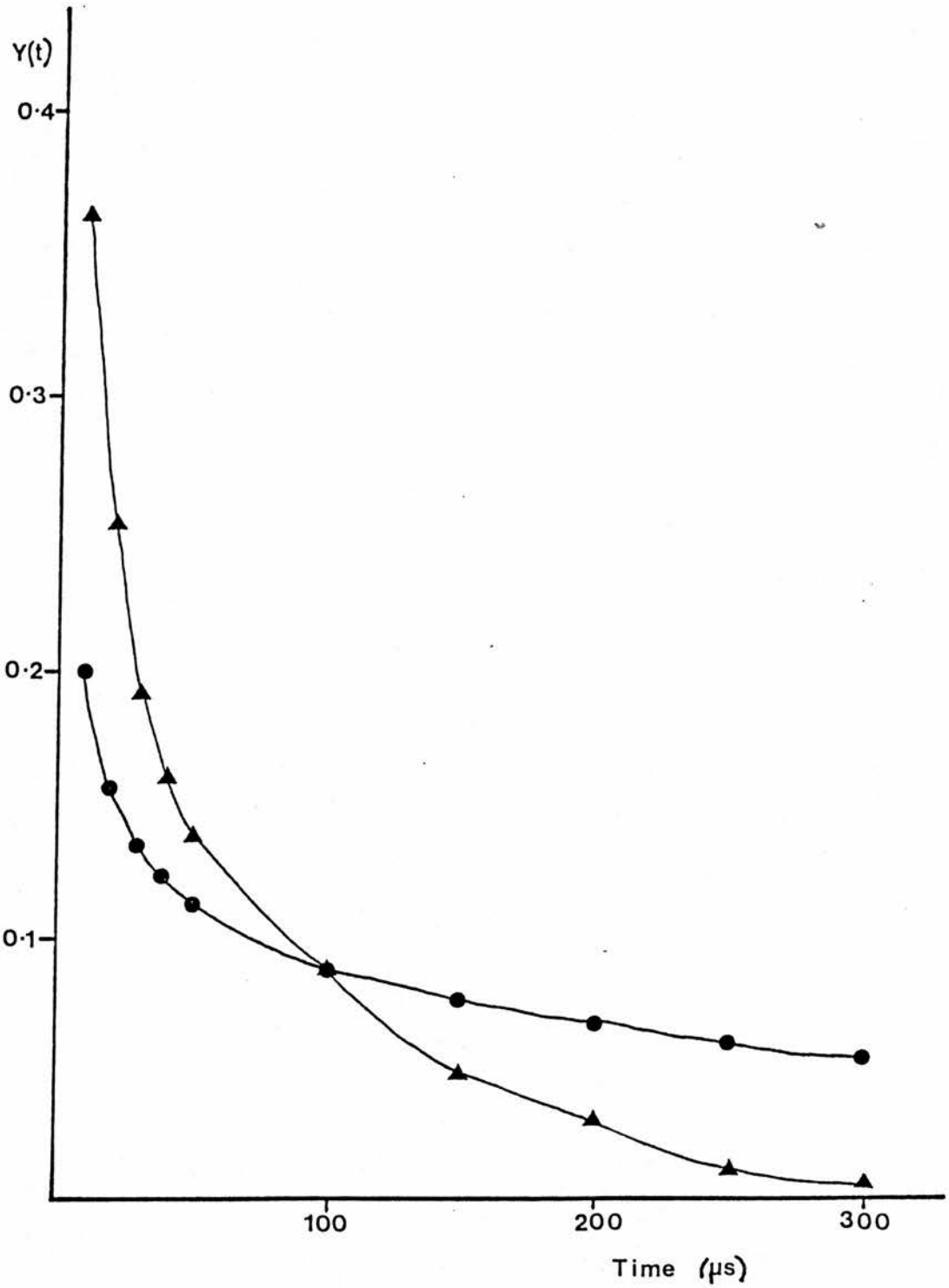

Fig.(3.13)

Superposition of the theoretical and experimental decay kinetics.

likely that the assumption was unreasonable. Unfortunately however, this meant that further quantitative work on this sample could not be done. Langer had made this assumption in his treatment of manganese electroluminescence in CdF_2:Mn,Y [38]. It could be possible therefore that a reappraisal of his results is needed.

It was thought that the system response time could be distorting the shape of the decay in the region where Auger quenching takes place. The Auger decay time was estimated to be ~1.5 μs using $\tau_q = 1/\gamma n$. The response time of the system was determined by measuring the decay of an led and was found to be ~3 μs. The system response time was decreased to 60 ns by reducing the load resistor in the photomultiplier tube from 27 kohms to 390 ohms. The decay of the ZnS:Mn diode was then recorded, but the shape of the decay was found to be no different from the decay which was recorded with the slower system response time. It was concluded therefore that the shape of the decay was not distorted by the system response time.

Another unexplained feature of the decay curves is the time constant of the slow exponential part of the decay which is found to be about 0.5ms rather than the expected value of about 1ms. It was thought that this may be due to thermal quenching. This theory was examined by recording the decay curve for a 50V reverse bias pulse in the same way as previously at a variety of temperatures ranging from room temperature (290K) to 370K. The resulting decay curves are shown in fig.(3.14). As the temperature is increased there was no decrease in the time constant for the slow part of the decay as would be expected if

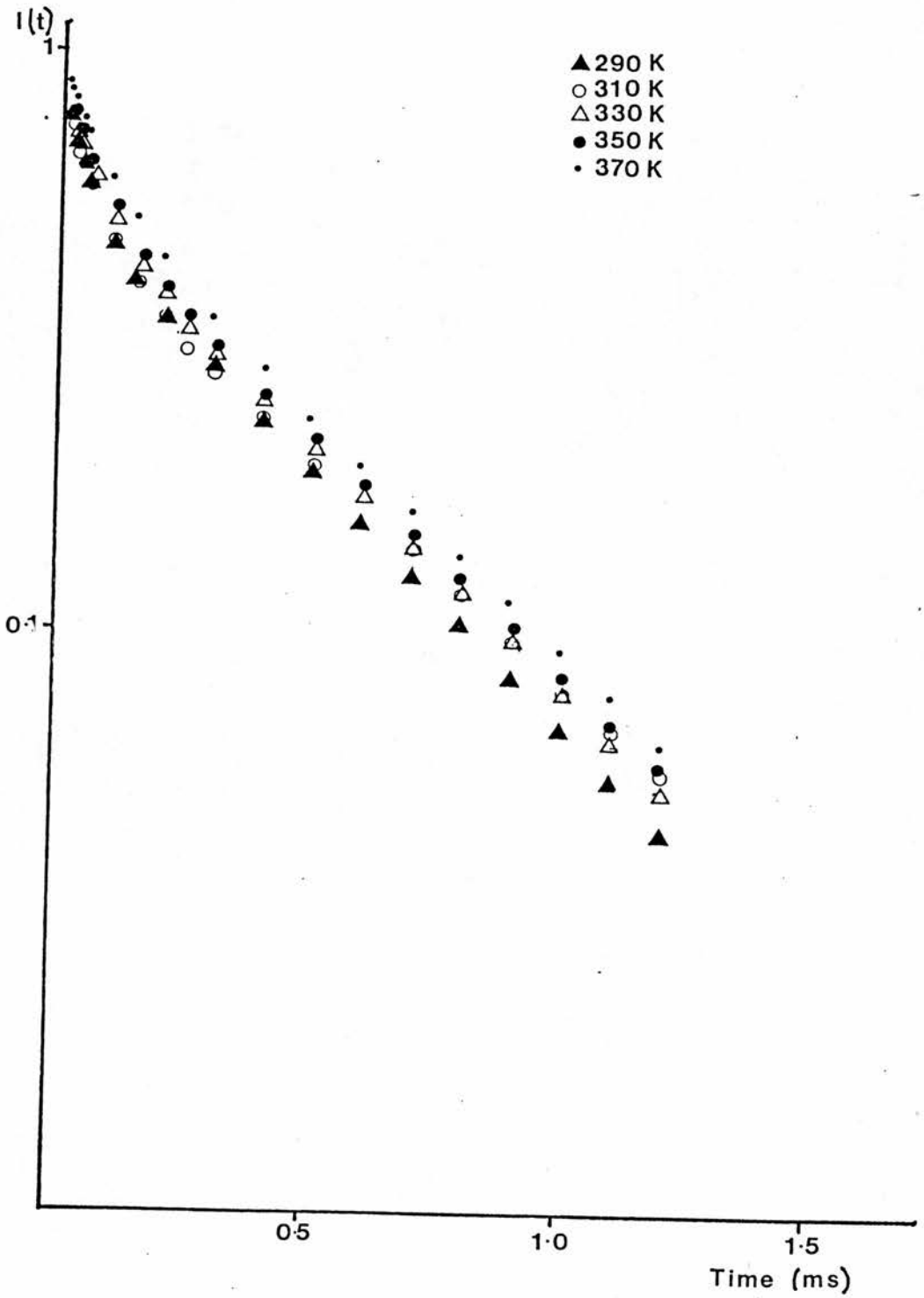

Fig.(3.14)

Decay of the ZnS:Mn sample for a 50V reverse bias pulse at several temperatures.

thermal quenching were responsible for the shorter time constant at room temperature. There was a slight decrease in the fast proportion of the decay with increasing temperature which is due to a slight variation of the depletion width with temperature. It was concluded that there was no thermal quenching in the sample.

The reason for the 0.5ms time constant is unexplained at present.

CONCLUDING REMARKS.

The work in this chapter has shown that it is possible to determine the emitting region in ZnS:Mn Schottky diodes as was intimated by J.M. Langer [38]. The emitting region was estimated from the experimental results to be over a small region which is slightly larger than the depletion region width for zero bias. This was in qualitative agreement with the theoretical emitting region which was determined. A quantitative analysis of the results could not be performed because of the difficulty in separating fast decay due to the Auger quenching from the non-exponential decay.

A sample which would be ideal for this type of experiment would need to have a large emitting region as discussed previously (the sample used here had an emitting region which was barely large enough for the non-exponential decay to be observed) and also a small value of Δ. This would make the assumption that $N_o^*(x)$ is constant over the region more reasonable and the experimental results could then be compared with the

theoretical non-exponential decay to reveal the fast proportion of the decay.

CHAPTER 4

ELECTROLUMINESCENCE OF ZnS:RE SCHOTTKY DIODES.

INTRODUCTION.

In this chapter we look at the electroluminescence of ZnS:RE Schottky diodes and in particular we measure the emission spectra and the decay times of the diodes. By comparison of these measurements with the work done on ZnSe Schottky diodes by Turvey and Allen [42] we obtain evidence of intervalley transitions in the conduction band which are characterised by broad emission spectra and fast decay times, and hence show that there are energetic electrons in the diodes with energies up to 2.8eV above the conduction band edge. This means that when we discuss the rare-earth emission we already know that there are hot electrons in the diodes which could excite the rare-earth centres. In fact we observe no spectral components due to the internal $4f^n$ transitions of the rare-earth and hence show that the presence simultaneously of hot electrons and luminescent rare-earth centres in the diodes is not sufficient to guarantee rare-earth emission.

The established excitation mechanism of the rare-earth centres in ZnS is impact excitation as was shown by Krupka [25]. There is however some controversy about the evidence, as for example Marrello et al. [43] were unable to repeat Krupka's results. In this chapter we show that as well as the broad emission band due to the interband transitions there are several other electroluminescent emission bands in ZnS:RE diodes which are dependent on the rare-earth dopant. We show that the presence of these bands indicates that Krupka's data could be interpreted in terms of an energy transfer mechanism. We

conclude that the excitation of the rare-earth is likely to be by the impact of hot electrons for some conditions and by energy transfer for others. This is the same situation as we have for manganese in ZnS:Mn and ZnSe:Mn as was shown in the second chapter of this thesis.

EXPERIMENTAL METHODS.

4.1 Growth and preparation of the samples.

The ZnS:RE samples used in this chapter were grown by H.Hartmann using the method described in [44]. The starting powder materials (ZnS and the rare-earth in metallic form) were fired at 1250 °C in a N_2-CS_2 gas stream and were subsequently grown into crystals by iodine transport. Some of the samples were codoped with lithium as it has been shown [45] that this cleans up the photoluminescence spectrum from self-activated or Cu-related emissions and also enhances the RE^{3+} emission. The crystals were made conducting by immersion in a Zn/Al bath with 2-4% Al for 90 hrs at 800 °C. This process typically gave room temperature resistivities of ~ 10^3 ohm cm. The rare-earth concentration was ~ 10^{19} cm^{-3} and electron microprobe analysis on ZnS:Sm showed that the samarium had not been removed by the Zn/Al treatment. The samples used were ZnS:Sm,Li (T56a), ZnS:Eu,Li (T38a,b) and two samples of ZnS:Tb (T34a D and E).

The samples were polished with jeweller's rouge and then placed under propanol in an ultrasonic cleaner to remove all traces of the rouge. The samples were then etched in a dilute solution of HCl for 30 seconds and then rinsed thoroughly with de-ionised water. Any excess water was removed from the samples with propanol. 1mm aluminium Schottky contacts were evaporated onto the samples. Large area silver paste ohmic contacts were made on the other side of the samples. This type of ohmic contact was used in preference to indium contacts as they gave

more light emission.

4.2 Measurement of the emission spectra.

The sample was placed directly in front of the slits of a Rank-Hilger D330 or a Zeiss SPM2 monochromator. A reverse bias d.c. voltage was applied to the sample and the resultant electroluminescence was detected from the output slit of the monochromator by a Hamamatsu R955 photomultiplier tube. The output from the photomultiplier was fed into a Spex DPC2 photometer which was operated in photon counting mode. This enabled the detection of the small signal produced which had previously been difficult to measure. (Initially the experiment had been attempted by chopping the light emission from the sample and measuring the output from the monochromator using an EMI 9558B photomultiplier tube which fed into a Brookdeal 401 lock-in amplifier). The experiment was operated digitally for greater accuracy. The wavelength on the monochromator was set manually to 350 nm and the photometer integrated the output signal over a period of 20 seconds. The wavelength was then increased by 5 nm and the operation was repeated until the wavelength reached 800 nm whereupon the sensitivity of the tube was dramatically reduced. As each integration took 20 seconds, the whole spectra took about 45 minutes to record, so it was important to check the consistency of the results. This was done by repeating a previous measurement whenever the wavelength increased by 100 nm. Also, at the end of the run several measurements were repeated over a whole range of wavelengths. The voltage to the sample was then switched off and the background signal was measured over a range of wavelengths and this signal was then

subtracted from the measurements taken.

The experiment was repeated several times for each applied voltage to a given sample. The lower voltage used was determined by the smallest signal which could be measured accurately over the background signal, and the highest voltage used was determined by the maximum power dissipation in the sample. Samples of ZnS:Sm,Li, ZnS:Tb (D and E) and ZnS:Eu,Li were used in the experiment.

In order to pick out the $4f^n$ spectral lines observed by D. Hommel [46] in photoluminescence experiments at 570 nm, 610 nm, 650 nm and 720 nm the experiment was repeated for the ZnS:Sm,Li sample, but the wavelength was increased in steps of 1 nm over a 20 nm region centred around each wavelength where the fine structure was expected. However, no $4f^n$ lines could be clearly resolved above the noise background.

4.3 Calibration of the system for measuring spectra.

The calibration source used to calibrate the system was of the black body type. The source was produced by heating a cylinder of graphite to 850 °C in a nitrogen atmosphere in a furnace. The temperature in the furnace was kept constant by a Control and Readout Ltd. 405 temperature controller. The light from the black body source was collected by a lens and focussed onto the slits of the monochromator. The signal was measured for each wavelength used in the spectra measurements with an integration time of 20 seconds, and again the background signal was subtracted from the measurements. The resulting spectrum of

the black body source was compared with the theoretical spectrum of a black body source at that temperature to give a calibration curve for the system. Unfortunately however, as a black body source at 850 °C was used for the calibration, an accurate calibration could only be found for wavelengths greater than 450 nm. This minimum wavelength could have been lowered by increasing the temperature of the black body source, but it was not possible to increase the temperature much further. The calibration was repeated for both the Rank-Hilger and the Zeiss monochromators.

4.4 Measurement of the decay time.

Reverse bias pulses of height 200V were applied to the sample from an Avtech AVR-3-C pulse generator. The sample was placed directly in front of an EMI 9558B photomultiplier tube which detected the light output from the sample. The signal was processed with a Brookdeal 415/425A boxcar system the output of which was monitored on a chart recorder. In order to reduce the noise in the signal as much as possible the pulse generator was operated at its upper frequency limit of 1kHz, this meant that the maximum pulse width which could be applied was 5 μs.

As very fast decay times were to be measured several problems were encountered in setting up the experiment. When the sample was placed in a typical spring contact holder then the holder itself picked up electrical noise from the pulse generator. This problem was solved by screening the sample by placing the sample holder in an earthed metal box with a small hole to enable light emission. Another problem was the pick-up

of electrical noise from the pulse generator by the boxcar. This was reduced to a minimum by the careful placing of the cables in the experimental set-up which were then taped in place.

Once the problem of electrical noise was sorted out, there was still the system response time to consider. The fall time of the applied pulse was measured on a chart recorder and found to be ~ 9 ns so this did not produce a problem. The response time of the system was tested by recording the decay of a red LED which should have a decay time of < 10 ns. The first modification that was made to the usual procedure for measuring decay times as was used in chapters 2 and 3 was that the input impedance of the boxcar was reduced from 100 kohms to 50 ohms. This improved the response time of the boxcar but also decreased its sensitivity. The output resistor R_L in the dynode chain of the photomultiplier tube produced a long time constant because of the RC network in the circuit. The decay of the LED was measured as 2.8 μs with the original value of R_L which was 27 kohms. The measured decay time was successively reduced as R_L was decreased until it reached 16 ns when R_L was 390 ohms and the input impedance of the boxcar was 50 ohms (an input impedance of 100 kohms gave a decay time of 53 ns). This was considered to be a reasonable value for the response time of the system. The disadvantage of having such a low value of R_L was that it greatly reduced the sensitivity of the tube. The signal level was lower than it might be because only voltages up to 200V could be applied from the pulse generator which meant that the current through the samples was lower than the maximum possible current. Because of this, the low value of R_L and the low input impedance of the boxcar, the overall system sensitivity had been greatly

reduced. This meant that a signal which would normally have been easy to detect could only be detected by applying a very high tube voltage which led to very noisy decay curve traces. Unfortunately, in order to preserve the fast system response time the time constant on the boxcar which could be used to reduce the noise on a signal had to be kept at its minimum value.

Initially it was hoped that the wavelength dependence of the decay of the ZnS:RE samples could be determined using a monochromator but the signal level was too low to do this. Instead, the wavelength dependence was determined by placing filters in front of the sample. Wratten and interference filters with a 10 nm passband were used in measuring the decay of the ZnS:Sm,Li sample. The low light intensity from ZnS:Tb sample E meant that only Wratten filters could be used. The decay of ZnS:Tb sample D and the ZnS:Eu,Li sample were not studied in detail.

4.5 Measurement of the quantum efficiency.

The experiment was set-up as described in section 4.2 but an ammeter was placed in series with the sample to measure the current through the sample. The light output from the sample was measured for a given wavelength on the photometer with an integration time of 20 seconds (again the background signal at this wavelength was subtracted from the measured signal). The current through the sample was also measured and the relative quantum efficiency which is proportional to the light output/current was determined as a function of the applied voltage for any desired wavelength.

RESULTS.

4.6 Calibration of the system.

The flux of photons (i.e. the number of photons per unit area per unit time) emitted from a black body source in an energy interval δE is $N(E)\,\delta E$. The power in this flux is $h\nu\, N(E)\,\delta E$.

The power in the interval $\delta\lambda$ from a black body source is given theoretically by $W(\lambda)\delta\lambda$, where by Planck's radiation law,

$$W(\lambda) = \frac{2c^2h}{\lambda^5[\exp(hc/\lambda kT)-1]}. \qquad (4.1)$$

We have then that

$$W(\lambda)\delta\lambda = h\nu\, N(E)\,\delta E \qquad (4.2)$$

i.e.

$$N(E) = \frac{W(\lambda)\,\delta\lambda}{h\nu\quad\delta E} \qquad (4.3)$$

$$= \frac{W(\lambda)\lambda^2}{h\nu\quad hc} \qquad (4.4)$$

$$\text{i.e.}\quad N(E) \propto \lambda^3 W(\lambda) \qquad (4.5)$$

When the black body spectrum is recorded with the experimental system we measure

$$L_1 = CN(E) \qquad (4.6)$$

where C is the calibration coefficient for the system. When the

spectrum of a sample is recorded we measure

$$L_2 = CN'(E) \qquad (4.7)$$

where N'(E) is the number of photons emitted by the sample per unit area per unit time at that wavelength. Substituting in the value of C from eq.(4.6) and substituting for N(E) using (4.5), we have that

$$N'(E) \propto L_2 \frac{\lambda^3 W(\lambda).}{L_1} \qquad (4.8)$$

The calibration coefficient for the sample is therefore $\lambda^3 W(\lambda)/L_1$. This was plotted as a function of wavelength for the Zeiss and Rank-Hilger monochromators in fig.(4.1).

4.7 The emission spectra.

The emission spectra were calibrated using the calibration curves in fig.(4.1) and the results shown here are the calibrated results.

The emission spectra of the ZnS:Sm,Li sample are shown in fig.(4.2) for applied voltages of 140V, 180V and 220V. It can be seen that there is little change in the shape of the spectra with voltage. The spectrum of the sample consists of a broad band similar to that observed by Turvey and Allen in a ZnSe Schottky diode [42] which was attributed to intervalley transitions in the conduction band.

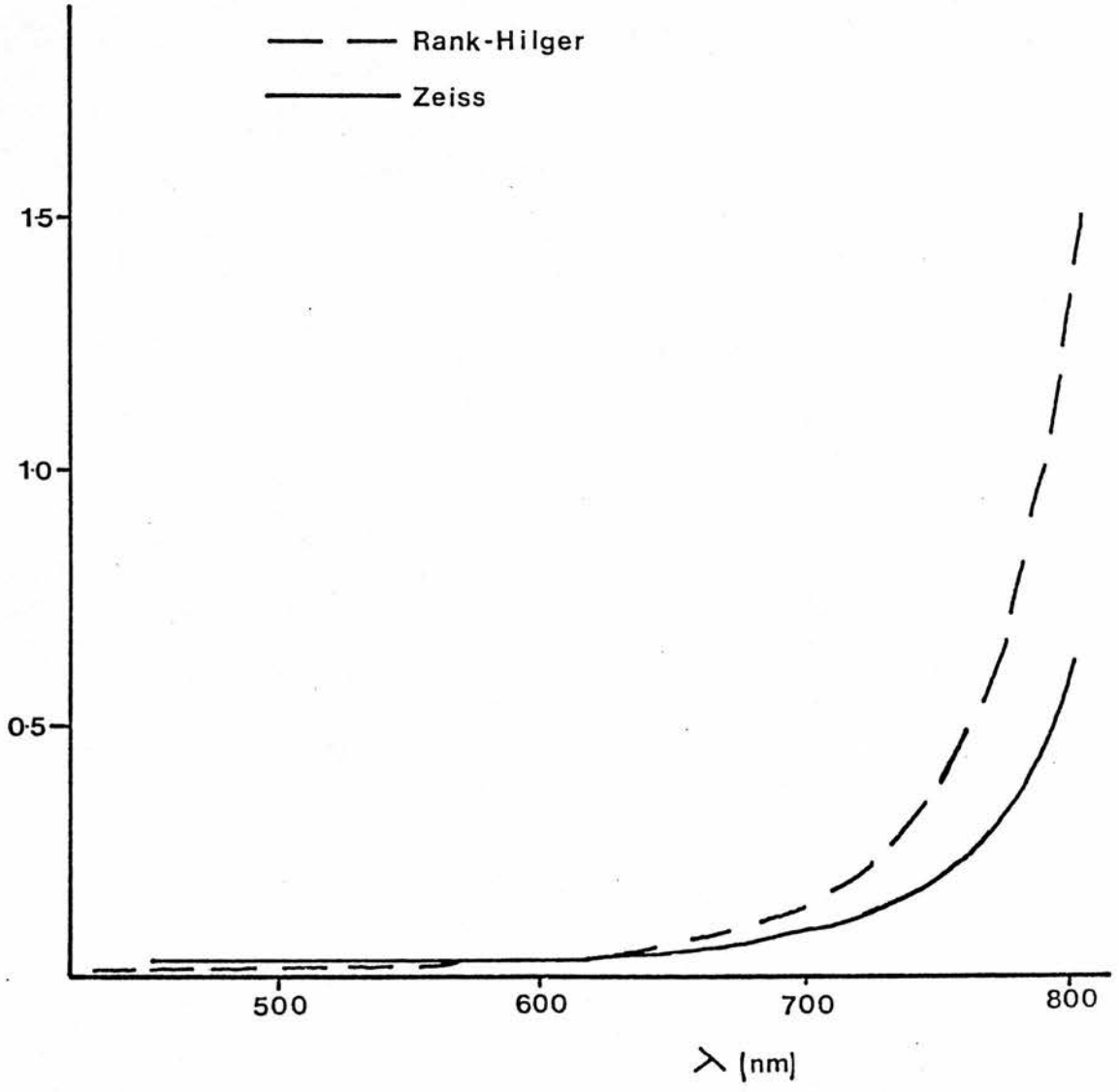

Fig.(4.1)

Calibration curve for the Hamamatsu R955 tube with the Zeiss SPM2 and Rank-Hilger D330 monochromators.

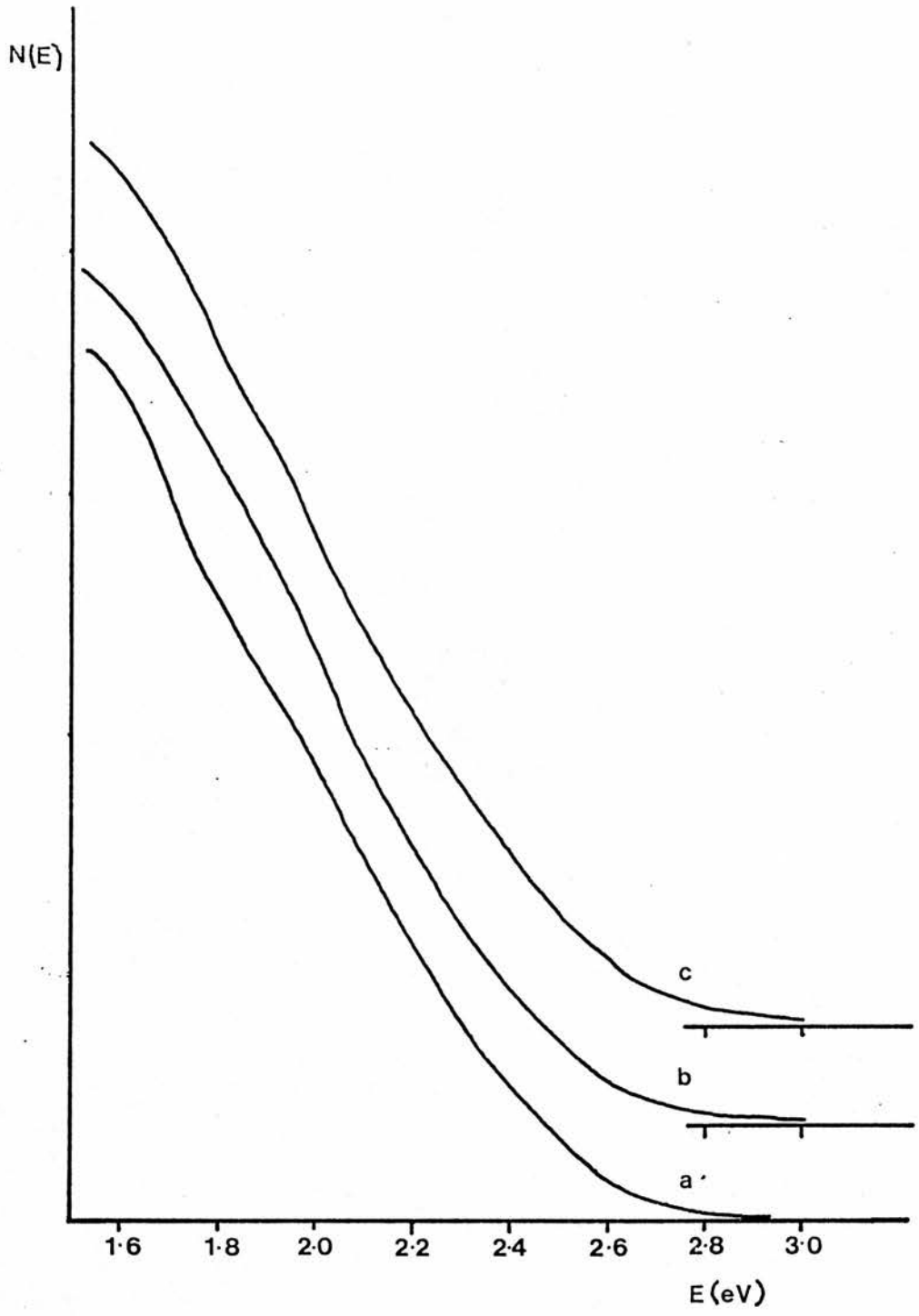

Fig.(4.2)

The calibrated EL emission spectra in terms of the relative photon flux per unit energy range of the ZnS:Sm sample at a)220V b)180V c)140V.

The spectra of ZnS:Tb samples D and E and the ZnS:Eu,Li sample are shown in figs.(4.3) to (4.5). They have the same broad shape as the ZnS:Sm,Li sample but in addition there is a green band similar to that seen in photoluminescence spectra [46] of varying strength. The spectra of each sample taken with an applied voltage of 180V were plotted on the same graph as shown in fig.(4.6) where the different relative intensities of the green band can be clearly seen.

When the resolution of the experiment was increased over the regions where $4f^n$ spectral lines were expected, no $4f^n$ spectral lines were observed above the noise background.

4.8 Decay times of the ZnS:RE samples.

The work in this section concentrated on the decay of the ZnS:Sm,Li and ZnS:Tb (E) samples.

4.8.1 Decay of the ZnS:Sm,Li sample.

The decay of the ZnS:Sm,Li sample with a Wratten 29 filter is shown in fig.(4.7). The decay consists of two parts, a very fast decay which has a decay time of <16 ns, the response time of the system, and a slower component which has a decay time of ~84 ns. The fast decay is indicative of intervalley transitions in the conduction band as was also indicated by the shape of the spectrum.

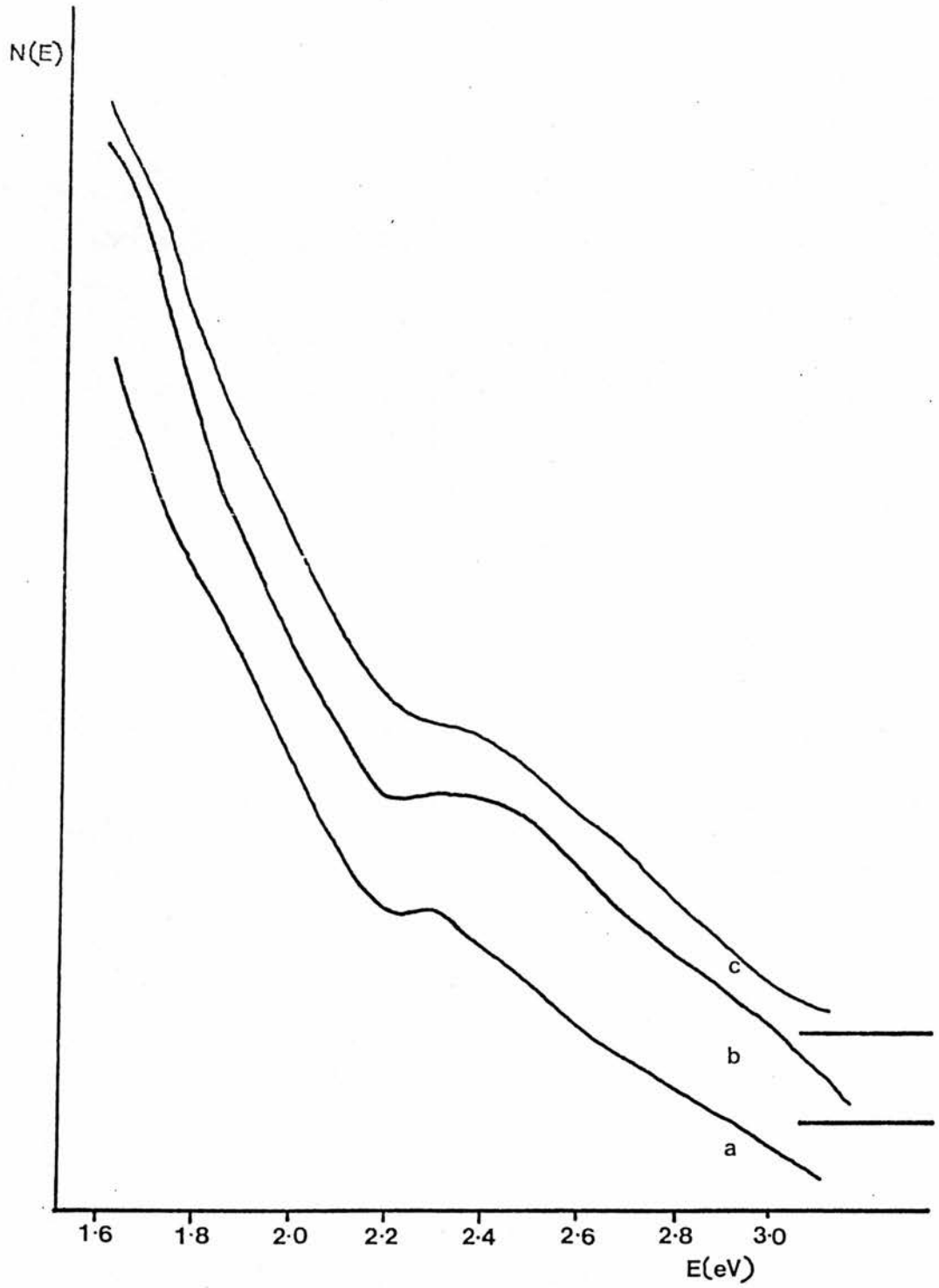

Fig.(4.3)

The calibrated EL emission spectra in terms of the relative photon flux per unit energy range of ZnS:Tb sample E at a)220V b)180V c)140V.

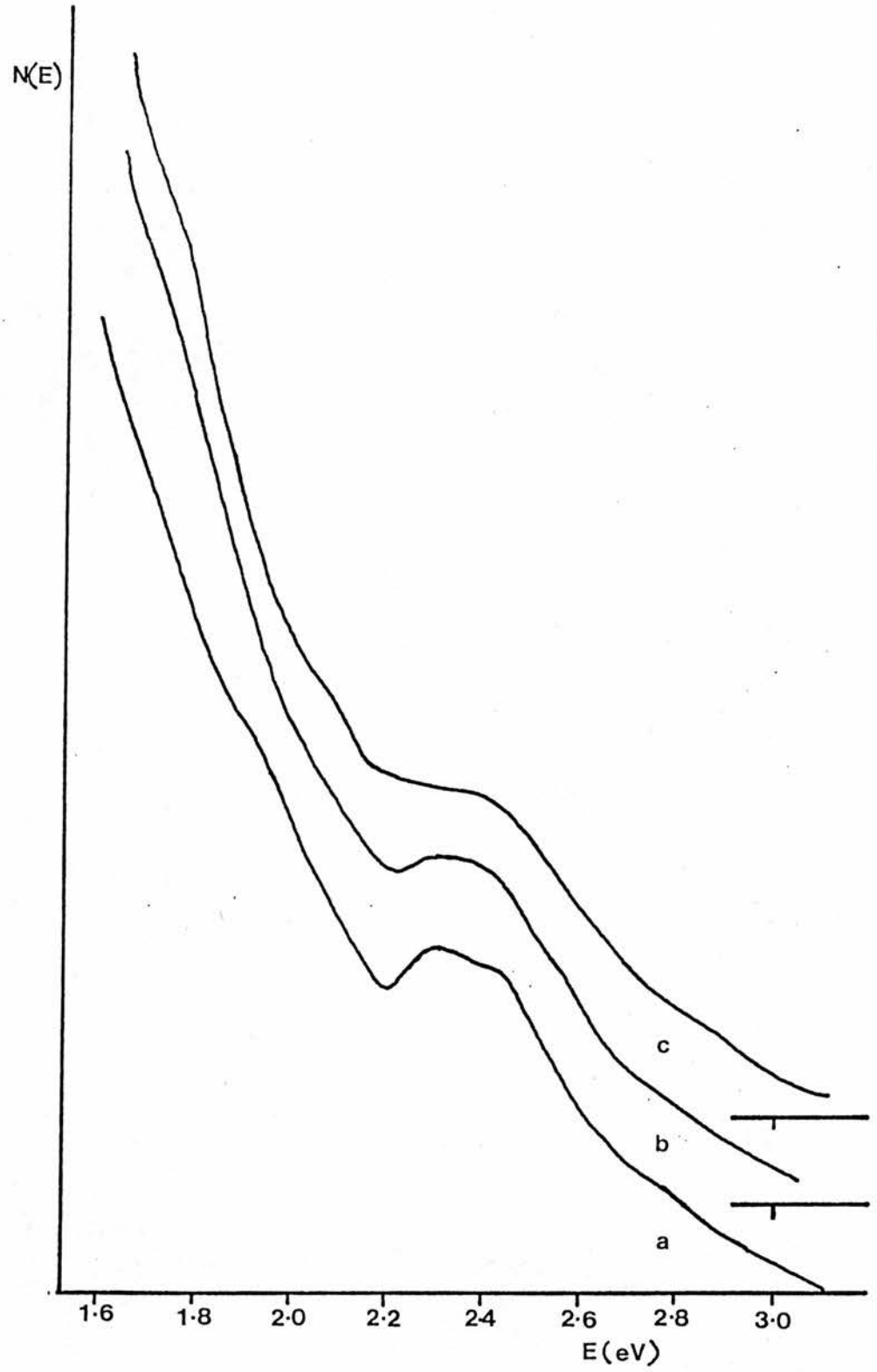

Fig.(4.4)

The calibrated EL emission spectra in terms of the relative photon fluxper unit energy range of ZnS:Tb sample D at a)250V b)220V c)180V.

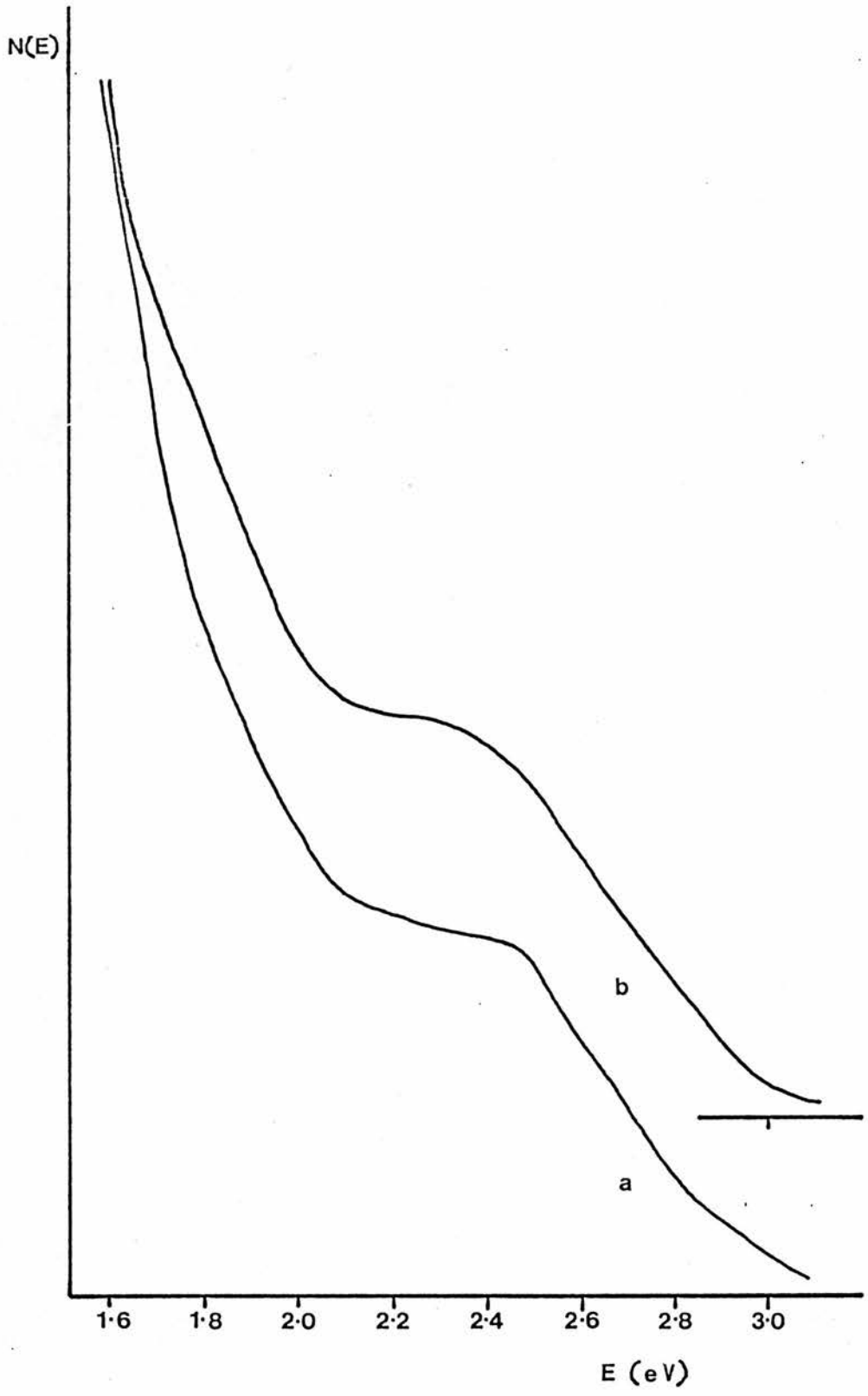

Fig.(4.5)

The calibrated EL emission spectra in terms of the relative photon flux per unit energy range of the ZnS:Eu sample at a)220V b)180V.

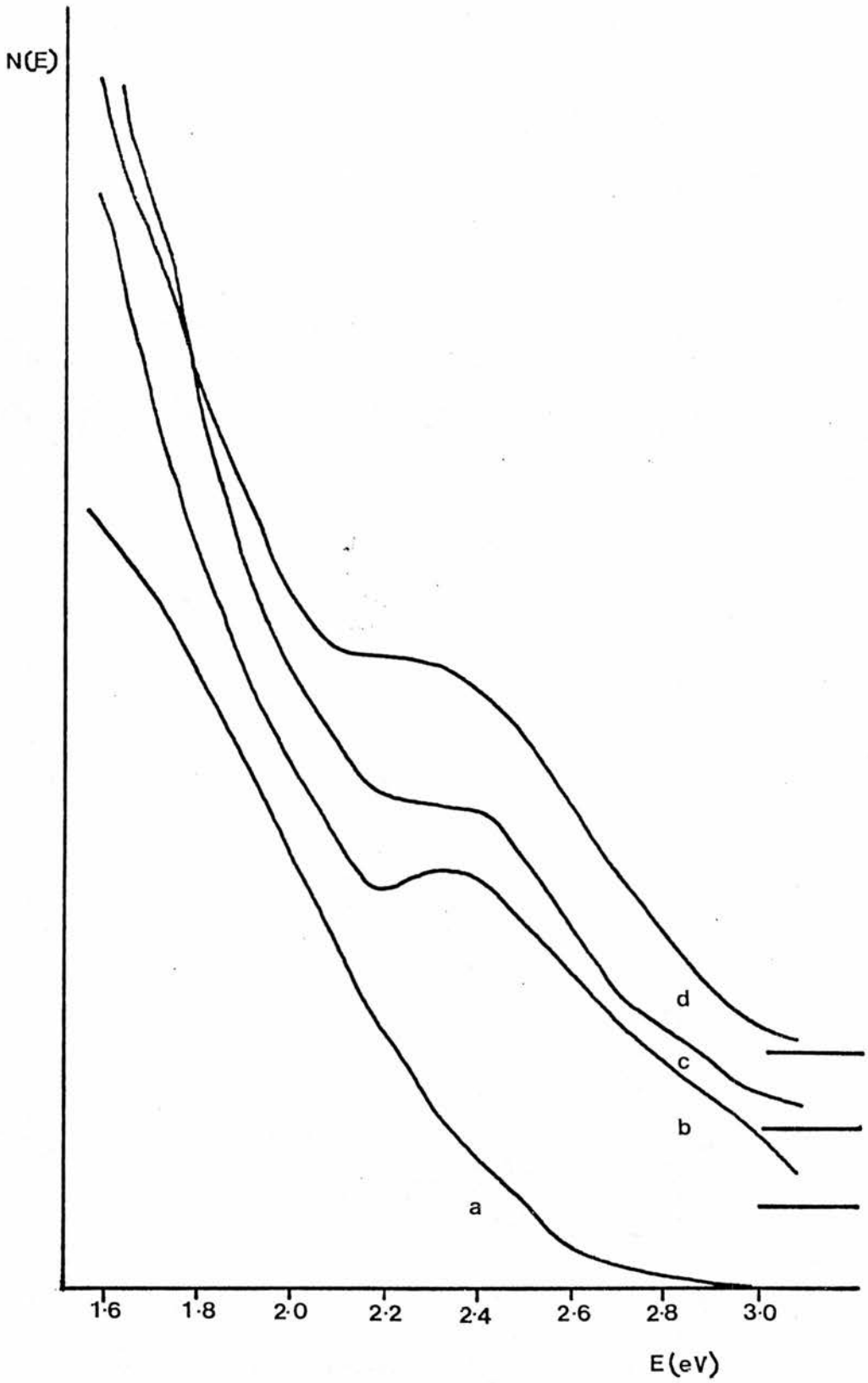

Fig.(4.6)

The calibrated EL emission spectra in terms of the relative photon flux per unit energy range of a)ZnS:Sm, b)ZnS:Tb sample E, c)ZnS:Tb sample D and d)ZnS:Eu at 180V.

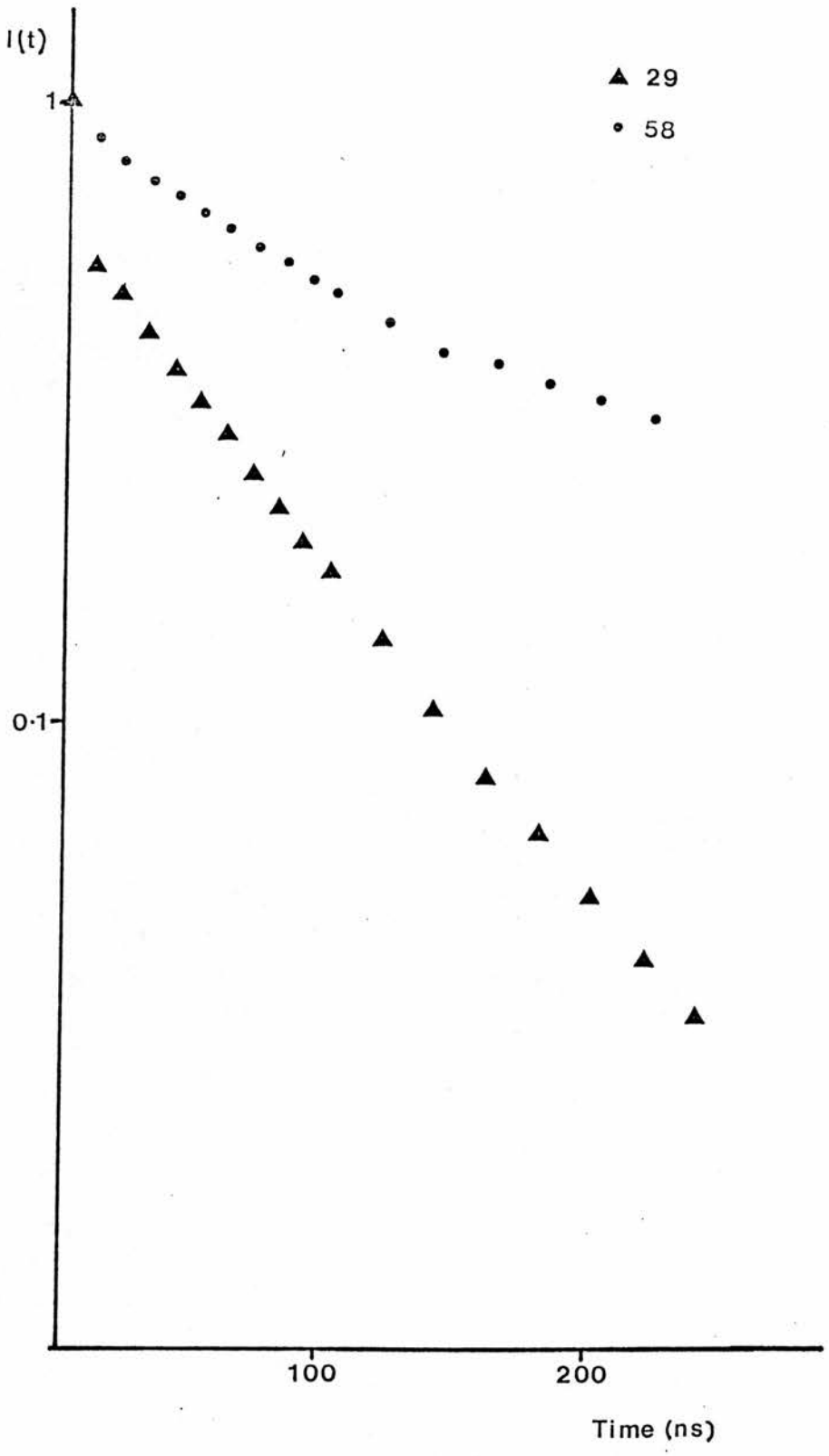

Fig.(4.7)

The decay of ZnS:Sm with Wratten 29 and 58 filters.

When a Wratten 58 filter was used the shape of the decay changed dramatically as is shown in fig.(4.7). Here, over the same time scale used for the ZnS:Sm,Li sample the very fast decay seems to be masked by a slower decay of decay time ~ 150 ns. The time base on the boxcar was lengthened to 10 μs and the resulting decay is shown in fig.(4.8). The decay consists of two parts, one part having a decay time of ~ 150 ns as was also shown in more detail on the previous graph and the other part having a much longer decay time of ~ 2.8 μs.

When a Wratten 75 filter was used the decay was again in two parts as is shown in fig.(4.8). The faster decay again had a decay time of ~ 150 ns, but the longer decay was slightly faster with a decay of ~ 2.0 μs. Similar results were obtained using Wratten 16 and 38 filters. The relative intensity of the slower component was not as great with the 75, 38 and 16 filters as it was with the 58 filter. Finally, a Wratten 47B filter was used and again the decay consisted of two parts, the fast part having a decay of ~ 145 ns and the weak slower component having a decay time of ~ 1.25 μs. The transmission curves of the Wratten filters are shown in fig.(4.9).

In order to determine the spectral variation of the decay time more accurately interference filters were used which had a passband of 10 nm. Firstly, interference filters with passbands between 500nm and 540 nm were used in order to isolate the 2.8 μs decay which was measured with the Wratten 58 filter. The resulting decays are shown in fig.(4.10). As with the 58 filter the decay consisted of two parts with decay times of 150 ns and

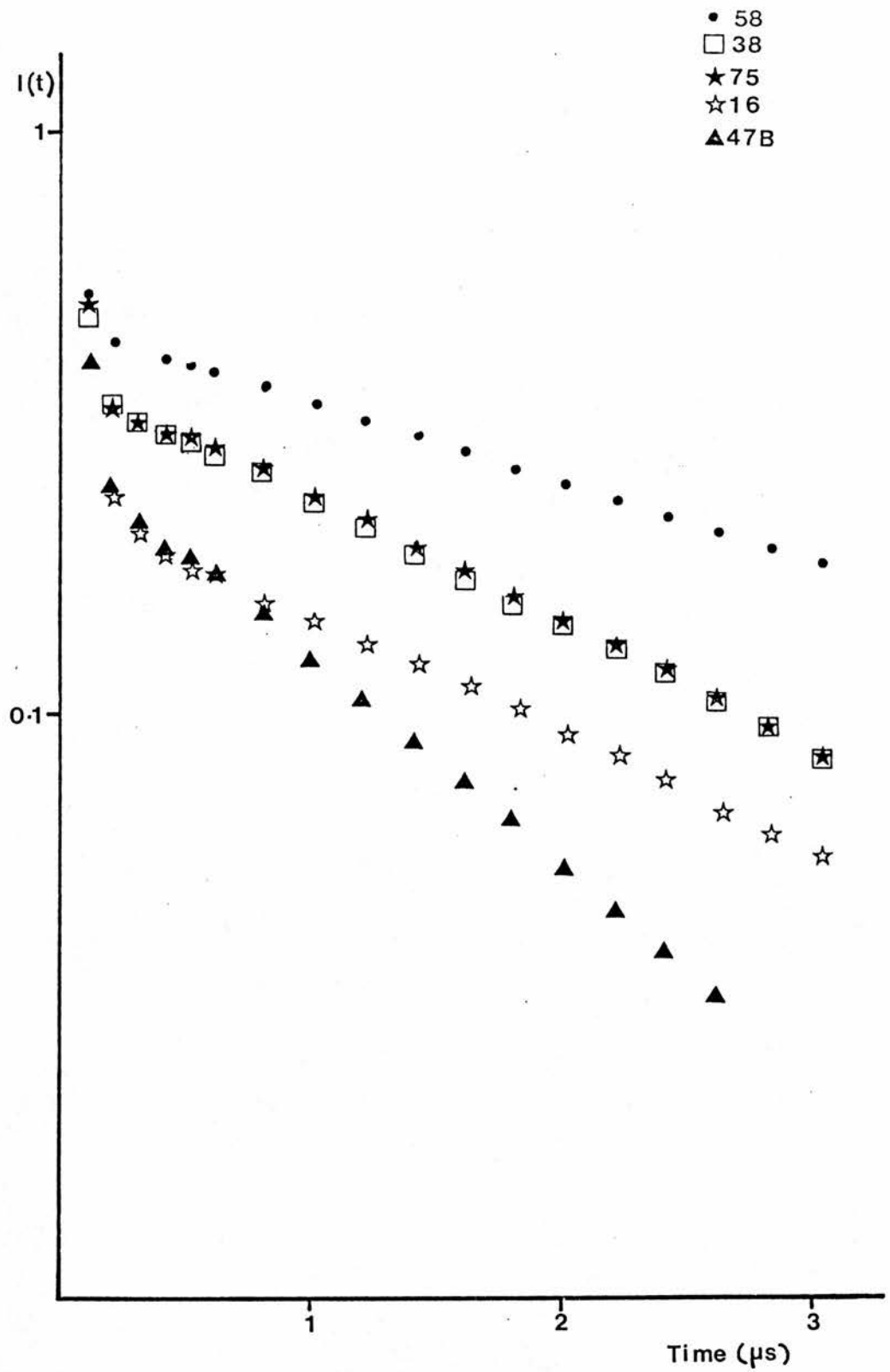

Fig.(4.8)

The decay of ZnS:Sm with 58, 16, 75, 38 and 47B Wratten filters.

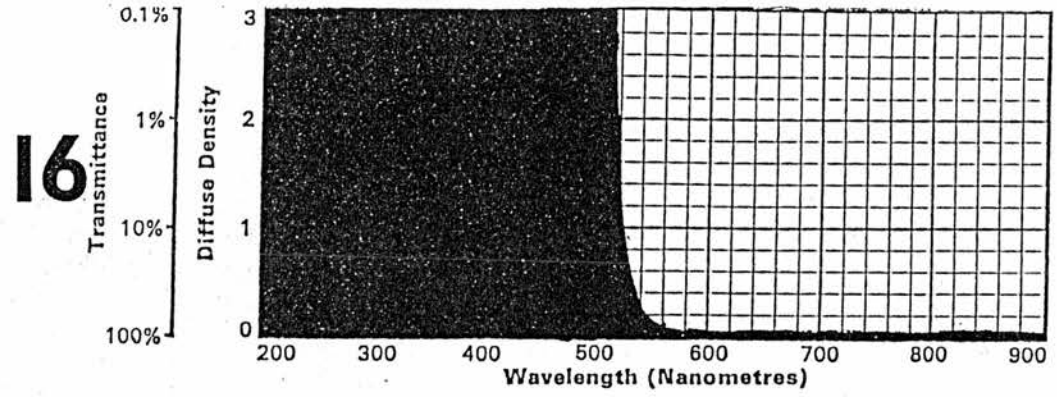

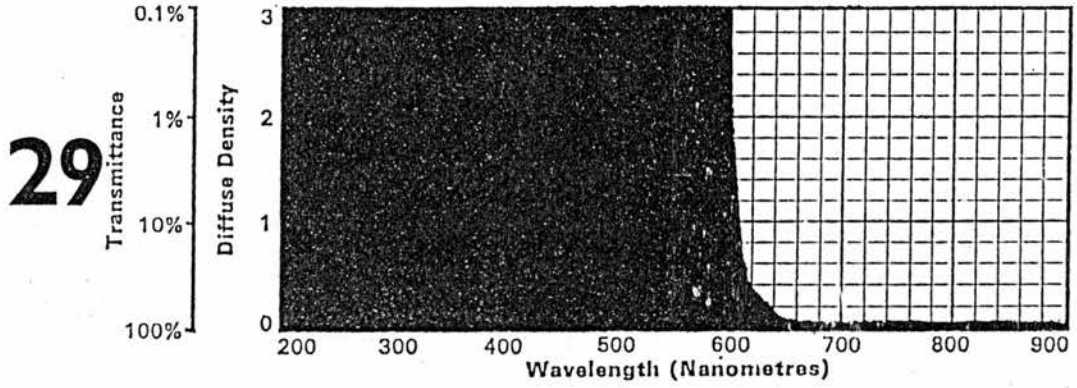

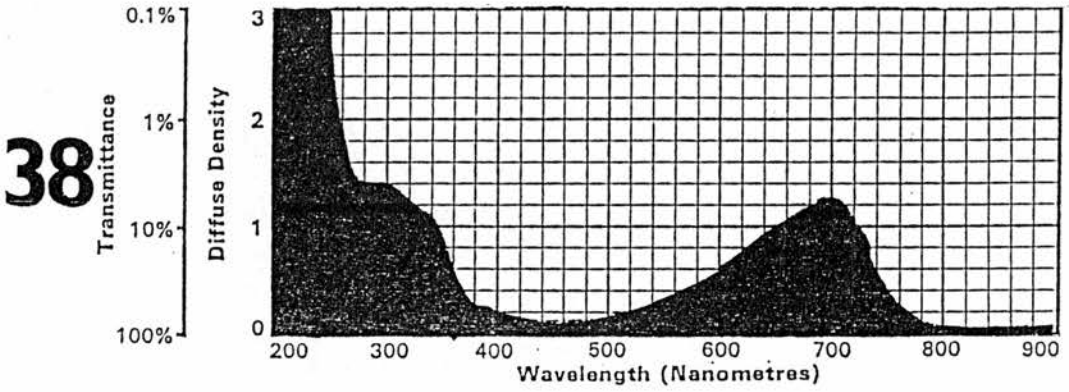

Fig.(4.9)

The transmission curves of the Wratten filters

used in the experiments.

47B

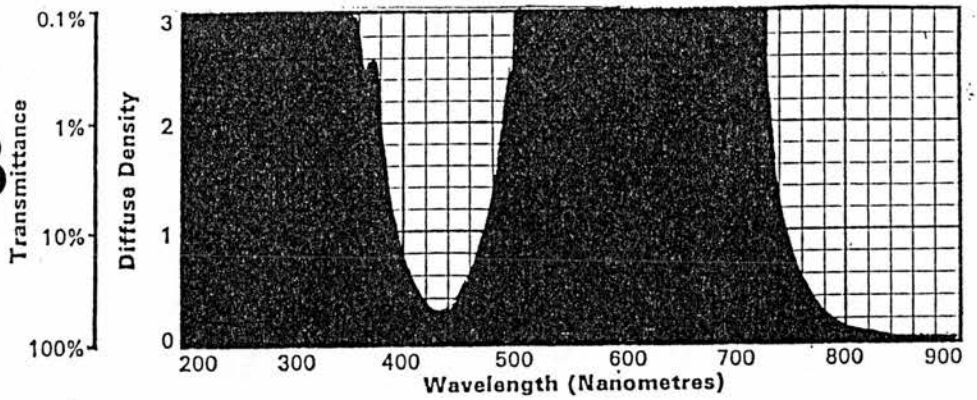
0.1%
1%
10%
100%
Transmittance
Diffuse Density
3
2
1
0
200
300
400
500
600
700
800
900
Wavelength (Nanometres)

58

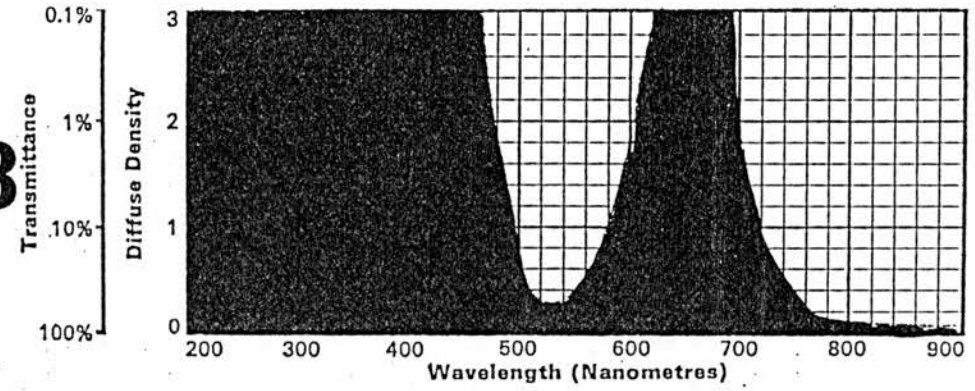
0.1%
1%
10%
100%
Transmittance
Diffuse Density
3
2
1
0
200
300
400
500
600
700
800
900
Wavelength (Nanometres)

75

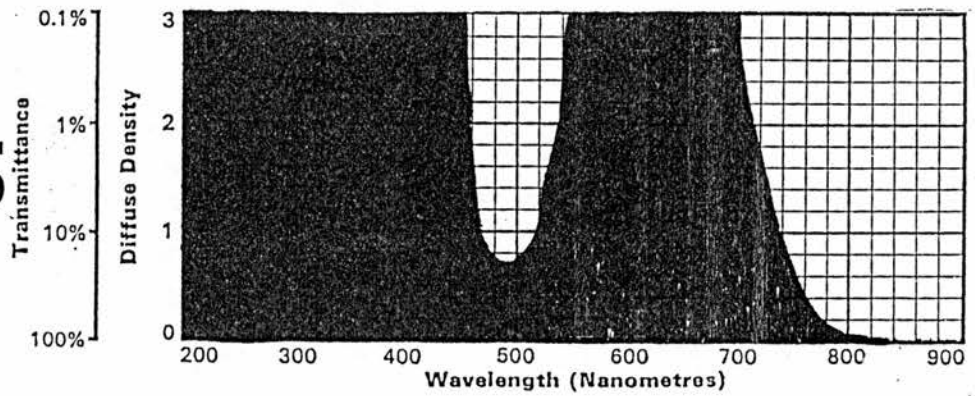
0.1%
1%
10%
100%
Transmittance
Diffuse Density
3
2
1
0
200
300
400
500
600
700
800
900
Wavelength (Nanometres)

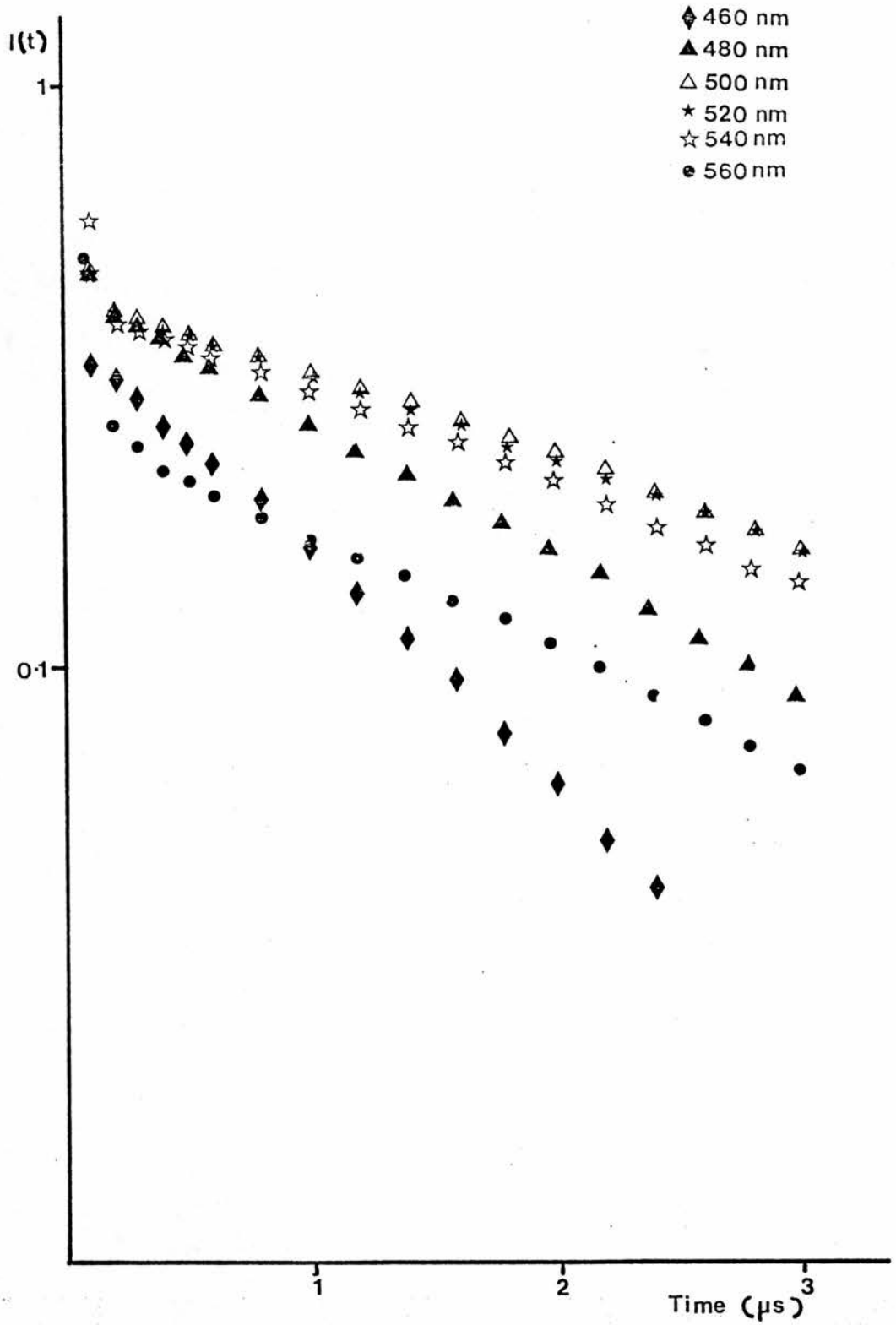

Fig.(4.10)

Decay of ZnS:Sm with several interference filters.

2.8 μs. The relative intensity of the slow decay was about the same for each of the filters used. This implies that the band peaks at 520 nm and is fairly broad.

When 480 nm and 560 nm filters were used the decay was similar to that found with the Wratten 75, 38 and 16 filters, the decay times being ~ 150 ns and 2.0 μs. With a 460 nm filter the decay is similar to that obtained with the Wratten 47B filter with the two parts of the decay having decay times of 100 ns and 1.2 μs.

It should be noted that as the width of the applied pulse was 5 μs, then if there are any centres present in the material with a decay time >>5 μs their decay will not be detected as the centres will not be sufficiently excited by the applied pulse. In order to detect any previously unobserved long decays the time-base on the boxcar was increased. The resulting decays taken without a filter are shown in fig.(4.11) as the applied pulse width is increased from 10 μs to the maximum possible value of 100 μs. A decay with lifetime ~ 20 μs was observed the relative intensity of which increased with increasing applied pulse width, though the intensity was still weak at the maximum applied pulse width of 100 μs. The spectral variation of the long decay with an applied pulse width of 100 μs was examined using filters, though as the applied pulse frequency had to be reduced to 50 Hz the noise on the signal increased so only the more efficient filters could be used. When Wratten 29 and 47B filters were used the long decay was not observed. However, when a Wratten 58 filter was used the long decay was observed with a decay time of ~ 20 μs and an increased relative intensity as

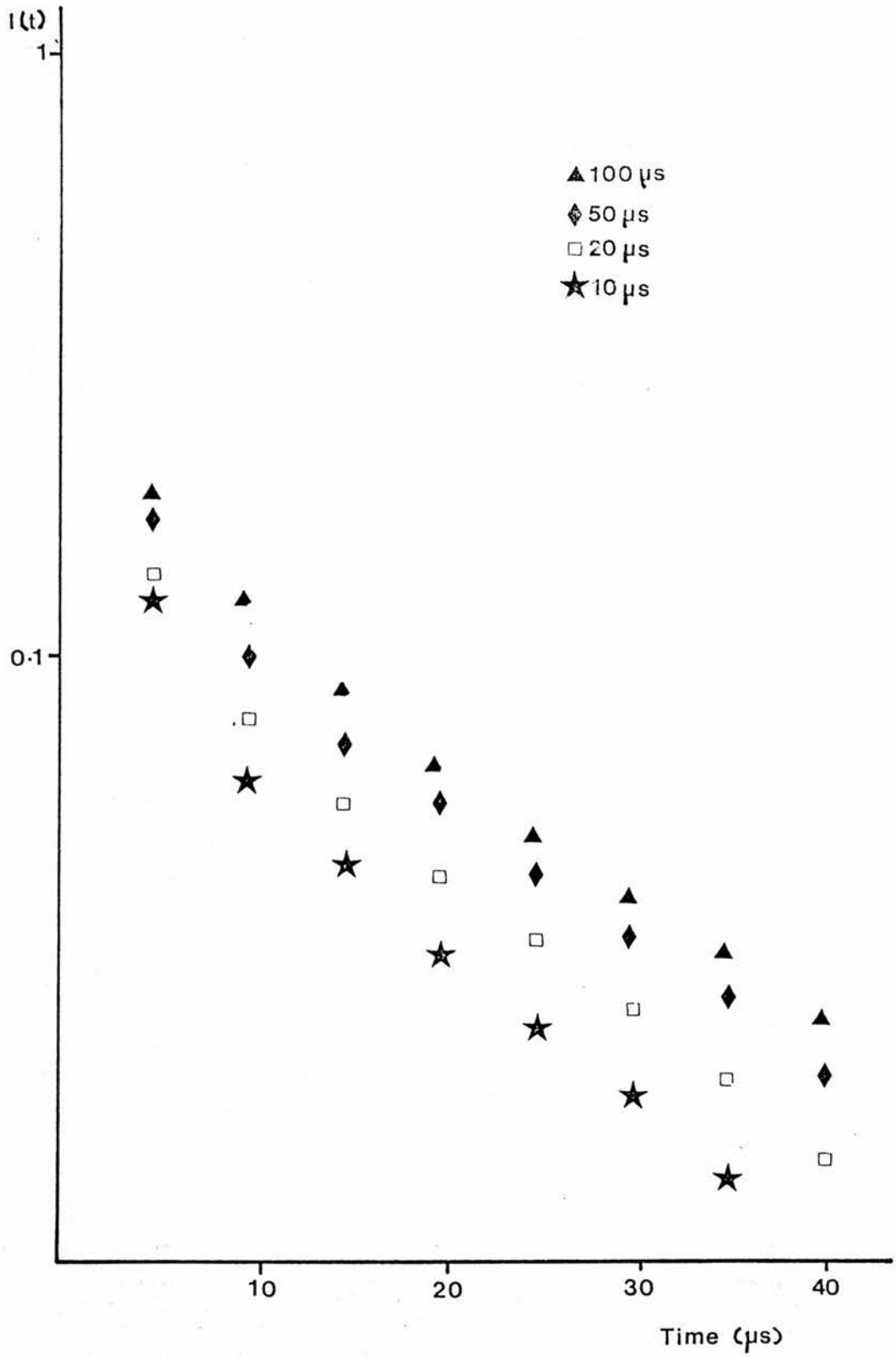

Fig.(4.11)

Decay of ZnS:Sm for several applied pulse widths.

shown in fig.(4.12). This implies that the long decay peaks somewhere in the green.

The decay of the ZnS:Sm,Li sample has different rates in different parts of the spectrum. There are components in the green with decay times of 2.8 μs and 20 μs. There is a component at 460 nm with a decay time of ~ 1.2 μs and one below 600 nm with a decay time of ~ 84 ns. There is also a broad band from approximately 480 nm to 600 nm with a decay time of 2.0 μs. There are therefore at least four electroluminescent emission bands in addition to the broad band due to the inter-band transitions.

4.8.2 Decay of ZnS:Tb sample E.

The signal produced by this sample was less than that from the ZnS:Sm,Li sample so it was only possible to examine the spectral variation of the decay time with Wratten filters. The decay of the sample with a Wratten 29 filter is shown in fig.(4.13). The decay consists of two parts, a very fast decay with a decay time of < 16 ns and a slower component with decay time ~ 76 ns. The decay is very similar to that of the ZnS:Sm,Li sample with the same filter.

The decay of the sample was measured with a Wratten 58 filter and the results are shown in figs.(4.13) and (4.14). The decay consists of three components, one with a very fast decay time of ~ 20 ns, one with a decay time of ~ 165 ns and the other with a decay time of 285 ns. Similar results were obtained using a Wratten 16 filter where the three decay times are 20 ns, 120 ns

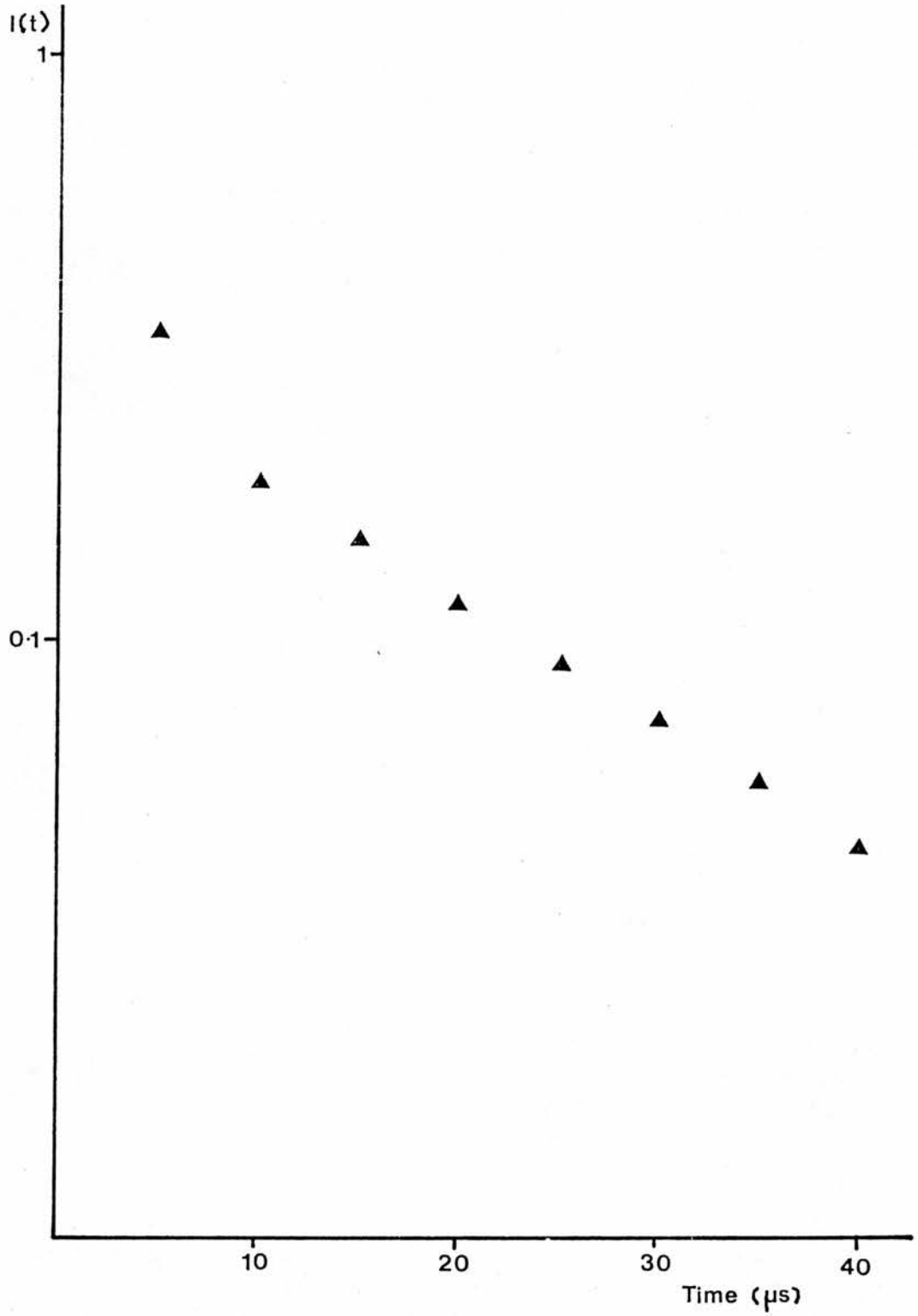

Fig.(4.12)

Decay of ZnS:Sm with a Wratten 58 filter and an applied pulse width of 100 us.

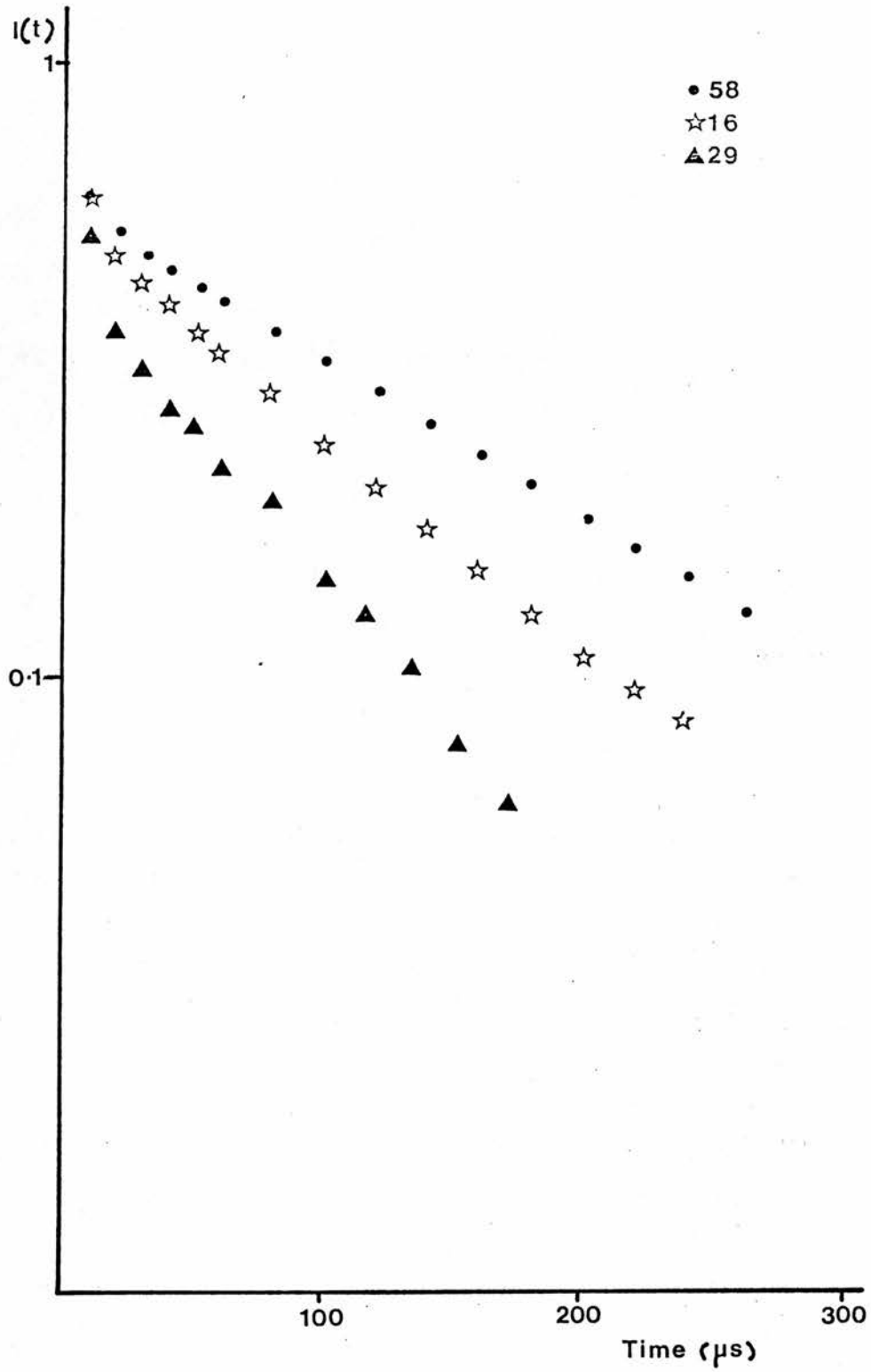

Fig.(4.13)

Decay of ZnS:Tb sample E with 29, 58 and 16

Wratten filters.

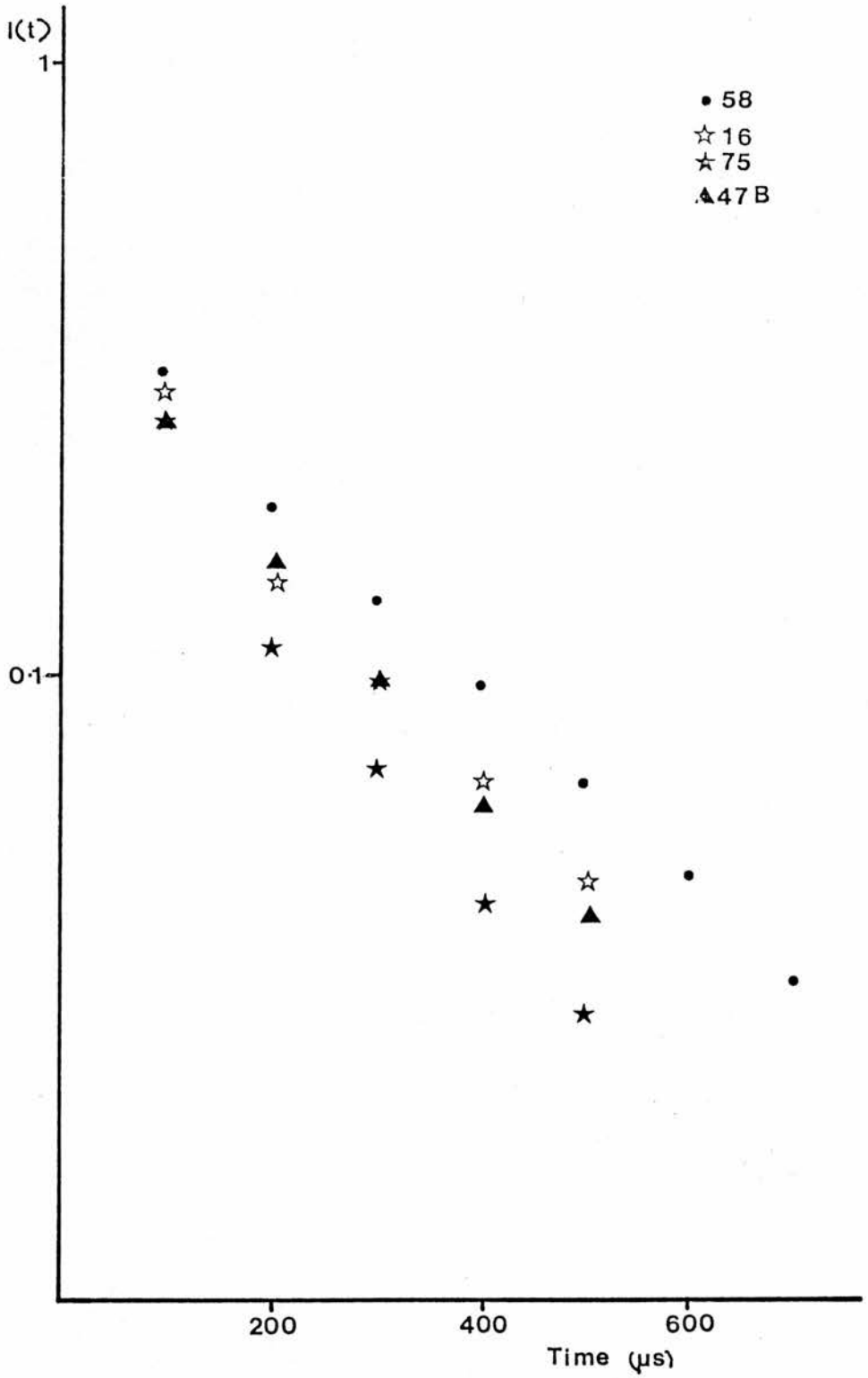

Fig.(4.14)

Decay of ZnS:Tb sample E with 58, 16, 75 and 47B Wratten filters.

and 265 ns. Results using 75 and 47B filters were difficult to take and the decay time could only be recorded using a timebase on the boxcar of 5 μs. The results give a long decay in both cases with a decay time of ~ 220 ns.

The decay was then recorded using a timebase of 50 μs on the boxcar to look for any long decay components. The resulting decay for an applied pulse width of 100 μs and without any filters is shown in fig.(4.15). The figure shows that there is a longer decay component with a decay time of ~8.7 μs. Because of the low signal level it was not possible to record the decay very accurately when filters were used at this pulse width. It was possible however, to see that the long decay disappeared completely when a Wratten 23A filter was used. This implies that the peak of the long decay must be < 570 nm.

It was not possible to make any firm conclusions about the electroluminescent emission bands in this sample. The decay does not seem to change greatly when different filters are used. Also, the time range over which the decay is exponential seems very short, i.e. for the results taken with the Wratten 58 filter the decay is exponential between 30 μs and 270 μs and then between 200 μs and 600 μs.. This implies that the decay could be non-exponential. Another point to note is the similarity of the of the decay of both samples when a Wratten 29 filter is used. The decay in this region of the spectrum does not seem to depend on the rare-earth dopant but may be a property of the ZnS host lattice.

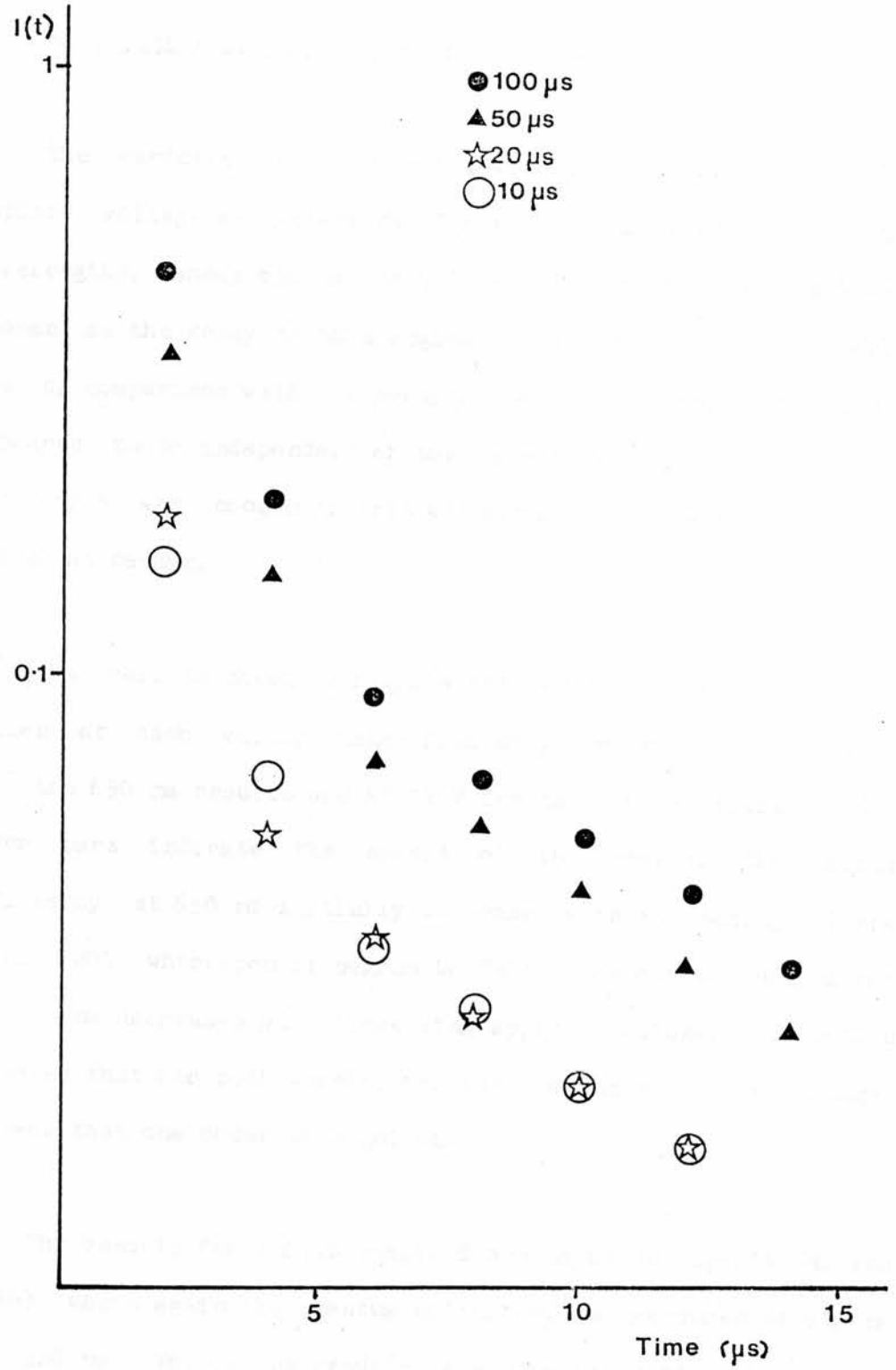

Fig.(4.15)

Decay of ZnS:Tb sample E for several applied pulse widths.

4.9 The relative quantum efficiency results.

The variation of the relative quantum efficiency with applied voltage was determined for the ZnS:Sm,Li sample at two wavelengths, namely 650 nm and 520 nm. The 650 nm wavelength was chosen as the decay in this region contained no slow components and by comparison with the results for ZnS:Tb sample E the decay appeared to be independent of the rare-earth dopant. The 520 nm wavelength was chosen as this was around the peak of the 2.8 μs and 20 μs decays.

The results shown in figs.(4.16) and (4.17) are the average values at each voltage taken from many runs normalised at 160V for the 650 nm results and at 140V for the 520 nm results. The error bars indicate the spread of the results. The quantum efficiency at 650 nm initially increases with increasing voltage until 180V whereupon it begins to fall. The quantum efficiency at 520 nm decreases with increasing applied voltage. It should be noted that for both wavelengths the quantum efficiency changes by less than one order of magnitude.

The results for ZnS:Tb sample E are shown in figs.(4.18) and (4.19) where again the quantum efficiency was measured at 650 nm and 520 nm. The 650 nm results were normalised at 210V and the 520 nm results at 110V. (The normalisation point was taken as the voltage at which the results had the least scatter). The quantum efficiency at 650 nm again peaks but this time at the higher voltage of 240V. This peak however was less easily observed because of the large scatter in the results between 250V

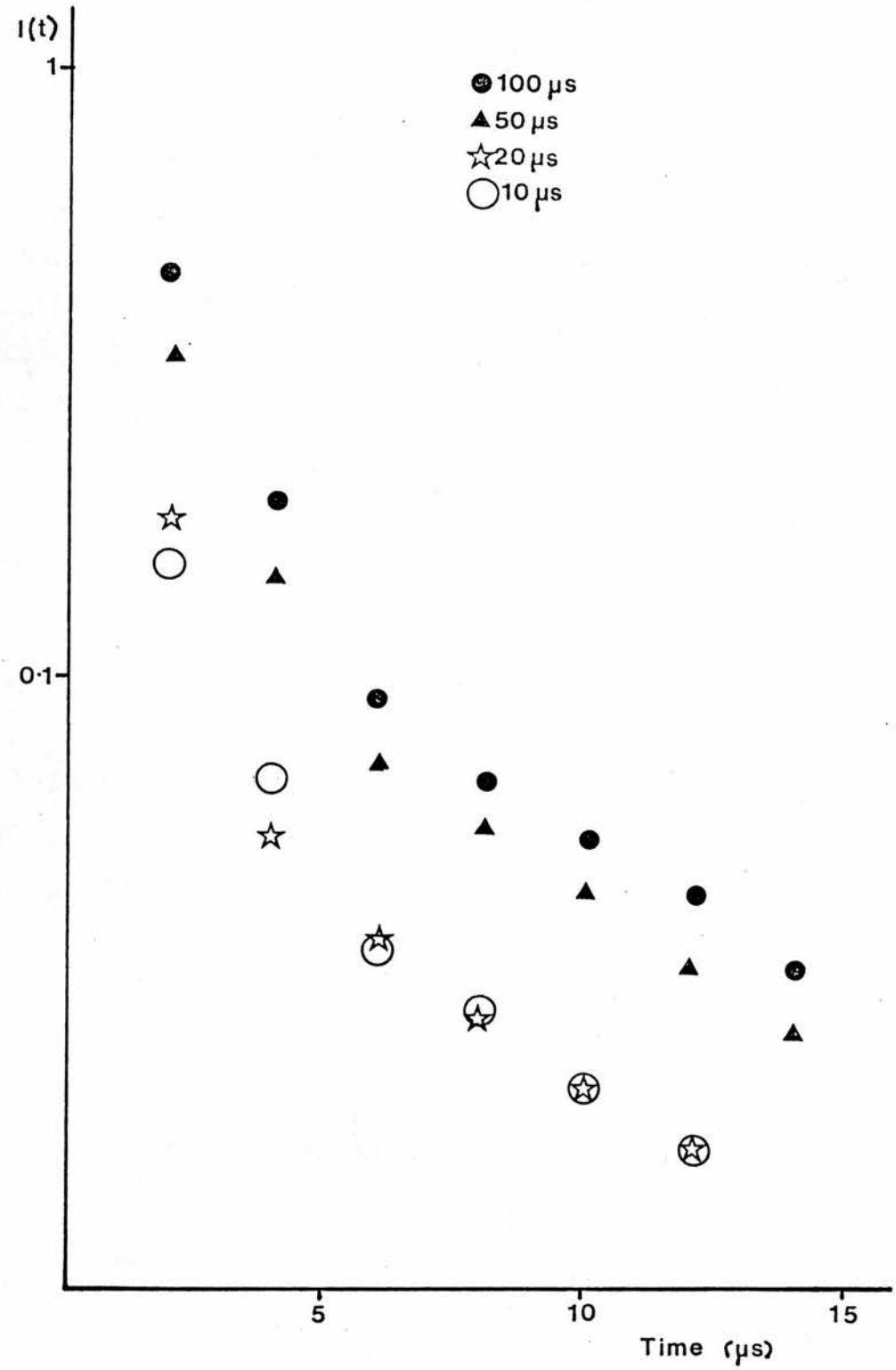

Fig.(4.15)

Decay of ZnS:Tb sample E for several applied pulse widths.

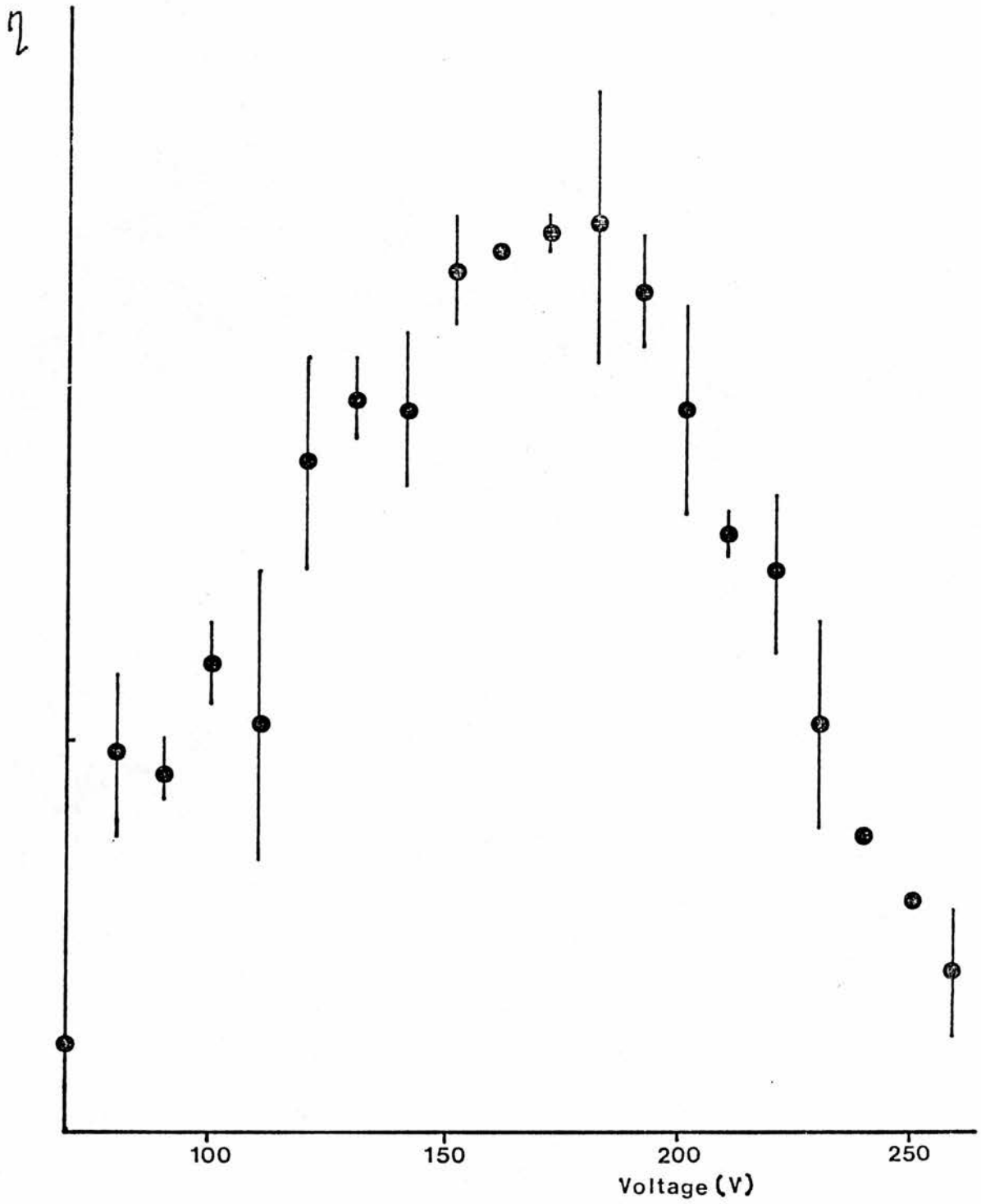

Fig.(4.16)

Variation of the relative quantum efficiency with applied voltage for the ZnS:Sm sample at 650 nm.

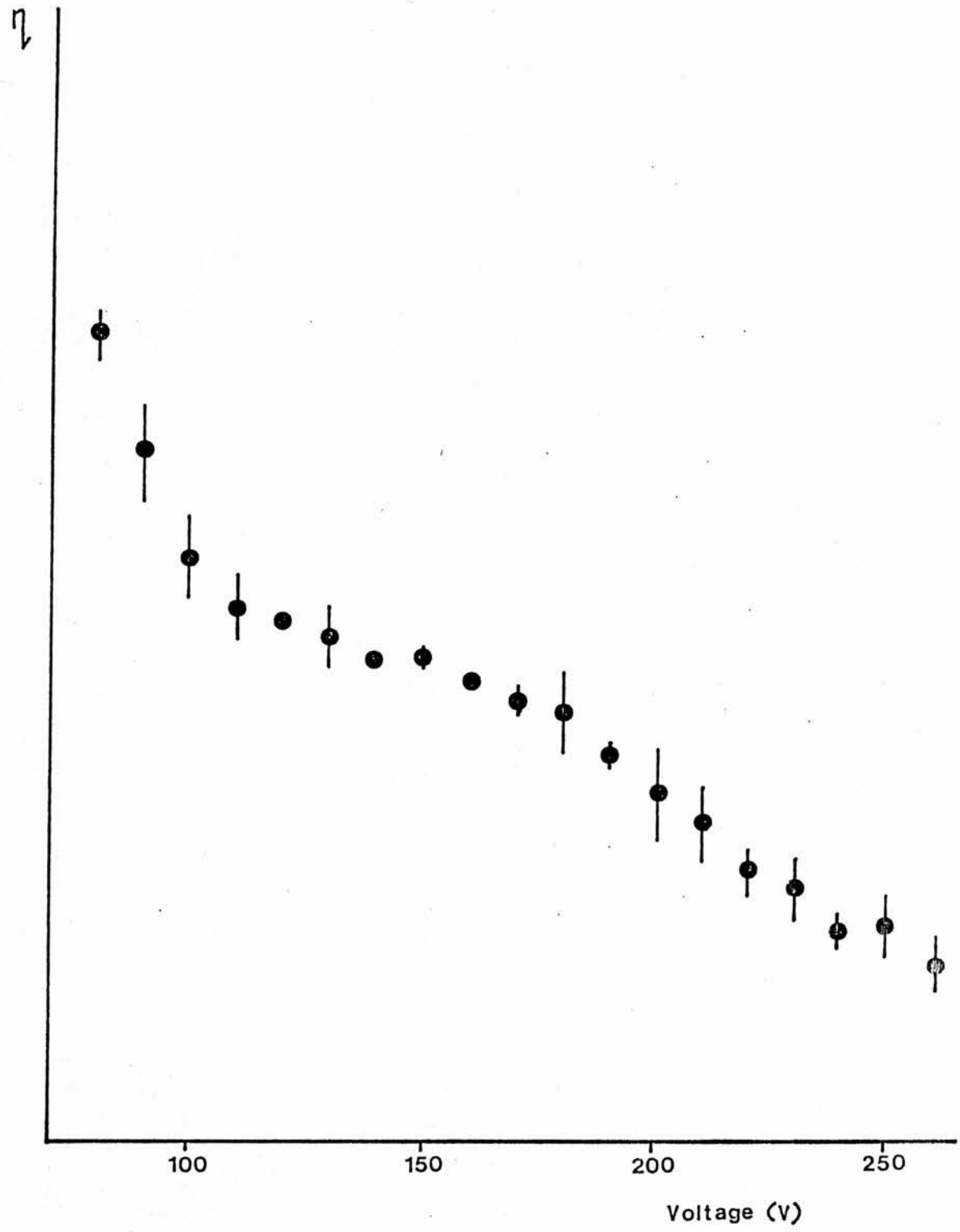

Fig.(4.17)

Variation of the relative quantum efficiency with applied voltage for the ZnS:Sm sample at 520 nm.

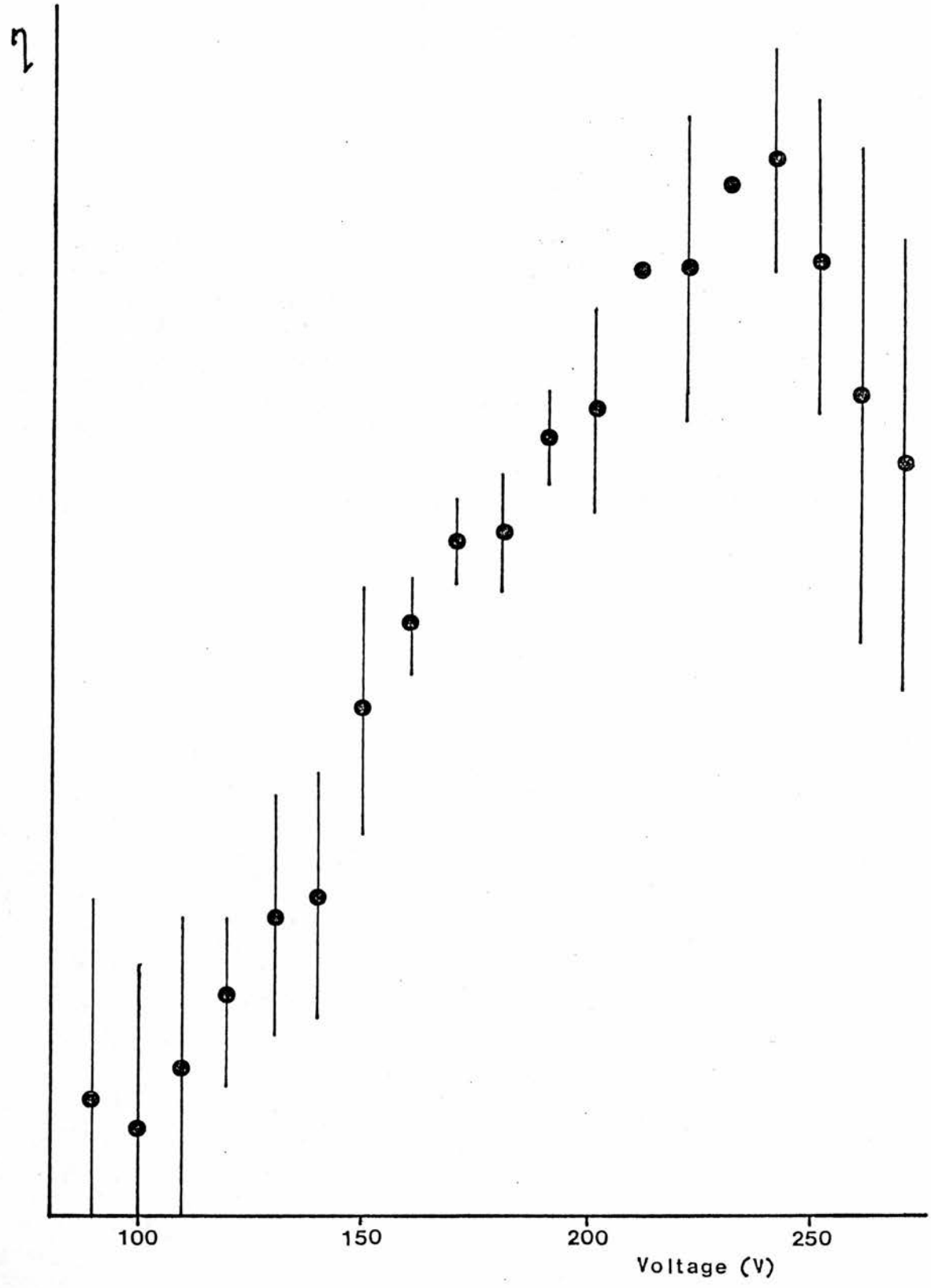

Fig.(4.18)

Variation of the relative quantum efficiency with applied voltage for ZnS:Tb sample E at 650 nm.

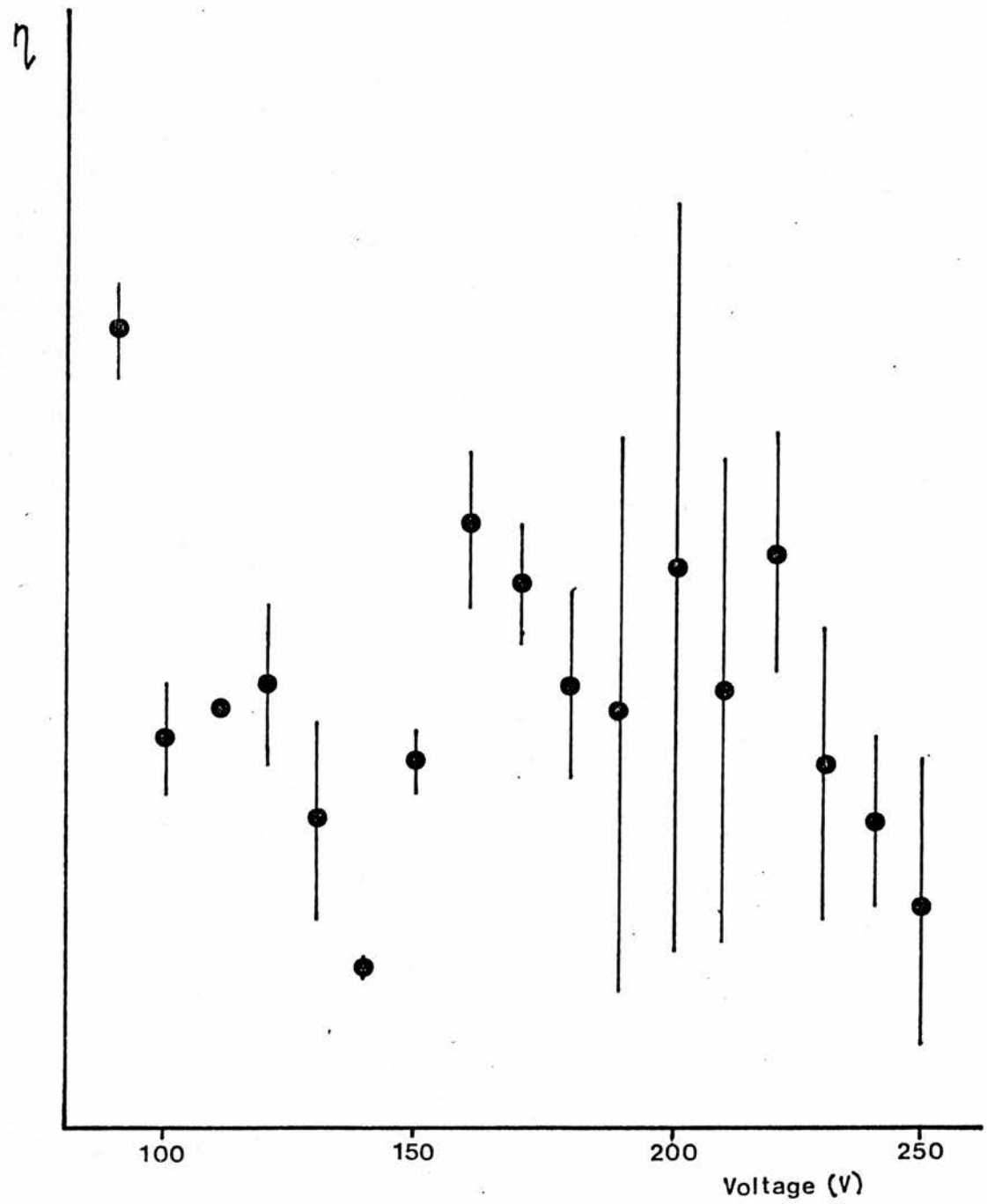

Fig.(4.19)

Variation of the relative quantum efficiency with applied voltage for ZnS:Tb sample E at 520 nm.

and 270V. Again the quantum efficiency changes over less than one order of magnitude. It is impossible to say with any accuracy how the quantum efficiency varies with voltage at 520 nm because of the large error bars involved. It is possible however, to say that there is very little change of the quantum efficiency with the applied voltage.

DISCUSSION.

The decay measurements on the ZnS:Sm sample show that there are at least four emission bands in addition to the intervalley transition band. The green band is most likely to be a donor-acceptor recombination in which donors are associated with residual copper acceptors [47,48]. The decay of this donor-acceptor recombination is non-exponential as the decay time will depend on the separation of the donor-acceptor pairs. This means that both the 2.8 μs and 20 μs decays could be due to donor-acceptor recombination. The decay of ZnS:Tb sample E also appears to be non-exponential. The non-exponential decay appears to be similar over quite a large spectral range namely between 430 nm and 600 nm. However, the broad band due to donor-acceptor recombination observed in ZnS:Cu,Al phosphors by Era et al. [47] had limits of 450 nm and 620 nm at room temperature. Although the spectral variation of the long decay of lifetime ~ 8.7 μs could not be determined accurately, it is known that that the emission band which produces this decay peaks at a wavelength of < 570 nm. This would be appropriate if the decay was due to the discussed donor-acceptor recombination.

The decay of the green band is different for each rare-earth. This may be because the rare-earth is a component of the donor-acceptor pair. Because the donor-acceptor recombination has a non-exponential decay it is possible that the observed differences in the decay could be due to differences of excitation intensity or of pair concentration but as the samples were made and excited under similar conditions this is unlikely.

The broad band emissions from the ZnS:RE samples and the fast decay times recorded with the Wratten 29 filter are generally similar to the observations made by Turvey and Allen in n-type ZnSe Schottky diodes [42]. This is taken as evidence of intervalley transitions in the conduction band and shows that there are energetic electrons in the diodes with energies up to 2.8eV above the conduction band edge. Luminescence due to this type of transition will be discussed in more detail in the next chapter. No electroluminescent spectral components attributable to internal $4f^n$ transitions could be clearly resolved above the background noise level. This means that the presence simultaneously of sufficiently energetic electrons and of luminescent rare-earth centres is not sufficient to guarantee rare-earth emission. This result is expected as the impact excitation cross-section of the rare-earths was found to be very small [49]. Rare-earth emission would only be expected if there was a resonance between the energy levels of the rare-earth and the band structure of ZnS as there is in ZnS:Mn. If there was such a resonance in these rare-earth samples then the quantum efficiency against voltage plots would have a sharp peak similar to that observed in ZnS:Mn in chapter 3 of this thesis and by Neil Gordon [41]. The relative quantum efficiency against voltage plots shown in figs.(4.16) and (4.18) have very broad peaks and this therefore implies that there is not a resonance between the energy levels of the rare-earth centres and the band structure of ZnS.

In contrast to this, Bryant et al. have observed rare earth emission along with broad bands in ZnS:RE diodes [50]. The explanation of this difference lies in the method of doping the ZnS with the rare-earth. In our samples the rare-earth was introduced as described in 4.1 by firing ZnS and rare-earth in metallic form at 1250 °C in a N_2-CS_2 gas stream. Bryant's samples however, were ion implanted at 77K with a rare-earth using an ion beam energy of 20keV and a fluence rate of 1×10^{15} cm^{-2}. This method produced a lot of defects in the sample. Bryant explains his results in terms of a "defect-molecule" theory. The defect-molecules involve rare-earth ions together with damage-induced lattice defects. When the defect-molecule is excited by collisions with the hotter electrons several decay modes are possible. One of these modes is a multiphonon non-radiative decay and another is one in which the molecule is Auger de-excited to the ground state as a result of a collision with a conduction band electron at one stage of the non-radiative phonon decay. A third mode of decay is that at some stage of its decay the defect molecule may internally transfer its energy into the rare-earth ions with an efficiency determined by the corresponding transition probability between the rare-earth ion levels involved. Thus the rare-earth emission that Bryant observes is entirely due to the presence of defects which were formed by the ion implantation process.

In other ZnS:RE systems made by other techniques (i.e. thin film ACEL devices [51-54]) bright $4f^n$ electroluminescence is seen with a rare-earth concentration only an order of magnitude greater than used here. This calls into question the relative

importance of energy transfer and impact excitation of the luminescent centre. Already there is evidence for both types of excitation mechanism in the literature and these will be discussed in the following.

Krupka [25] measured the ratio of the emissions from the Tb^{3+} $^5D_3$ and $^5D_4$ levels as a function of field in ZnS:Tb thin films. The two transitions which he measured are shown schematically in fig.(4.20). He found that as the field increased the ratio of the emission from the $^5D_3$ level to the emission from the $^5D_4$ level increased. He took this as evidence of impact excitation. Krupka's data could not be explained in terms of energy transfer from one centre. The results in this chapter show that in principle more than one centre could be impact excited. If the voltage dependent efficiencies of the transferring centres differ then Krupka's results could be explained in terms of an energy transfer mechanism. Krupka considered this possibility but dismissed it on the basis of the following. He electrically excited a structure which contained an undoped ZnS layer and observed four broad bands. He then found that the relative intensities of the two high energy bands which might constitute "intermediate states" which would transfer energy to the Tb^{3+} ion did not vary as a function of applied voltage. He then repeated the procedure with a structure containing ZnS:Gd active layers to see if the introduction of a trivalent rare-earth into the ZnS gave rise to additional states. He again found that the relative intensities of the observed broad bands did not vary with the applied voltage. Hence he eliminated energy transfer from an intermediate level as a possible mechanism and concluded that the mechanism was the

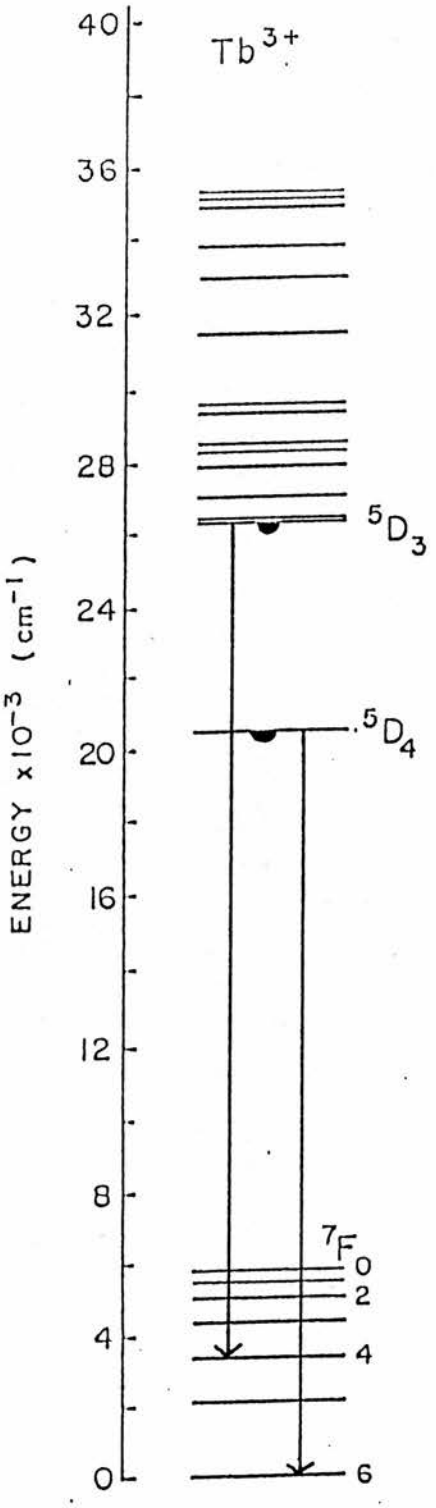

Fig.(4.20)

Energy levels of the Tb^{3+} ion.

direct impact excitation of the Tb^{3+} ion by hot electrons. However, the results in this chapter show that the broad bands are not necessarily independent of the rare-earth doping. Because of the requirement of charge compensation other centres are present in similar concentrations to that of the rare-earth and may take part in energy transfer processes. Hence Krupka's elimination of the energy transfer mechanism would only have been valid if he had measured the voltage dependence of the broad bands in the same material as that with which he performed the original experiments.

Marrello et al. [43] measured the electroluminescent efficiency as a function of the position of the doped probe layer in double dielectric thin film ZnS ACEL devices. The experiment was done with an Mn-doped layer device and a TbF_3-doped layer device. The result was that the EL efficiency profile was much more uniform when a TbF_3-doped layer rather than a Mn-doped layer was used. This was a surprising result because if it is assumed that impact excitation is the major excitation mechanism then one would expect the TbF_3 EL efficiency profile to be steeper because hotter electrons are required to impact excite Tb luminescence than Mn luminescence. One possible way of explaining the results would be to assume that a significant fraction of the TbF_3 EL excitation is by resonant energy transfer. This is in direct disagreement with the work done by Krupka [25] and in order to resolve the difficulty Marrello et al. attempted to reproduce Krupka's results with their dielectrics and ZnS:TbF_3. However, they observed no change in the $^5D_3$ to $^5D_4$ Tb luminescence ratio. This result along with the results of their original experiment suggest that the excitation mechanism of Tb in their devices is

not primarily by hot-electron impact but is more likely to be by resonant energy transfer.

CONCLUDING REMARKS.

In this chapter we have established that there are hot electrons in the ZnS:RE diodes by observing the broad emission spectra and fast decay times of the diodes. We have shown that the presence simultaneously of hot electrons and luminescent rare-earth centres does not necessarily lead to rare-earth emission. This is because of the small impact cross-section of the rare-earth centres.

The results in this chapter also show that as well as the broad emission band due to the interband transitions there are several other electroluminescent emission bands in ZnS:RE diodes which are dependent on the rare-earth dopant. This means that the results obtained by Krupka in [25] which he used as evidence for a hot electron impact excitation mechanism can be interpreted in terms of an energy transfer mechanism. In order for Krupka to have conclusive evidence that the excitation mechanism is by the impact of hot electrons he would have to show that the relative intensities of the broad bands in the original samples did not vary with applied voltage. The quantum efficiency measurements in this chapter show that the relative intensities of the luminescence in different parts of the spectrum vary with the applied voltage, and that the way in which the relative intensities vary depends upon the rare-earth dopant.

Marrello et al. [43] have also thrown doubt on Krupka's results, and Tuenge et al. [55] found that the intensity ratio of the $^5D_3$ to $^5D_4$ emissions decreased with the applied voltage. With ZnS:Mn and ZnSe:Mn the excitation is by impact for some conditions and transfer for others as the results of chapter 2 showed. The results from this chapter show that the same is likely to be true of ZnS with rare-earths.

CHAPTER 5

LIGHT EMISSION FROM HOT ELECTRONS IN ZnS.

INTRODUCTION.

Light emission from hot electrons has previously been observed in reverse biased p-n junctions of Si [56-58], Ge [59,60], GaP [61,62] and SiC [63]. The emission from these junctions has been attributed to two processes acting together, namely, the direct (phonon-assisted) recombination of hot electrons and holes responsible for photons of higher energy, and radiative intraband transitions of carriers which contribute to the emission at the low energy end of the spectrum. The emission from hot electron transitions is characterised by broad electroluminescence spectra and fast decay times. Turvey and Allen [42] observed these characteristics in n-type ZnSe reverse biased Schottky diodes, the broad band electroluminescence ranging from 0.5eV - 2.6eV. The light emission was interpreted as being due to transitions of hot electrons between the various conduction band minima. The quantum efficiency of the electroluminescence was in accord with this interpretation. Similar spectra (though recorded over a restricted energy range) have been observed in ZnO [64] and GaP [65] and the emission in these materials has been interpreted as being due to intervalley transitions in the conduction band by comparison with the ZnSe results.

Skolnick [66] observed a broad band electroluminescence (1.5eV - 3.6eV) from ZnS:Mn,Cu powder devices. He attributed this blue electroluminescence to transitions within the conduction band by reference to the ZnSe results [42]. However, his spectra were not corrected for the system response. Chimczak

and Allen [26] corrected his spectra for the photomultiplier response (S20 and S1 photomultiplier tubes were used), whereupon the spectral shape appeared to be similar to that of the many blue emissions caused by impurities in ZnS. The only evidence for the emission in Skolnick's devices being due to intervalley transitions therefore is the fast decay time ~ 50ns. However, the decay time of the intervalley transitions is expected to be < 50ns, so this decay time will only be evidence of intervalley transitions if this was also the response time of the system. The response time of Skolnick's system was 25 ns. It is concluded therefore that the blue emission reported by Skolnick is not likely to be due to intervalley transitions in the conduction band.

In this chapter very broad electroluminescence spectra (0.6eV - 3.1eV) are observed from n-type ZnS reverse biased Schottky diodes. This electroluminescence is also shown to have a very fast decay time. The results are very similar to those observed in ZnSe diodes by Turvey and Allen [42], and are also interpreted in terms of hot electron transitions between the conduction band minima. The results are related to the band structure of ZnS, whereupon the high energy cut-off of the electroluminescence spectrum is found to correspond with X_3-Γ_1 transitions.

The term "hot electron" can be applied to a system where the effective temperature of the electrons is greater than the lattice temperature. In polar materials, the hot electrons are scattered less efficiently as the mean electron energy increases. This leads to electron runaway and dielectric

breakdown at a critical field, whereupon the electrons will populate the upper valleys of the conduction band. The theory of dielectric breakdown in solids was developed by Frohlich [67] and refined by Stratton [68]. In this chapter Stratton's formula for the dielectric breakdown field is applied to ZnS, and it is shown that for the fields used in these experiments the electrons are transferred to the upper valleys of the conduction band, where an increased effective mass prevents further electron runaway. This supports the prediction made from the experimental results, that the emission from the ZnS diodes is due to intervalley transitions in the conduction band. It is also shown by the application of Stratton's formula to a parabolic fit of the ZnS band structure that a simple parabolic band model cannot be applied to ZnS.

EXPERIMENTAL METHODS.

5.1 The samples.

Several samples of undoped ZnS were used for the work in this chapter. Two of these samples were grown and heat treated in 1974 namely ZnS 3(a) and (b), and one was grown and treated recently in this laboratory namely ZnS Ew1 Tr3. This sample was given a conductivity treatment at 950 °C for 170 hours in a Zn/Al mixture containing 6% aluminium. The samples were made into Schottky diodes using the techniques that have been described in previous chapters. ZnS 3(a) was used with its original indium ohmic contacts whilst ZnS 3(b) and ZnS Ew1 Tr3 had silver paste ohmic contacts. All the samples had 1mm evaporated aluminium Schottky contacts. The type of contacts used were changed for the last experiment which was the measurement of the near i-r spectra, and this new type of contact is discussed in section 5.2.2.

5.2 Measurement of the emission spectra.

5.2.1 In the visible region.

The experimental procedure was as described in section 4.2 of chapter 4 with one modification. An ammeter was put in series with the diode so that the current could be monitored throughout the course of the experiment. This enabled a further check on the consistency of the results. Spectra were recorded at several applied voltages for all of the above samples of undoped ZnS.

5.2.2 In the near i-r region.

The type of detector chosen to measure the i-r spectra of the samples was a Mullard 61SV PbS photoconductive cell as it had a spectral response ranging from 0.3 to 3.5 μm. The cell was biased from a Brandenburg 472R stabilised d.c. supply using the circuit shown in fig.(5.1). The value of the load resistor (750 kohms) was chosen so that half of the applied voltage was dropped across the cell as this gave the best signal to noise characteristics.

The diodes were operated under pulsed drive conditions so that phase sensitive techniques could be used to process the signal. High voltage pulses with a 1:1 duty cycle were obtained using a Farnell E350 stabilised d.c. supply and a transistor switching circuit which was triggered by a Thandar TG102 pulse generator. The schematic for the switching system is shown in fig.(5.2). One advantage of using a pulsed power supply is that the diode contacts are then much more stable for high current flow. Another advantage is that for a given power dissipation in the diode, twice the light output is obtained from an electrically pulsed diode compared with an optically chopped system.

As the sensitivity of the PbS cell was not as great as other types of detector (such as photomultiplier tubes) the signal levels involved in this experiment were very small. It was important therefore to produce an optically efficient experimental set-up. For this reason a high efficiency Bausch &

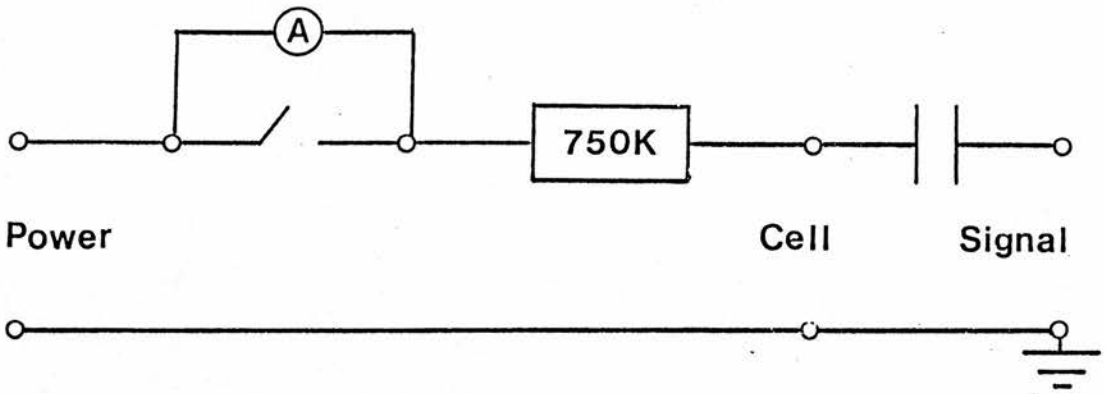

Fig.(5.1)

Bias circuit for the PbS cell.

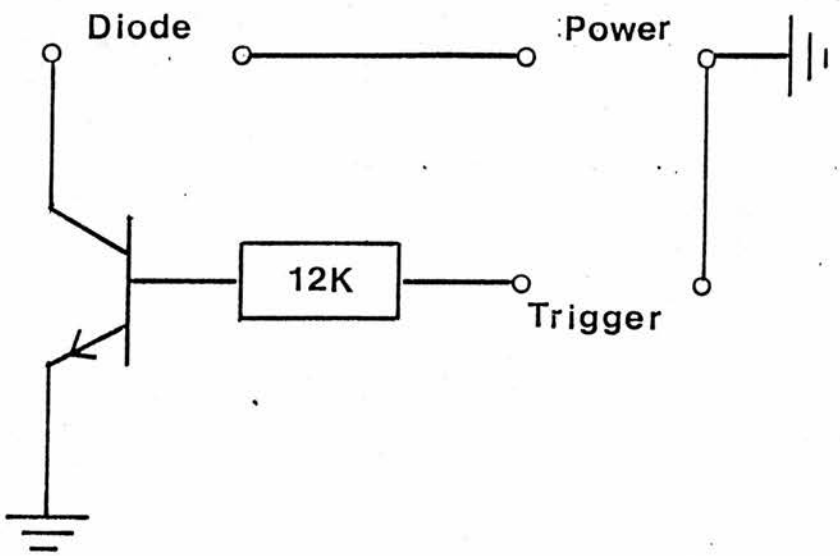

Fig.(5.2)

Schematic of the voltage switching system.

Lomb monochromator was used. The wavelength calibration of the monochromator was checked using the 1.01, 1.13 and 1.53 μm lines of a mercury lamp. A fast aspherical collimating element was used to collect as much of light as possible from the diode. This collimated beam was reduced to a parallel beam which was smaller than the entrance slit of the monochromator so that all of the available light passed through the monochromator. The light output from the monochromator was detected by the PbS cell which was placed immediately in front of the exit slit. The signal from the cell was processed by a Brookdeal 401A lock-in amplifier the output of which was monitored on a chart recorder. A schematic representation of the experimental set-up is shown in fig.(5.3).

Unfortunately, even with this optimised experimental set-up the signal level (<1μV) was still below the noise level. The noise was found to come from two sources namely, noise on the mains supply and electrical interference from the pulse generator and voltage switching system. Several steps were taken to reduce this noise to a minimum. Firstly, a mains stabilising unit was used. Secondly, the lock-in amplifier, PbS cell power supply and the chart recorder were put on a separate earth system. Thirdly, both the cell and sample power supplies were kept as far away as possible from the rest of the experiment. Fourthly, the signal from the cell was passed through a high pass filter centred on the pulse frequency. These four steps reduced the mains noise to an acceptable level of <0.1μV.

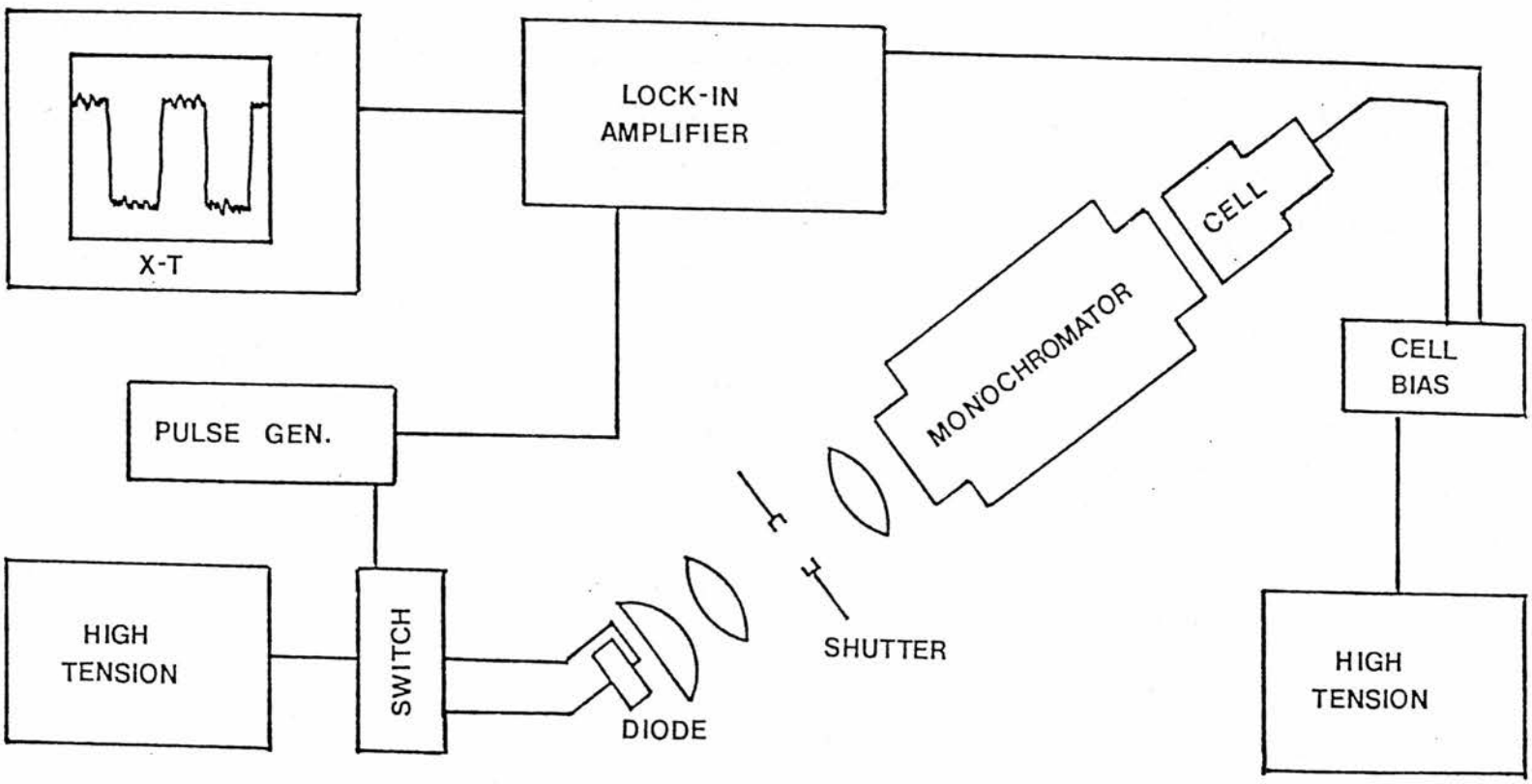

Fig.(5.3)

Schematic representation of the experimental set-up

for recording i-r spectra.

The electrical interference from the voltage switching system was reduced by the following. Firstly, the wires from the transistor switching box to the sample holder were reduced to the shortest length possible (about 5 cm). Secondly, the output from the pulse generator was reduced to the minimum voltage which still triggered the transistor switch. Similarly, the reference signal from the pulse generator to the lock-in amplifier was attenuated to such a level that the reference untriggered indicator on the lock-in was just extinguished. As the transmission of the interference greatly increases with frequency, the operating frequency was chosen to be 270 Hz which was not a multiple of the mains frequency. This was low enough not to be highly transmissive but was significantly higher than the mains frequency so that the mains filtering system still worked well. After these steps were taken there still remained a residual interference level. It was found however, that this was due to high frequency Fourier components from the edges of the square switching pulses and consequently was 90^{c} out of phase with the signal. It was found that the best way to maximise the signal was to phase maximise the interference and then change the phase by 90°. At this phase setting the electrical interference could not be observed above the mains noise level.

Once the noise had been reduced to an acceptable level ($<0.1\mu V$), the diodes had to be made as efficient as possible. This was achieved in the contact making process. After several trials of different types of contact, the following contact system was found to be the most efficient. Firstly, both surfaces of the sample were ground with 600 grade silicon

carbide, all traces of which were then removed by cleaning in propanol in an ultrasonic bath. Both surfaces were then polished with jeweller's rouge and were cleaned as previously. The sample was then etched for 1 minute in 10% HCl, rinsed in deionised water and then rinsed in propanol which removed the water. A large area aluminium Schottky contact was then evaporated onto the front surface of the sample. The sample was then set in dental wax on a microscope slide with the back surface of the sample uppermost. This surface was etched in caustic soda for 20 minutes, rinsed in deionised water, etched in 10% HCl for 30 minutes and then rinsed in deionised water followed by propanol. The wax prevented the caustic soda from damaging the aluminium Schottky contact. An indium contact was then infused onto the surface of the sample following the procedure described in chapter 2. This formed an ohmic contact. The wax was then removed from the sample using toluene in an ultrasonic bath and the sample was again cleaned in propanol. The sample was then placed in a spring contact holder with the large area Schottky contact against the metal plate and the spring contact touching the indium dot. A negative bias was applied to the Schottky contact so that the diode was operated under reverse bias. The advantage of the large area contact was that higher currents could be passed through the sample with lower current densities. Greater contact stability could consequently be achieved and there was a large area of light emission. Typically, rms currents between 5 and 7 mA were passed depending on the size of the sample.

The spectra of the diodes were recorded as follows. Reverse bias voltage pulses were applied to the diodes and the current was set to a given level and monitored throughout the experiment. There were no problems however with current fluctuations for this type of contact. The wavelength was set to 1.2 μm and an optical shutter was placed in front of the monochromator. The background noise level was then recorded. This took about 10 minutes as a long time constant (10-30 seconds) and a low frequency filter were used on the lock-in amplifier. The shutter was then manually removed and the signal level was recorded, again for about 10 minutes. The shutter was then replaced and the background level was re-recorded. The wavelength was then changed and the whole procedure was repeated. This technique produced a series of battlements on the chart recording from which the true optical signal could be observed irrespective of any residual interference. Results were taken every 0.1 μm between 0.7 and 1.6 μm. At the end of the run the 1.2 μm result was repeated as a check on the consistency of the results. The run was started at 1.2 μm as at this wavelength the signal was largest so this gave the most accurate check on the consistency. The same procedure was repeated for the second grating where the results were taken every 0.2 μm between 1.6 and 2.0 μm. As a manual optical shutter was used we could be completely certain that the results were independent of the electrical interference. The shutter also provided a good method of observing the smaller signals (such as at 0.7 μm) over the noise background and eliminated the problem of background drift.

5.3 Measurement of the decay time.

The decay times of the samples in the visible region were measured following the procedure described in section 4.4 of chapter 4. For these samples however, a Stanford SR280 boxcar system was used so some minor modifications were made to the experimental method. The input impedance of this boxcar was 1 Mohm and this could not be reduced to 50 ohms as was the case for the Brookdeal boxcar. This meant that the output resistor in the dynode chain of the photomultiplier tube R_L had to be reduced to the minimum workable value of 47 ohms. The system response time was again tested with a red LED, whose decay time was measured to be ~ 35 ns. No measurements were made on the spectral variation of the decay times of these samples.

5.4 Measurement of the relative quantum efficiency.

The diode was placed directly in front of an EMI 9558B photomultiplier tube. A voltage was applied across the diode and the current through the sample I and the output current of the photomultiplier tube L were measured. Initially the dark current of the tube was measured and this was subsequently subtracted from the results. It was important to determine the voltage dropped across the diode accurately and for this purpose a split contact holder was used, i.e. the base-plate of the holder which connects to the ohmic contact of the diode was cut in half. The ohmic contacts on the diode (either indium or silver paste) were suitably separated, and the voltage was applied across one contact and measured across the other. The relative quantum

efficiency L/I was thus determined as a function of the voltage dropped across the diode. The variation of the relative quantum efficiency with voltage in different parts of the spectrum was examined by placing interference filters in front of the diodes.

The relative quantum efficiency was also measured as a function of voltage for pulsed drive conditions and this was done as follows. Voltage pulses from an Avtech AVR-3-C pulse generator were applied across the diode. The voltage of the pulse was measured on an oscilloscope using the split contact holder technique. A 100 ohm resistor was placed in series with the diode and the current through the diode was determined by measuring the voltage dropped across the resistor on an oscilloscope. The diode was placed directly in front of the photomultiplier tube, the output of which was fed into a Stanford SR280 boxcar system. The signal consisted of a train of pulses and the gate of the boxcar was set to correspond with the middle 80% of the signal pulse. The averaged signal L was then read from the digital readout of the boxcar. Again, the relative quantum efficiency L/I could be obtained as a function of voltage dropped across the diode.

RESULTS.

5.5 The emission spectra.

The emission spectra in the visible region were calibrated using the calibration curve for the Zeiss spectrometer shown in fig.(4.1) of Chapter 4. The calibrated spectra for each sample are shown for several applied voltages in figs.(5.4) to (5.6). It should be noted however, that as the tube's sensitivity drops towards 1.55 eV the signal levels between 1.55 eV and 1.70 eV are small and the calibration coefficient is large, hence any small discrepancy in the measurement of the signal is magnified in this energy range. A small discrepancy can easily be introduced, for example, during the process of subtracting the background noise level from the signal level, particularly for the lower voltage results where the signal level is at its lowest.

The emission spectra of the ZnS Ew1 Tr3 sample shown in fig.(5.4) are very broad with a high energy cut-off at 3.10 eV. The shape of the spectra are unlike those due to impurities but are similar to those observed by Turvey and Allen [42] in ZnSe diodes which were due to intervalley transitions in the conduction band of the semiconductor. The emission spectra do not vary with the applied voltage except in the low energy region where there appears to be more light emission for the lower voltage. This variation with voltage however, cannot be taken to be a real effect because of the problems of accuracy in this energy range which were discussed in the previous paragraph.

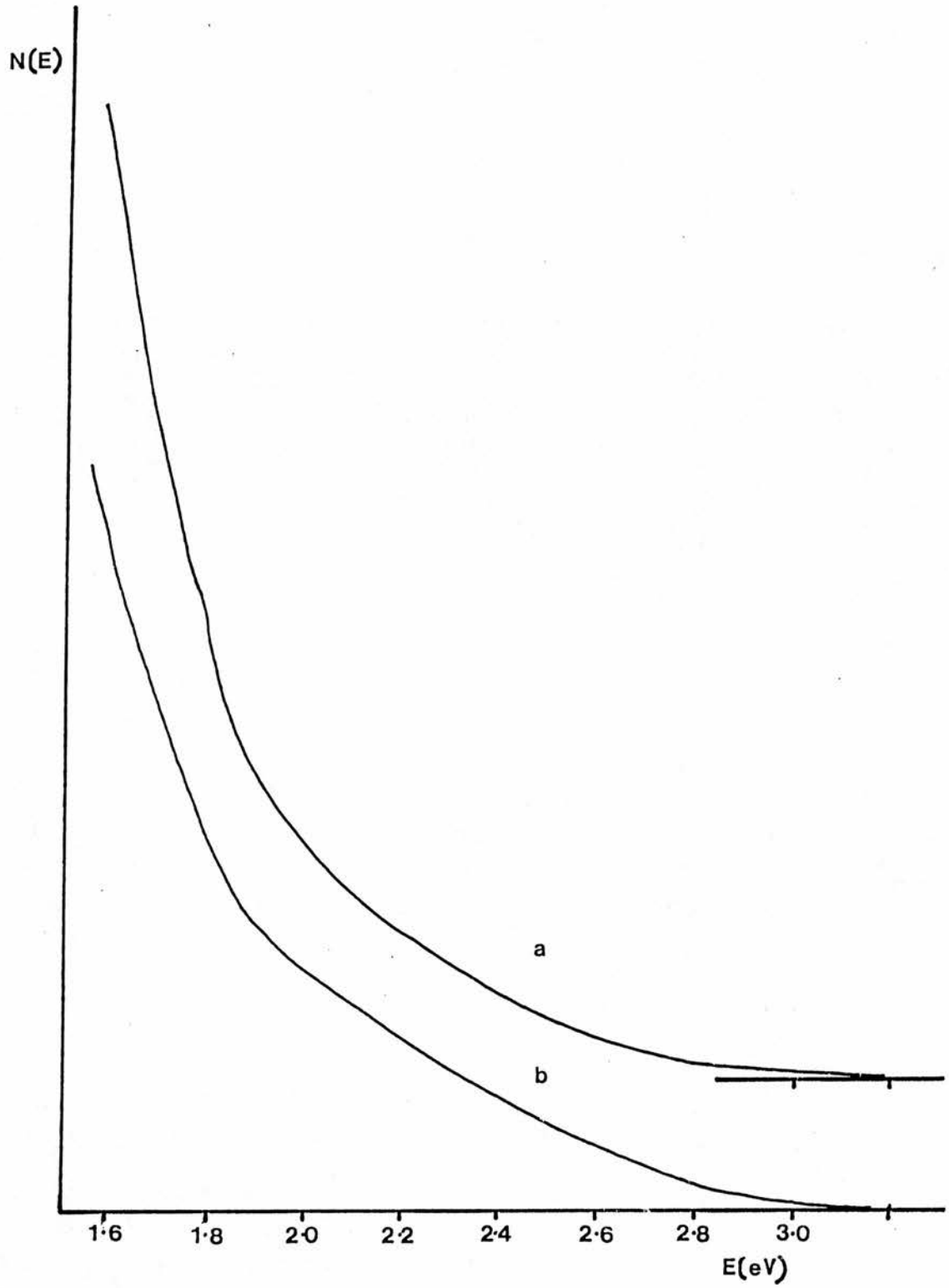

Fig.(5.4)

Emission spectra of ZnS Ew1 Tr3 at (a)70V, (b)110V.

The broad underlying emission spectra of the ZnS 3(a) sample shown in fig.(5.5) have the same basic shape as those for the previous sample, again with a high energy cut-off at 3.10 eV, but superimposed on the very broad spectra there is a broad blue band which peaks at 2.55 eV (485 nm). The intensity of this blue band decreases with increasing applied voltage whilst the shape of the underlying broader band remains unchanged. A similar blue band (though of lesser intensity) is seen in the ZnS 3(b) spectra shown in fig.(5.6). Again the intensity of the blue band decreases dramatically with increasing applied voltage. The underlying broad spectra of this sample have the same overall shape as the previous two samples with slightly more light emission in the low energy region. For this sample, there also seems to be more light emission in the low energy region for the lower voltage, but again this effect cannot be assumed to be real for the reasons discussed previously.

The calibration procedure described in section 4.3 of chapter 4 was also used to calibrate the i-r spectra measuring system. However, it was found that the low dispersion of the glass lenses in the i-r made it impossible to focus a perfect black body source onto the slits of the monochromator for wavelengths $> 1.3\ \mu m$. An alternative calibration of the system was obtained by the following. A correction was applied to take account of the spectral response of the cell using data supplied by the manufacturers. Also as the dispersion of the monochromator was linear in wavelength, the spectra were multiplied by a factor of λ^2 to account for this. Thus the major causes of spectral distortion have been accounted for in

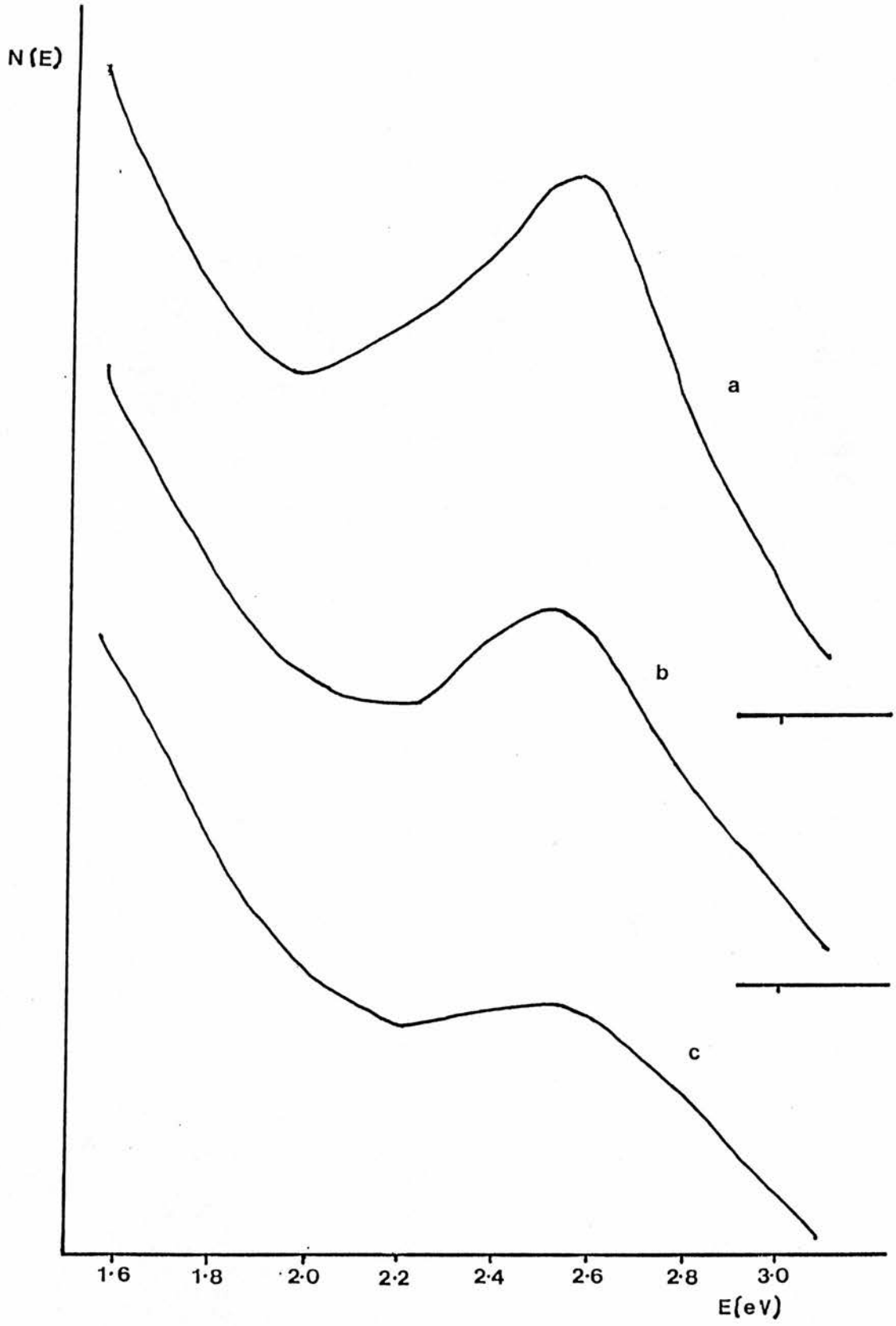

Fig.(5.5)

Emission spectra of ZnS 3 (a) at (a)45V, (b)60V, (c)72V.

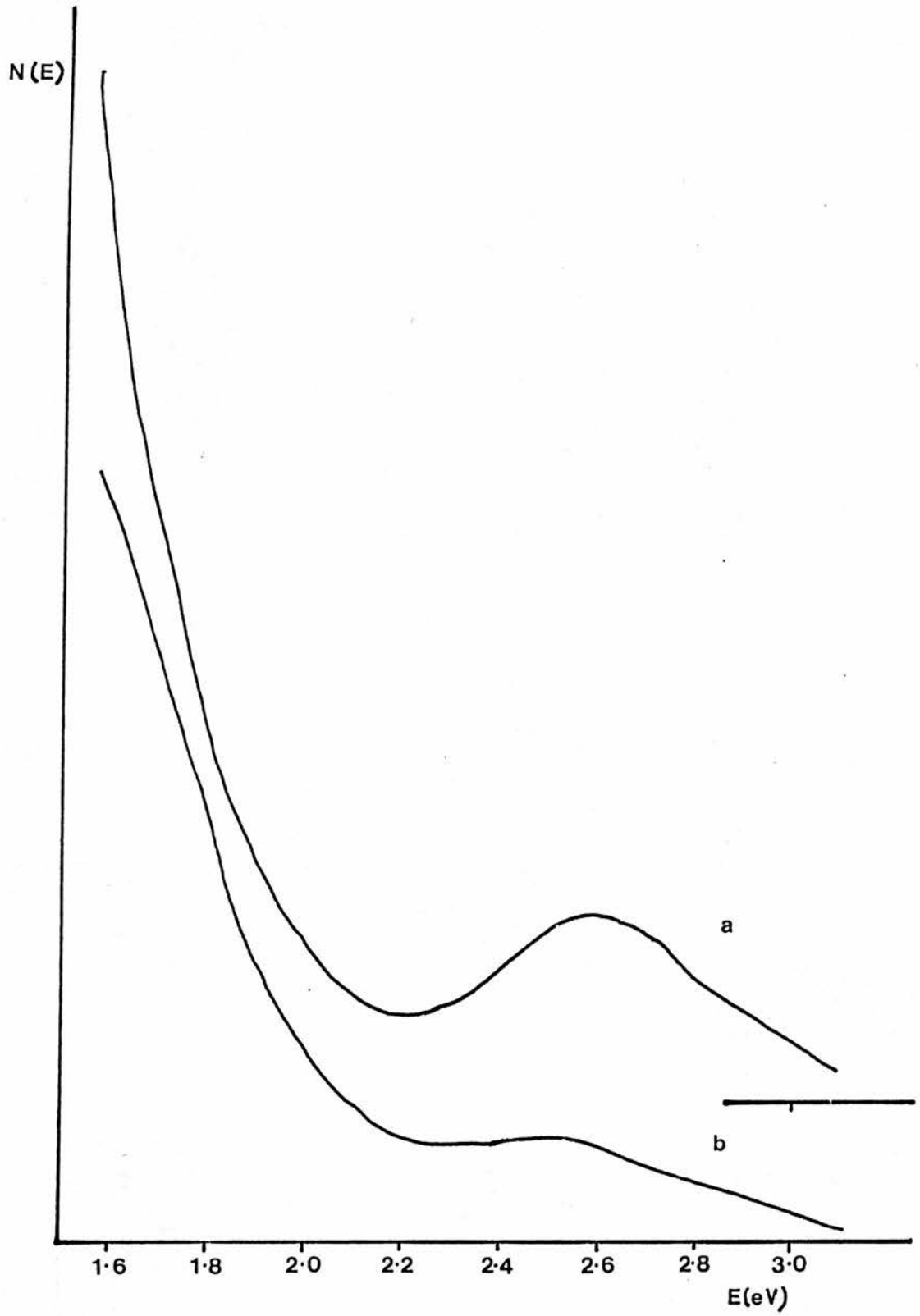

Fig.(5.6)

Emission spectra of ZnS 3 (b) at (a)50V, (b)60V.

the calibration. The calibration curve for the system obtained by applying these corrections is shown in fig.(5.7). It should be noted that this calibration does not take into account the transmission efficiency of the lenses in the system. It can be seen from fig.(5.8) however, that the transmission curve for crown glass is flat over the spectral range covered in the experiment so the presence of the lenses in the system should have a negligible effect on the calibration. The upper wavelength limit of 2.0 μm was originally chosen as it is unreasonable to expect glass optics to work well at wavelengths greater than this.

The i-r spectra shown in this chapter were calibrated using the calibration curve of fig.(5.7). This calibration curve was in good agreement with the calibration curve obtained using the black body source up to 1.3 μm whereupon the source could no longer be treated as a perfect black body for the reasons discussed previously. This shows that the method of calibration used here has a fairly high degree of accuracy.

The calibrated spectra of the samples are shown in fig.(5.9). As the signal levels involved in the experiment were low the spectra were only recorded at one voltage for each sample, this voltage being the one which corresponded to the maximum possible power dissipation in the diode. It can be seen from the figure that the spectrum for each of the samples has the same basic shape. The spectra are very broad peaking at ~ 1.05 eV, and are similar to those observed in ZnSe diodes using the same type of detector as K.Turvey [69]. The spectra follow on well from the spectra recorded in the visible region where the

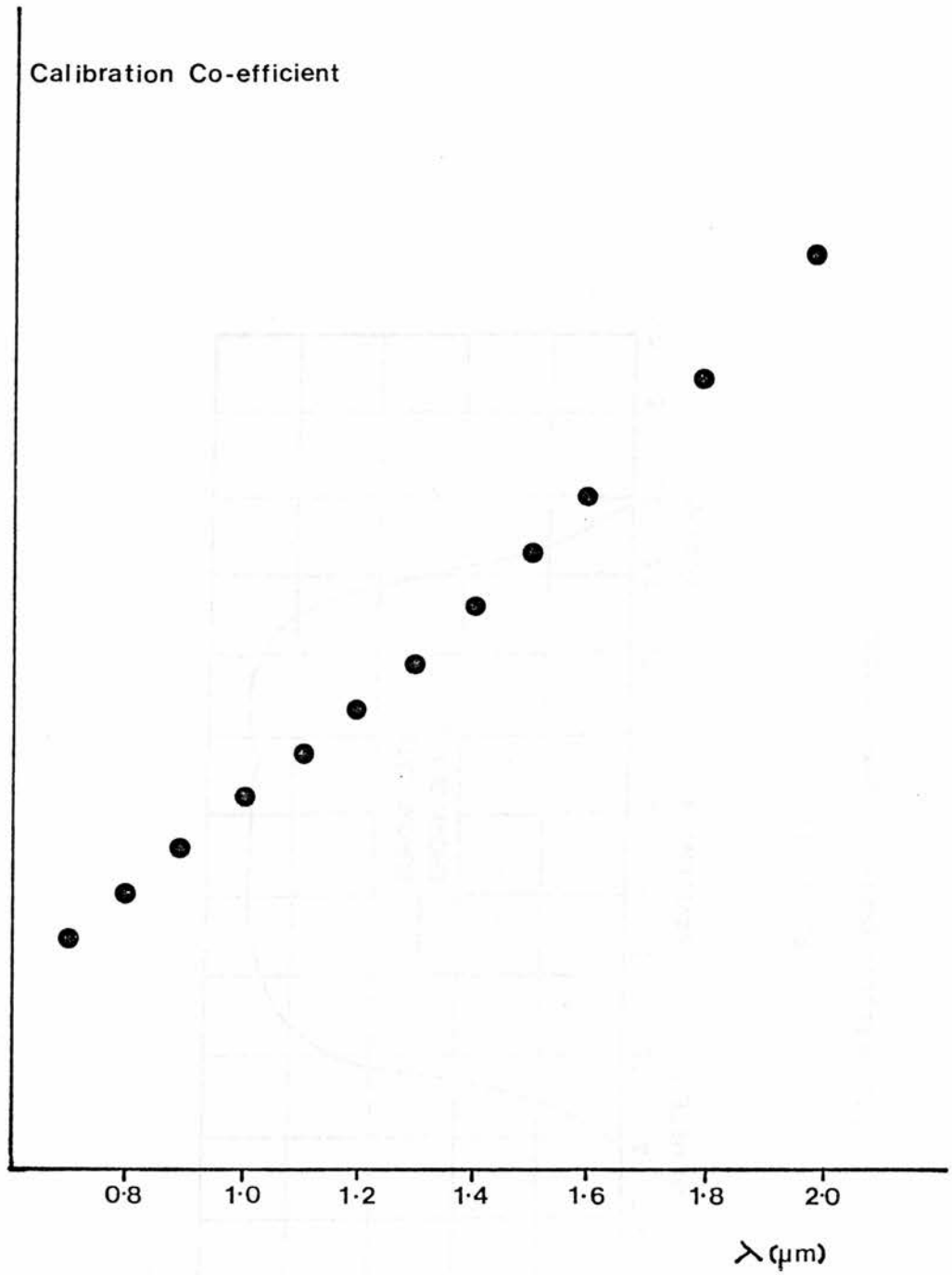

Fig.(5.7)

Calibration curve for the i-r spectra measuring system.

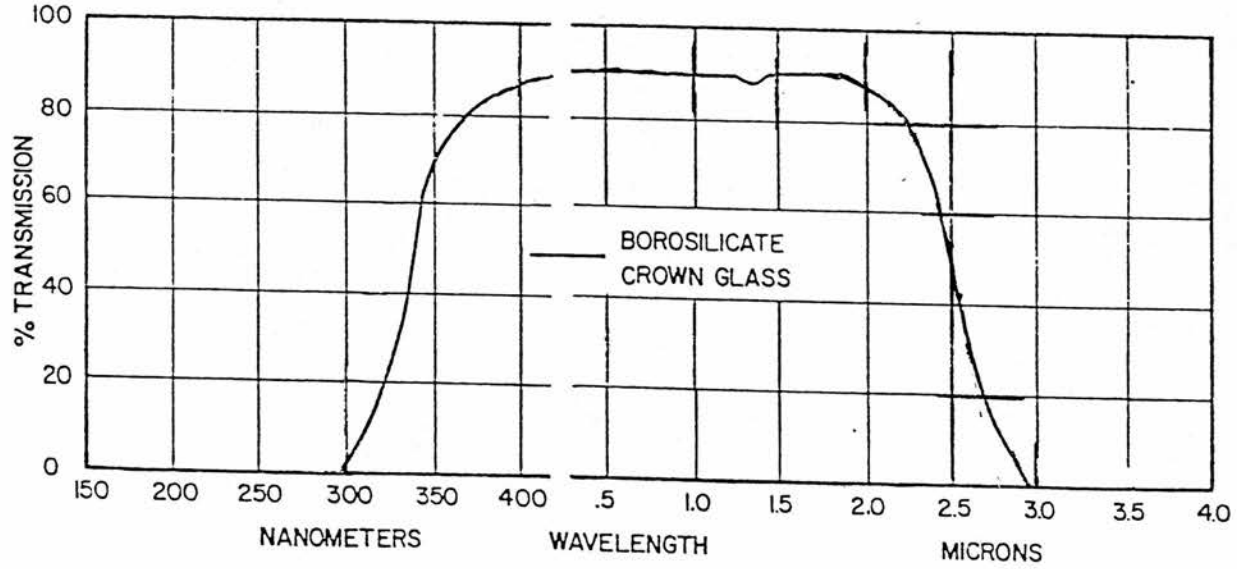

Fig.(5.8)

Transmission curve of crown glass.

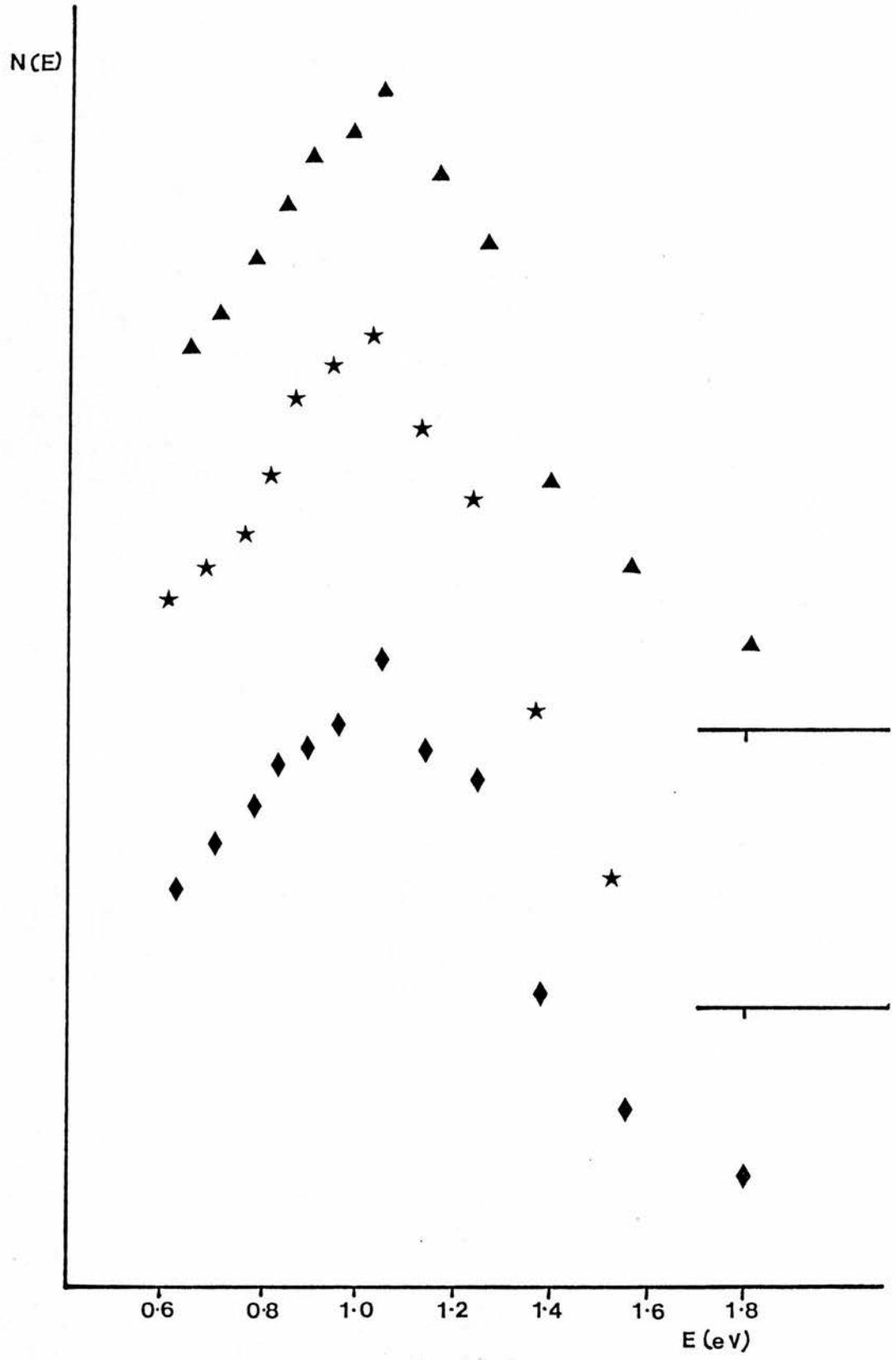

Fig.(5.9)

I-R emission spectra of ▲ZnS 3(a),

★ZnS Ew1 Tr3, ♦ZnS 3(b).

light emission increases with decreasing energy. A plot of the combined spectra is shown in fig.(5.10) for the ZnS Ew1 Tr3 sample.

5.6 Decay times of the samples.

The decay time was measured in the visible region of the spectrum (i.e. an S20 response photomultiplier tube was used). For every sample the decay time was measured to be < 35 ns, the decay time of the LED which was used to test the response time of the system. This implies that the decay time of the samples is < 10 ns. There was no evidence of any longer decay components in the recorded decay curves of the samples. The applied pulse had a width of 10 μs and the voltage was 150 V for the ZnS 3(a) and ZnS Ew1 Tr3 samples and 100 V for the ZnS 3(b) sample.

The decay time could not be measured in the i-r region of the spectrum as the response time of the i-r detector was not good enough to measure the fast decays involved in the experiment. However, as the shape of the spectrum in this region is totally unlike that due to an impurity, it can be assumed that the light emission is due to intervalley transitions in the conduction band. This will be substantiated in the discussion section of this chapter. Hence, the decay time in this region can be assumed to be < 10 ns also, although it cannot be determined experimentally.

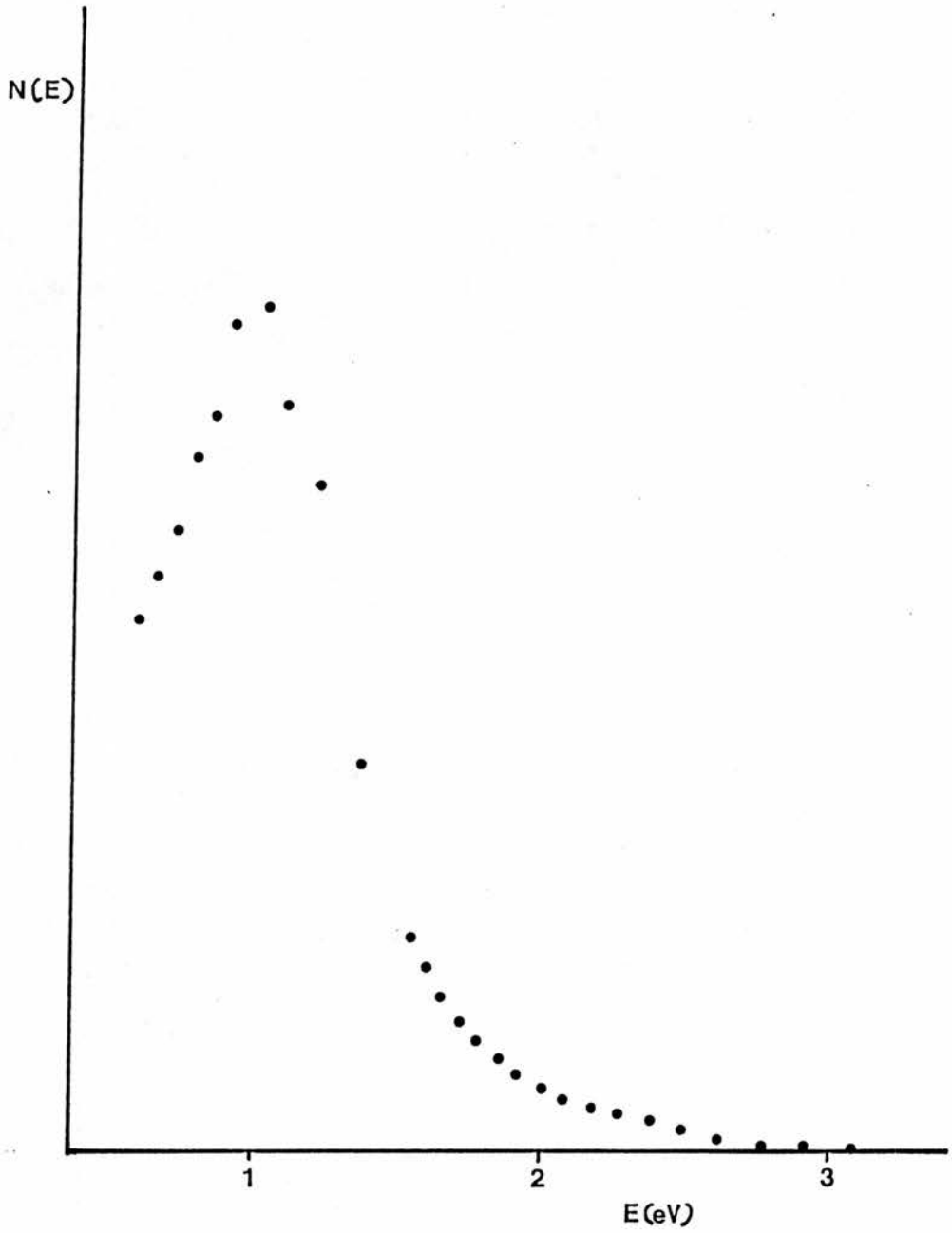

Fig.(5.10)

Combined visible and i-r emission spectra of ZnS Ew1 Tr3.

5.7 The relative quantum efficiency results.

The variation of the relative quantum efficiency with the average field in the junction for d.c. drive conditions is shown in fig.(5.11) for the ZnS 3(a) sample at two wavelengths namely 488 nm and 640 nm. The average field was determined from the donor density of the sample as described in chapter 3. The 488 nm interference filter was chosen as this corresponded to the peak of the blue emission. The relative quantum efficiency of the underlying broad band was examined using the 640 nm interference filter. It would have been preferable to use a longer wavelength filter but as the response of the S20 tube falls with increasing wavelength, this was the longest wavelength filter which could be used for reasonable signal levels. The figure shows that for higher fields the relative quantum efficiency increases more rapidly in the red than in the blue. This is consistent with the emission spectra results where the prominence of the blue band was seen to decrease with increasing applied voltage. Similarly, fig.(5.12) shows that for the ZnS 3(b) sample the relative quantum efficiency again increases more rapidly in the red than in the blue. This is consistent with the emission spectra shown in fig.(5.6). In contrast however, the variation of the relative quantum efficiency with field does not change much with wavelength for the ZnS Ew1 Tr3 sample as is shown in fig.(5.13). This is again in agreement with the emission spectra results as the spectra of this sample did not have a blue band.

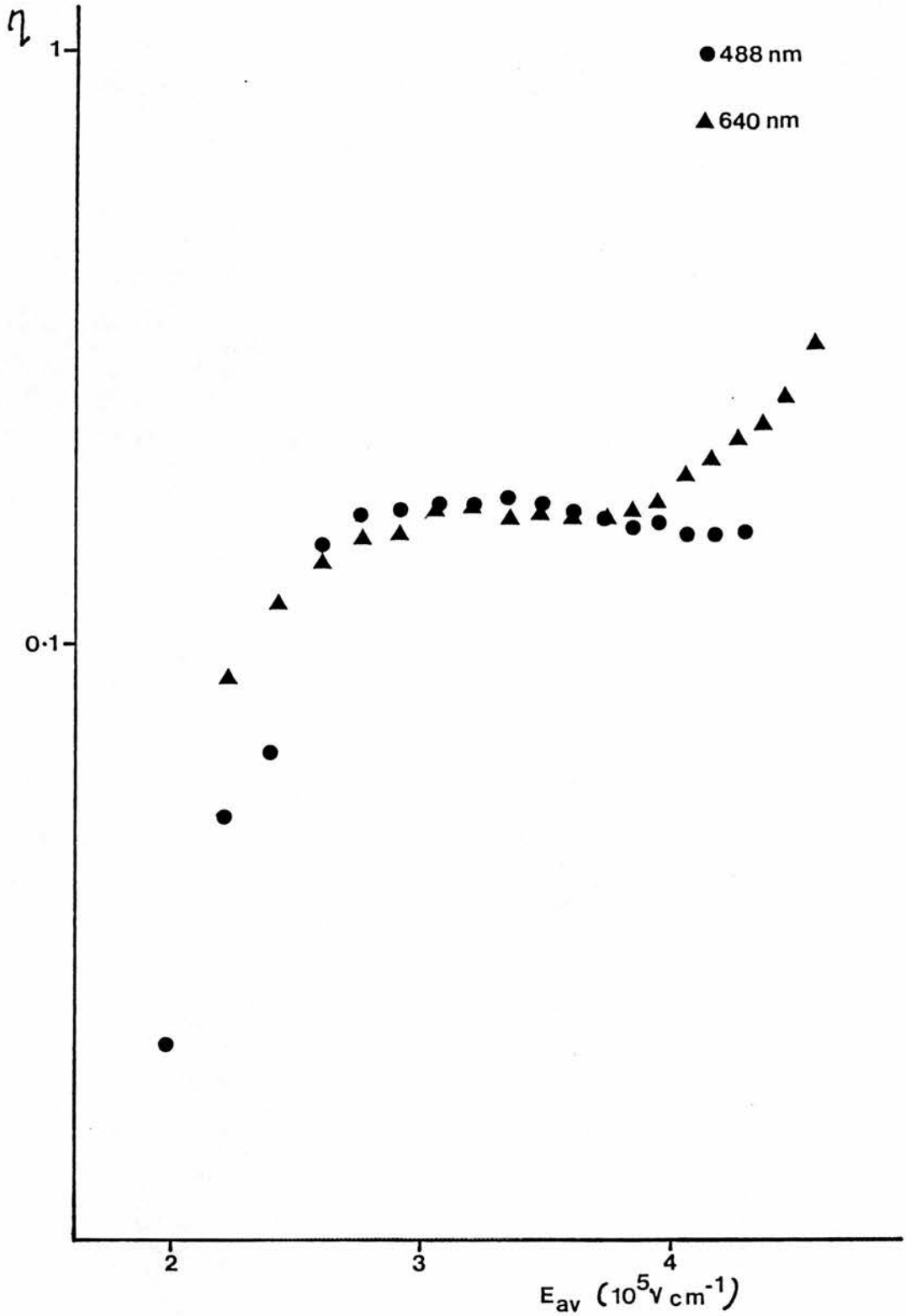

Fig.(5.11)

Relative quantum efficiency (d.c.) of ZnS 3(a).

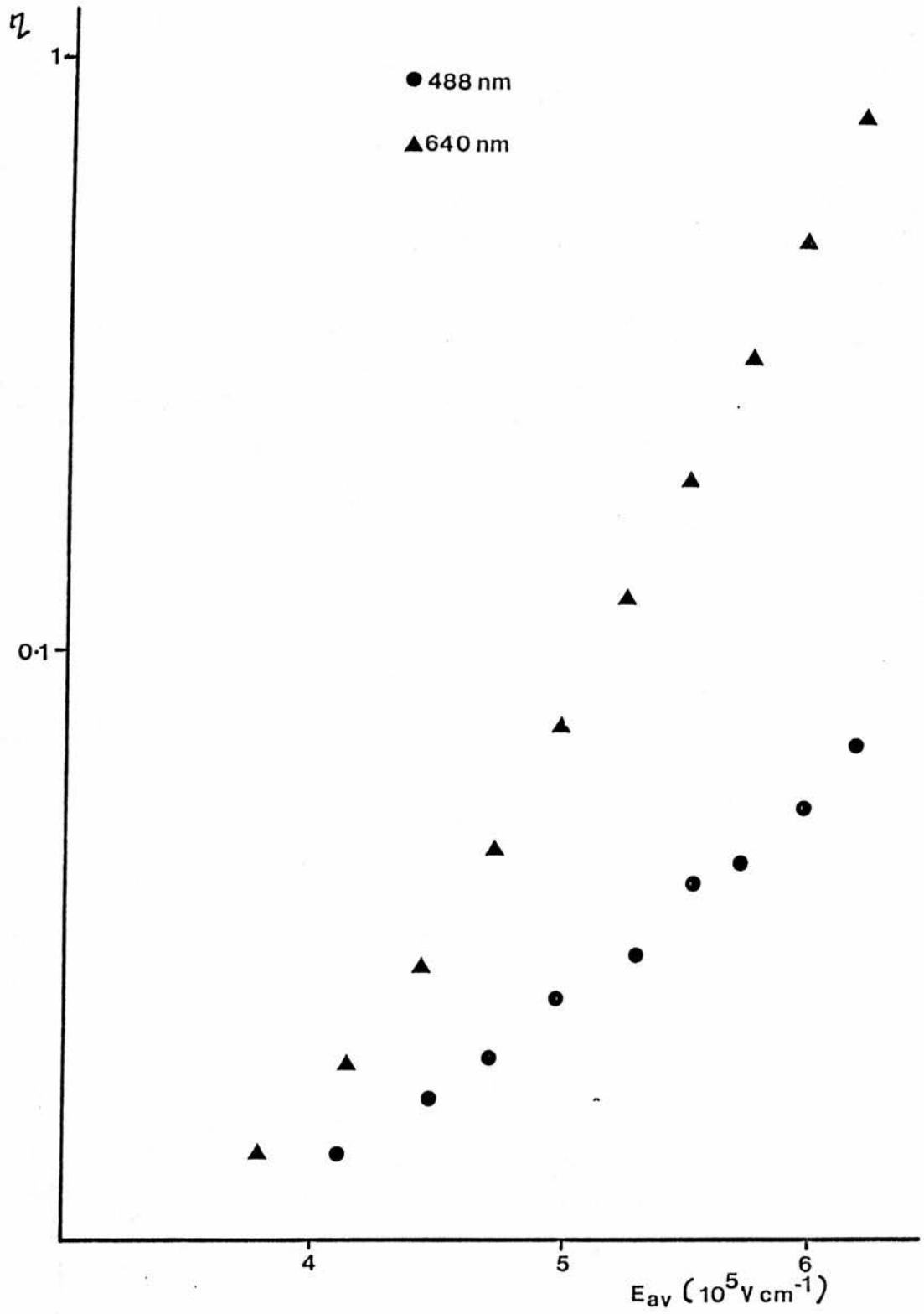

Fig.(5.12)

Relative quantum efficiency (d.c.) of ZnS 3(b).

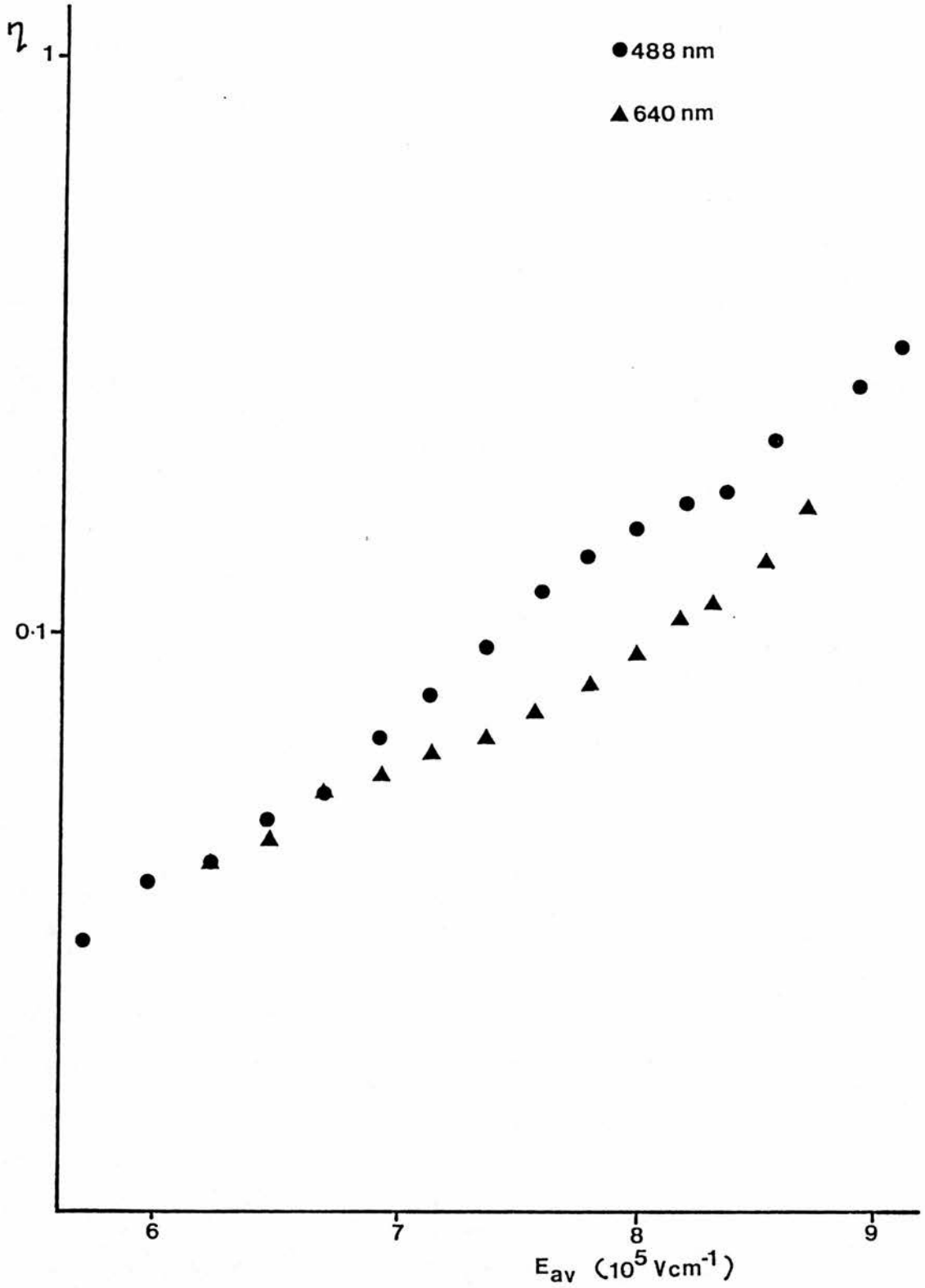

Fig.(5.13)

Relative quantum efficiency (d.c.) of ZnS Ew1 Tr3.

The relative quantum efficiency results for applied d.c. voltages are not very informative as the results are obviously distorted by other emission processes. The decay time measurements showed that for an applied pulse width of 10 μs the decay was fast with no slower components. This means that for an applied pulse of this width we are observing the effects of the fast broad emission band alone. Therefore, the results taken with an applied pulse width of 10 μs should give an accurate indication of how the relative quantum efficiency of the broad emission band varies with the average field in the junction. The results for all the samples are shown on the same plot in fig.(5.14). The relative quantum efficiency increases with increasing field until a maximum is reached at $\sim 5.5 \times 10^5$ Vcm^{-1}. The efficiency then falls as the field is increased further until the field reaches $\sim 8 \times 10^5$ Vcm^{-1} whereupon the efficiency begins to increase slightly again.

The relative quantum efficiency of the samples does not have the same variation with field when the applied voltage is pulsed rather than d.c. This was even the case for the ZnS Ew1 Tr3 sample where no blue bands were observed in the emission spectra. This difference was examined by determining the variation of the relative quantum efficiency with field for several applied pulse widths between 5 μs and 100 μs (this was the maximum pulse width available from the Avtech pulse generator). The results are shown in fig.(5.15) for the ZnS Ew1 Tr3 sample. The results for the 5 and 10 μs pulse widths are similar, but as the pulse width is increased further the maximum in the quantum efficiency disappears and the quantum efficiency

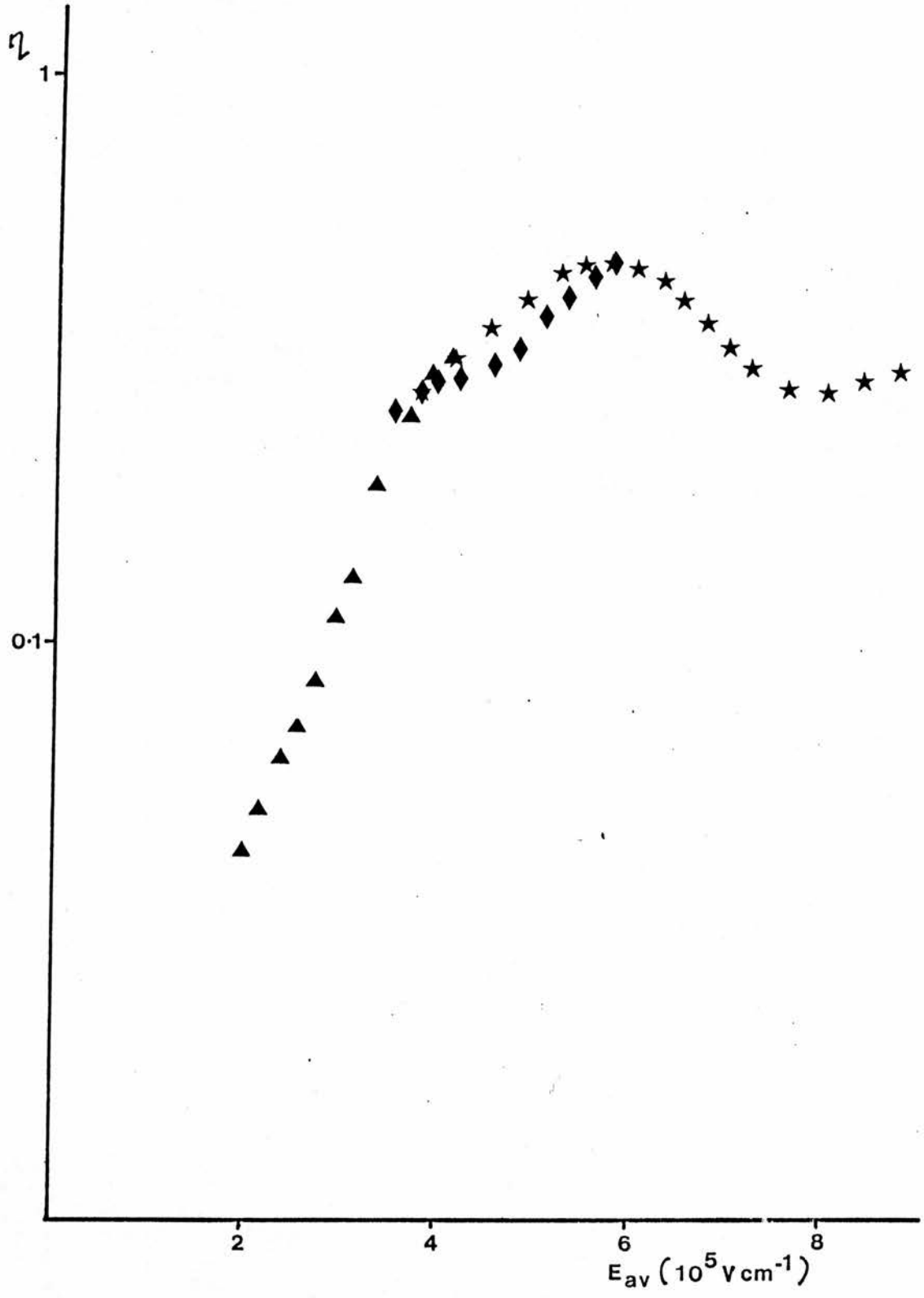

Fig.(5.14)

Relative quantum efficiency (pulsed) of

▲ZnS 3(a), ★ZnS Ew1 Tr3, ♦ZnS 3(b).

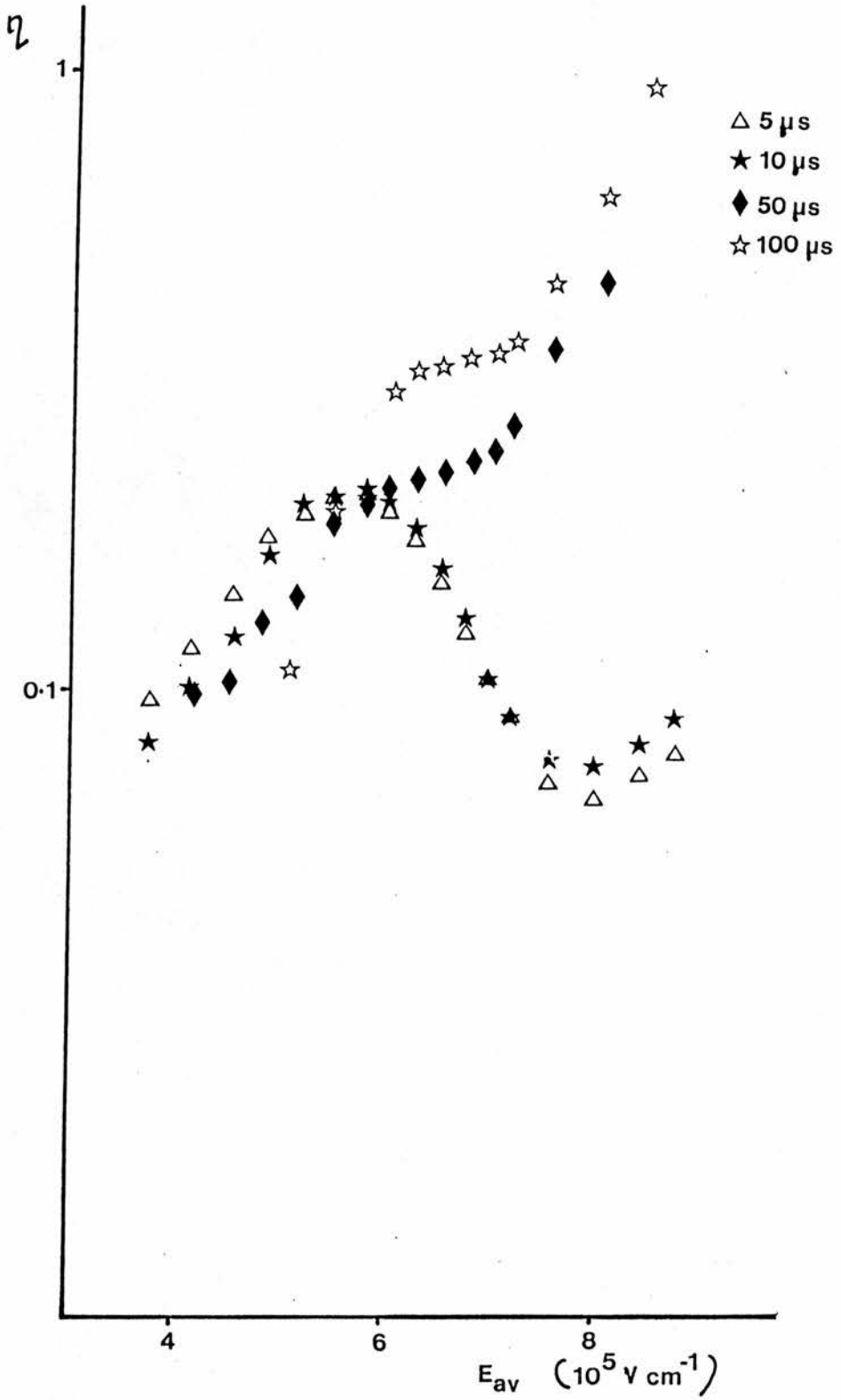

Fig.(5.15)

Relative quantum efficiency of ZnS Ew1 Tr3

at various pulse widths

continues to increase as the field increases. This was how the relative quantum efficiency varied with field for applied d.c. voltages. Hence, as the pulse width is increased the effects of other emission processes influence the results. The d.c. results are therefore of little interest other than to explain the prominence of the blue band at different voltages for samples ZnS 3(a) and (b).

DISCUSSION.

It is evident from the broadness of the electroluminescence emission spectra of the ZnS diodes that the light emission is not due to impurities. This is substantiated by the following. Firstly, the shape of the underlying broad spectrum is the same for different preparations of ZnS. Secondly, if the emission was due to impurities, then a similar luminescence emission should be observed for ultra-violet excitation. However, the photoluminescence spectra of samples ZnS 3(a) and (b) which were obtained by T.D. Thompson in this laboratory using an excitation light between 350 nm and 400 nm were quite different from the electroluminescence spectra. The photoluminescence spectra, which are shown in fig.(5.16), consist of a band ranging from 420 to 600 nm and peaking at ~ 490 nm. These spectra are very similar to the blue band which was superimposed on the broad electroluminescence spectra of the samples. Similar blue bands have been observed by other authors in both photo- and electroluminescence experiments for example, Bryant et al. [70] and Kukimoto et al. [71]. The emission mechanism of the blue band is thought by the mentioned authors to be donor-acceptor recombination of the isolated Al donor and an Al-Zn vacancy complex acceptor.

As the electroluminescence is not due to impurities, there must be another emission mechanism. Photons with energy greater than the energy gap can result from the recombination of hot holes and electrons. Wolff explained the broad emission obtained from avalanching Ge junctions in this way [60]. In our case

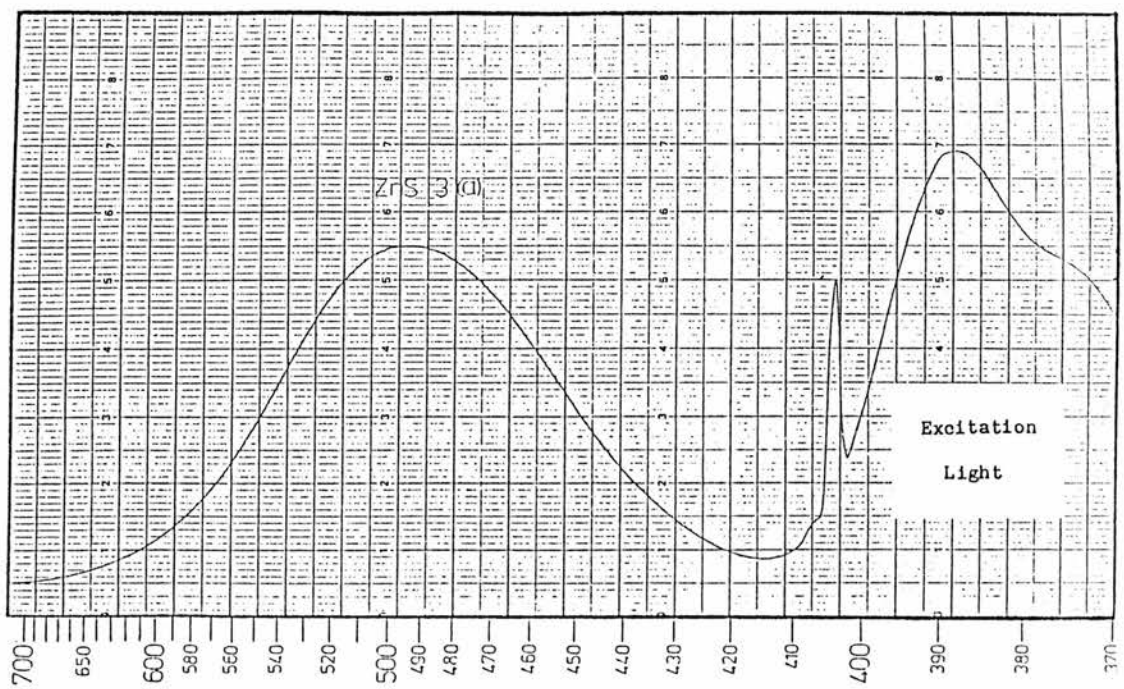

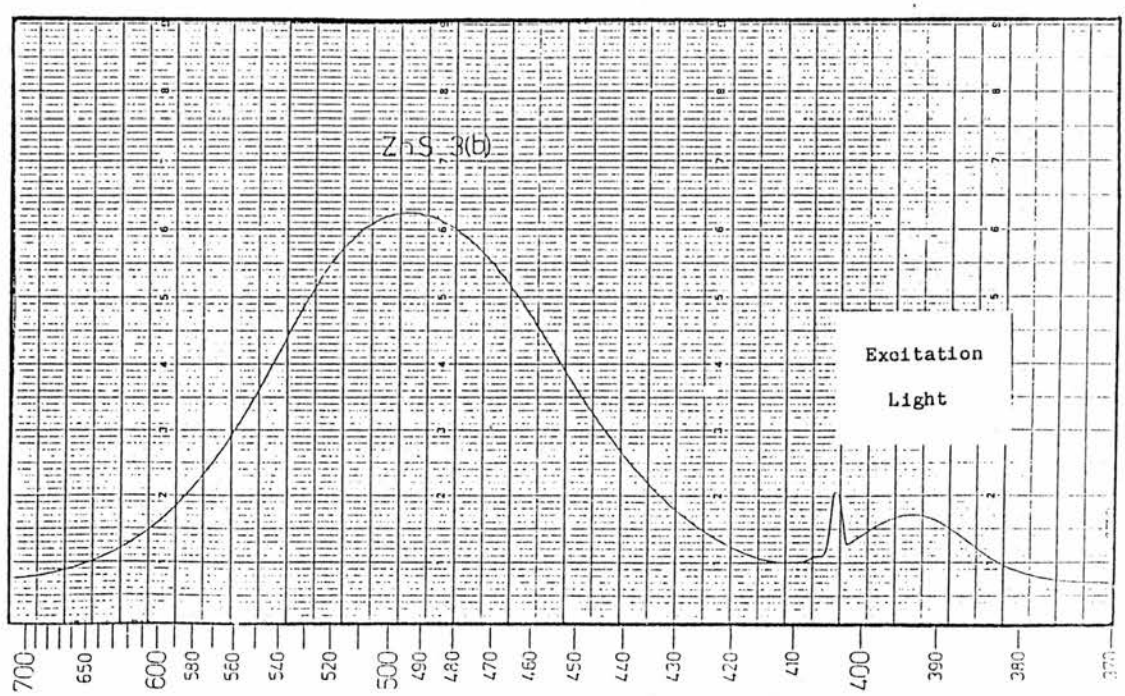

Fig.(5.16)

Photoluminescence spectra of samples

(a)ZnS 3(a), (b)ZnS 3(b).

however, the emission is below the energy gap and must therefore result from transitions wholly within the conduction bands or valence bands. From the measurements of the impact ionisation co-efficient in ZnS (T.D. Thompson and J.W. Allen [72]) it is known that band-to-band impact ionisation is negligible for the fields used in this experiment. The impact ionisation co-efficient was in fact measured for the twin of sample ZnS Ew1 Tr3 where band-to-band impact ionisation only began to be observed when the average field in the depletion region was $\sim 8 \times 10^5$ Vcm^{-1}. Therefore, the only carriers crossing the depletion region are electrons and it can be assumed that the light emission is associated with the transitions of electrons rather than holes. This again rules out the possibility of the emission being due to the recombination of hot electrons and holes.

The broad emission bands and fast decay times of the ZnS diodes are very similar to the results obtained with ZnSe Schottky diodes by Turvey and Allen [42]. In this case the emission was interpreted as being due to intervalley transitions in the conduction band of the semiconductor, in particular the $L_1 - \Gamma_1$, $X_1 - \Gamma_1$ and $X_3 - \Gamma_1$ transitions. This interpretation is also in agreement with our results for the ZnS diodes as it involves the transitions of electrons in the conduction band. Also, as the fields in the ZnS diodes are very high, typically $\sim 5 \times 10^5$ Vcm^{-1} (cf. 2×10^5 Vcm^{-1} for the ZnSe diodes), electrons will tend to congregate in the parts of the Brillouin zone where the group velocity is small and the effective mass is large, i.e. near the band minima. This is because scattering of the electrons is more efficient for slow incident particles. It

is likely therefore that at such fields, all the electrons have been transferred from the Γ valley. This implies that the emission is not due to transitions of hot electrons within the valley. This emission mechanism was proposed by Figielski and Torun [73] who used their formulation to explain the broad emission spectra observed by Chynoweth and McKay [58] in reverse-biased Si p-n junctions. In their formulation they assumed that the hot carriers had a Maxwellian distribution and that the band was parabolic. In this model transitions with high photon energy will only occur for the few electrons in the tail of the distribution. As the electron temperature changes with field, one would also expect the emission spectrum to change with field particularly at the high energy end. This is not the case for the results with ZnS diodes, where the spectra are seen to be invariant with voltage. The emission therefore appears to be due to intervalley transitions in the conduction bands and is therefore dependent on the band structure of the material. Further evidence for this is given by the similarity of the ZnS and ZnSe spectra, the two materials having very similar band structures.

It is important to see how our results relate to the band structure of ZnS. The critical point energies in the ZnS band structure as calculated by various methods are shown in table (5.1). From this table it can be seen that there is general agreement that the conduction band minima above Γ_1, are, in ascending order, L_1, X_1, X_3, Γ_{15} and L_3, though there appear to be large differences between the critical values for different computation methods. The high energy cut-off of the ZnS electroluminescence spectrum was 3.10 eV, so it seems unlikely

TABLE 5.1

SUMMARY OF THE CRITICAL POINT ENERGIES IN THE ZnS BAND STRUCTURE AS CALCULATED BY VARIOUS METHODS.

The critical point energies are given in eV with the origin taken at the lowest point of the conduction band.

CRITICAL POINT	(a)	(b)	(c)	(d)	(e)	(f)	(g)
L_{3C}	7.4	4.8	5.7	5.0		5.25	
Γ_{15C}	5.2	4.2	5.3	5.2	5.8	4.78	5.41
X_{3C}	2.3	2.2	2.7	2.3	2.6	2.32	3.80
X_{1C}	2.0	1.2	1.9	1.5	2.4	1.35	1.95
L_{1C}	1.5	1.2	1.7	1.6	1.7	1.39	1.83
Γ_{1C}	0.0	0.0	0.0	0.0	0.0	0.00	0.00
Γ_{15V}	-3.8	-3.8	-3.7	-3.7	-3.6	-2.26	-3.81
L_{3V}		-4.4	-4.0	-4.2		-3.10	-4.37
X_{5V}		-5.4	-4.8	-5.2		-4.45	-5.38

(a) First principles; Korringa, Kohn and Rostoker method.[74]

(b) First principles; Self-consistent orthogonalised plane wave.[75]

(c) Empirically refined, orthogonalised plane wave.[75]

(d) Pseudopotential method.[75]

(e) Modified orthogonalised plane wave.[76]

(f) Linear combination of Gaussian orbitals.[77]

(g) Linear combination of atomic orbitals.[78]

that the emission is due to $L_1 - \Gamma_1$ or even $X_1 - \Gamma_1$ transitions. Photons of this energy could be generated in $X_3 - \Gamma_1$ transitions although admittedly this would only be possible if the larger values computed for the $X_3 - \Gamma_1$ gap were almost correct. This was also found to be the case for the ZnSe results [69] where the high energy cut-off was 2.65 eV and the highest computed value for the $X_3 - \Gamma_1$ gap was 3.0 eV [79], more typical values being 2.1 eV [74]. The next valley higher than the X_3 valley is the Γ_{15} valley. However, it can be seen from the table that all the computed values of the $\Gamma_{15} - \Gamma_1$ gap are too high to give a high energy cut-off of 3.10 eV for $\Gamma_{15} - \Gamma_1$ transitions. It seems most likely then that the emission is due to transitions between the X_3 and Γ_1 valleys. It is impossible to determine from our results the occupancy of the L_1 and X_1 valleys, though it may be assumed that as the X_3 valley is populated then the X_1 and L_1 valleys are also likely to be populated. K. Turvey [69] showed by examination of the structure in the emission spectrum that this was the case for ZnSe diodes. However, it is now thought that this structure may just be an anomaly of the calibration, as the structure was not found to be reproducible when the experiment was repeated [80].

The variation of the relative quantum efficiency with field has a broad peak, the maximum value of the quantum efficiency occurring at $E_{av} \sim 5.5 \times 10^5$ Vcm^{-1}. This variation of the quantum efficiency can be interpreted in terms of the band structure of ZnS as follows. Initially the quantum efficiency increases with increasing field as more electrons are transferred to the X_3 valley. As the field is increased furtner, more

electrons are transferred to higher valleys and the efficiency of the X_3- Γ_1 transitions decreases. A similar peak in the quantum efficiency against field plot was observed in ZnS:Mn diodes by N.Gordon [41], although in this case the peak was sharper. Again this peak in the quantum efficiency can be explained in terms of the occupancy of the upper minima in the ZnS band structure. The peak in the quantum efficiency of the ZnS:Mn diodes is partly for the same reasons given for the undoped material but the sharpness of the peak is due to another factor. As the impact excitation of the manganese is thought to be an exchange process, the cross-section for impact excitation is sharply peaked in energy [49]. The quantum efficiency will therefore begin to decrease when the mean electron energy exceeds this peak energy. This would not be the case if a Maxwell-Boltzmann distribution of electrons was assumed. The ZnS quantum efficiency results and also those for ZnS:Mn diodes are therefore in agreement with the prediction made from the electroluminescence spectra results, that the emission is due to transitions from the X_3 valley to the Γ_1 valley.

From the experimental results it has been established that when there is a high electric field ($E_{av} \sim 5 \times 10^5$ Vcm^{-1}) across the depletion region of a ZnS Schottky diode, the electrons are transferred to the upper valleys of the conduction band. It would be interesting therefore, to determine the theoretical field for dielectric breakdown in ZnS. This will be discussed in the following. In polar materials, the efficiency of the LO phonon scattering mechanism does not effectively increase as the electron mean energy increases and this leads to electron runaway. Stratton [68] produced a formula for calculating the

breakdown field which corresponds to this electron runaway. At higher fields, other mechanisms come into play to limit the increase in energy of the electrons. For example, in SiO_2 [81], the electron energy distribution is initially stabilised by LO phonon scattering until a field of ~ $1MVcm^{-1}$ is reached where significant electron heating occurs. At higher fields the electrons are increasingly scattered by acoustic phonons and this scattering mechanism then stabilises the energy distribution. It will be shown that in ZnS the electron energy distribution can be stabilised by transfer of the electrons to the upper valleys of the conduction band where an increase in the effective mass leads to more efficient scattering.

Stratton [68] showed that the field for dielectric breakdown in polar materials is given by

$$F_c = (\varepsilon_\infty^{-1} - \varepsilon^{-1}) \frac{k\Theta m^*/m}{a_o \varepsilon} [2\ln\{2D/\gamma_o\}/3\pi]^{1/2} \qquad (5.1)$$

where ε and ε_∞ are the static and high frequency dielectric constants, $k\Theta$ is the (constant) phonon energy, a_o is the Bohr radius, D is a constant ($\ln D = 0.81$) and γ_o is the ratio of the Debye temperature to the lattice temperature. This formula was derived under the assumption that the lattice temperature was very much greater than the Debye temperature. This is not the case however in ZnS, where in fact $\ln \gamma_o$ can be assumed to be zero. The breakdown field in ZnS determined using this formula is therefore only approximate. However, the dielectric breakdown field in ZnSe calculated from this formula (2.8×10^4 Vcm^{-1}) is very close to the threshold field for the Gunn effect in ZnSe which was found to be 3.8×10^4 Vcm^{-1} by Ludwig and Aven [82].

Because of the similarity between ZnSe and ZnS, this gives us a good indication of the accuracy of the breakdown fields in ZnS determined using Stratton's formula.

The breakdown field in ZnS can be calculated using the known values of the dielectric constants $\varepsilon_\infty = 5.2$, $\varepsilon = 8.3$, the LO phonon energy $k\theta$ = 43meV [83,84] and the effective mass. The value of the effective mass depends on which of the valleys in the conduction band is being considered. Fig.(5.17) shows the band structure of ZnS drawn on an extended zone scheme for the conduction band in the (1,0,0) and (1,1,1) directions. A parabolic fit to this band structure is also shown in the figure and the effective masses of the electrons in these bands as determined from the parabolas are 0.8m in the (1,0,0) direction and 1.3m in the (1,1,1) direction. The breakdown fields estimated using Stratton's formula corresponding to these effective masses are 3.5×10^4 Vcm^{-1} and 5.3×10^4 Vcm^{-1} respectively. These fields are much lower than those in the ZnS diodes hence the electrons in the diodes will undergo electron runaway at these fields. (It should be noted that a parabolic fit was also made to a different band structure computation (Wang and Klein [77]) and this yielded almost identical effective masses to the above). This means that a simple parabolic band model cannot be applied to ZnS as this model provides no mechanism for the prevention of electron runaway at high electric fields. It can also be seen from fig.(5.17) that a parabola does not give a good fit to the ZnS band structure.

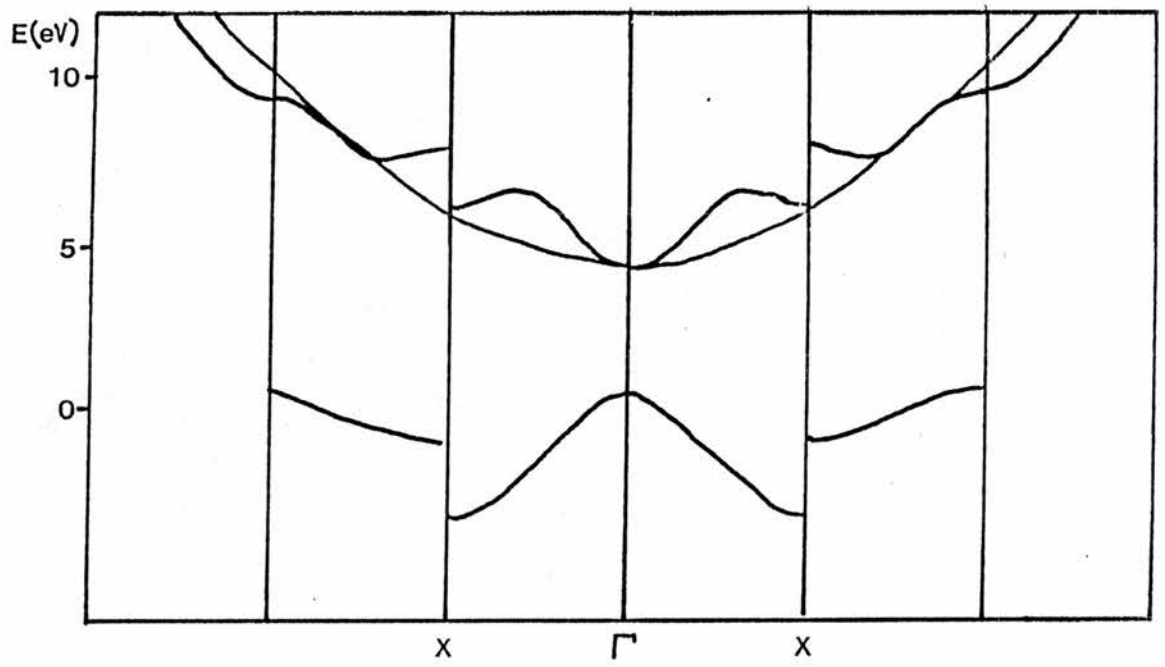

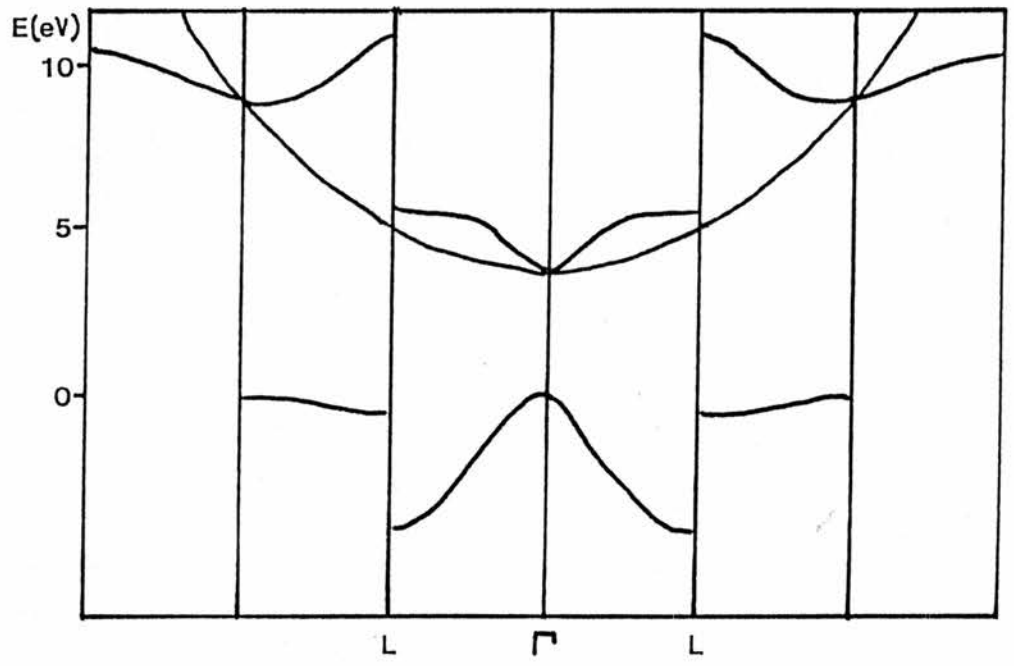

Fig.(5.17)

Band structure of ZnS on an extended zone scheme.

(Huang and Ching 1985).

As a simple parabolic band model is not applicable to ZnS, the breakdown field in the Γ_1 valley of the conduction band and the upper valleys will be estimated separately. The electrons in the Γ_1 valley have an effective mass of 0.27m [78], and this corresponds to an estimated breakdown field of 1.1×10^4 Vcm^{-1}. This field is much lower than the fields in the ZnS diodes, hence the electrons in the Γ_1 minimum will undergo electron runaway. The electrons will therefore be transferred to the upper valleys of the conduction band. It can be seen from fig.(5.17) that the X_1 and X_3 valleys are very flat and hence the electrons in these valleys have a large effective mass and low velocity and are therefore more strongly scattered. This means that the breakdown field in these valleys is much larger than that in the Γ_1 valley. However, no quantitative estimates of the breakdown field in these valleys can be made as there is a large variation in the shape of the valleys for different computations of the band structure, the bands being flat however, for every computation. It is concluded therefore that the electrons in the Γ_1 valley are transferred to the upper valleys of the conduction band at high fields where their increased effective mass prevents electron runaway. More evidence for this is given by the density of states in ZnS as calculated by the linear analytic tetrahedron integration method [77,78]. This density of states is shown along with the ZnS band structure as determined by Wang and Klein in fig.(5.18). It can be seen that the density of states in the Γ_1 minimum is very low, but it increases rapidly to reach a maximum in the X_3 minimum. This is in complete agreement with the experimental results from which it was predicted that the electroluminescence emission from ZnS Schottky diodes at high

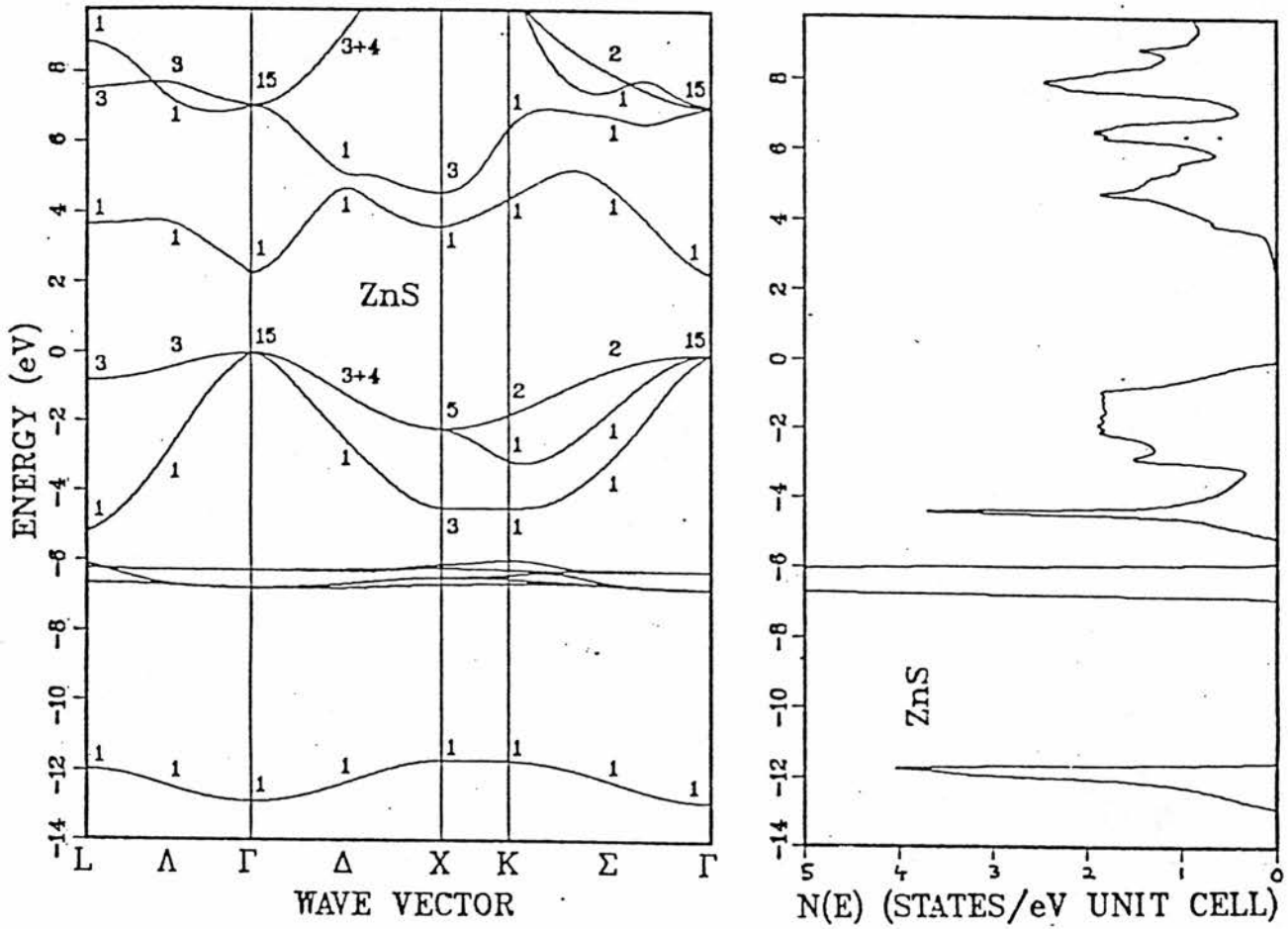

Fig.(5.18)

Band structure and density of states of ZnS.

(Wang and Klein 1981).

fields was due to electronic transitions between the upper valleys of the conduction band and the Γ_1 valley.

CONCLUDING REMARKS.

The ZnS diodes exhibited very similar characteristics (i.e. broad electroluminescence spectra and fast decay times) to the ZnSe diodes examined by Turvey and Allen [42]. The experimental results could be interpreted in terms of intervalley transitions in the conduction band as was the case for the ZnSe results. The experimental results were related to the band structure of ZnS, and the high energy cut-off of the electroluminescence spectra was found to correspond to $X_3 - \Gamma_1$ transitions.

The dielectric breakdown field in ZnS was determined using Stratton's formula [68] for the Γ_1 valley and the upper valleys of the conduction band separately. This showed that at high fields the electrons in the Γ_1 valley undergo electron runaway, but the electron energy distribution is stabilised by transfer of electrons to the upper valleys of the conduction band where an increase in the effective mass leads to an increase in the breakdown field. This was in complete agreement with the analysis of the experimental results and the computed density of states in ZnS [77,78].

A parabolic fit was made to the ZnS band structure in the (1,0,0) and (1,1,1) directions. Application of Stratton's formula to these parabolic bands showed that the electrons in these bands would undergo electron runaway at high fields with no

mechanism for stabilising the electron energy distribution. It was concluded therefore that a simple parabolic band model could not be applied to ZnS.

CHAPTER 6

CONCLUSIONS.

The various processes involved in the electroluminescent emission from ZnS Schottky diodes were studied separately. The acceleration of the electrons and the subsequent excitation of the luminescent centres takes place in the depletion region of the junction. The proportion of the depletion region over which the excitation of the centres takes place has been determined. Impact excitation is thought to be the dominant excitation process in Mn-doped material, but it has been shown that under some conditions the excitation can be an energy transfer process. In rare-earth doped material no evidence for an impact excitation mechanism was found. Direct evidence has been found for the presence of hot electrons in ZnS at the fields at which electroluminescence occurs. Light emission due to the transitions of these hot electrons in the conduction band has been observed in undoped material. Consequently, more information has been obtained on the distribution of the hot electrons in the conduction band of ZnS.

In ZnS:Mn and ZnSe:Mn two energy transfer processes have been found to occur simultaneously. For short applied pulse widths the light output from the diodes was very much greater than would be expected for an impact excitation process, and this was interpreted as being due to energy transfer into the manganese. The spatially dependent theory of energy transfer provided a good fit to the decay of the ZnS:Mn sample, the energy being transferred from the excited manganese centres to non-radiative centres. It was concluded that the two energy transfer processes could be treated independently in ZnS:Mn. In

ZnSe:Mn however, the situation was not as straight-forward as both energy transfer processes were found to affect the shape of the decay curve. The experimental results were interpreted using several models, but none of the models alone provided an entirely satisfactory fit to the data. A theory was formulated which combined the processes of energy transfer into and out of the manganese. Unfortunately, there were too many variables in the resulting expression to fit this theory to the data.

A qualitative estimate of the emitting region in ZnS:Mn was made from decay time measurements of the material. The manganese emitting region was found to be slightly larger than the depletion width for zero bias. This estimate was in agreement with the theoretical emitting region which was determined.

The electroluminescence of ZnS:RE diodes was studied. Evidence for the presence of hot electrons in the ZnS:RE diodes was given by their broad emission spectra and fast decay times. The simultaneous presence of the hot electrons and luminescent rare-earth centres was found not to be sufficient to guarantee rare-earth emission. This was thought to be due to the small impact cross-section of the rare-earth centres. Several other electroluminescent emission bands were observed in the ZnS:RE diodes, which were dependent on the rare-earth dopant. Consequently, it was shown that the results obtained by Krupka [25] which he used as evidence for an impact excitation mechanism, could be interpreted in terms of an energy transfer mechanism. It was concluded that the excitation in ZnS:RE diodes was likely to be by impact for some conditions and transfer for others as was the case for ZnS:Mn and ZnSe:Mn.

Light emission due to electronic transitions in the conduction band was observed in undoped ZnS diodes, and in particular the high energy cut-off of the emission spectrum was found to correspond to $X_3 - \Gamma_1$ transitions. A parabolic fit was made to the ZnS conduction band structure and application of Stratton's formula for the dielectric breakdown field [68] to this parabolic band showed that the electrons in the band would undergo electron runaway at high fields. Application of Stratton's formula to the different valleys in the conduction band showed that the electrons in the Γ_1 valley undergo electron runaway at the fields used in the experiments. The electron energy distribution was stabilised by the transfer of the electrons to the upper valleys of the conduction band where an increase in the effective mass leads to an increase in the breakdown field. This was in complete agreement with the experimental results. It was concluded therefore, that at high fields in ZnS the hot electrons occupy the upper valleys of the conduction band, in particular the L_1, X_1 and X_3 valleys where they have a low velocity and high effective mass. This differs from the proposal made by Mach and Muller [85], that in thin film ZnS devices a "streaming" or even a ballistic mode will be established in which the electrons are freely accelerated without any scattering processes. In this model it was assumed that the electrons remain in the Γ_1 valley with an effective mass of 0.3m. The analysis of our experimental results however, shows that this is unlikely to be the case as evidence for the occupancy of the upper valleys of the conduction band was found where the electrons are more efficiently scattered. It is unlikely therefore that the hot electrons in ZnS are ballistic.

The major innovation of this work is that the different mechanisms involved in electroluminescence have been studied separately. Previously, in the work on ZnS devices these mechanisms have been convoluted, and the analysis of the results has involved the deconvolution of the various mechanisms. Here, for example, the electroluminescent properties of the luminescent centres and the hot electrons have been studied separately. The presence of hot electrons in the rare-earth doped material was established. It was shown that the presence of these hot electrons and luminescent rare-earth centres was not sufficient to guarantee rare-earth emission. In undoped material the properties of the hot electrons themselves were studied and it was found that the electrons occupy the upper valleys of the conduction band. Thus, more information on the distribution of the hot electrons in ZnS was obtained at the fields at which electroluminescence occurs.

APPENDIX I

Kinetics of the energy transfer with a non-exponential decay.

Consider the theory in section (2.1) for the energy transfer from B centres to A centres. It is assumed in giving equation (2.12) that the decay of the A ions is purely exponential with lifetime τ . Now suppose that the decay of the A ions is given by equation (2.47) then equation (2.12) becomes,

$$\frac{dA^*}{dt} = \zeta AB^*(t) - A^*\left[\frac{1}{\tau_o} + \frac{K}{2}\left(\frac{1}{\tau_o t}\right)^{1/2}\right] \qquad (I.1)$$

where $K = \sqrt{\pi} c_n/c_o$.

Rearranging this equation and substituting for $B^*(t)$ we have,

$$\frac{dA^*}{dt} + A^*\left[\frac{1}{\tau_o} + \frac{K}{2}\left(\frac{1}{\tau_o t}\right)^{1/2}\right] = \zeta AB^*(0)\exp(-\zeta At) \; . \qquad (I.2)$$

This is a linear ordinary differential equation with integrating factor,

$$I(t) = \exp\left[\frac{t}{\tau_o} + K\left(\frac{t}{\tau_o}\right)^{1/2}\right] . \qquad (I.3)$$

The differential equation then becomes,

$$A^*\exp\left[\frac{t}{\tau_o} + K\left(\frac{t}{\tau_o}\right)^{1/2}\right] = \int AB^*(0)\exp\left[-\zeta At + \frac{t}{\tau_o} + K\left(\frac{t}{\tau_o}\right)^{1/2}\right]dt \; . \qquad (I.4)$$

We need to determine the following integral,

$$\int \exp\left[-\zeta At + \frac{t}{\tau_o} + K\left(\frac{t}{\tau_o}\right)^{1/2}\right]dt \; . \qquad (I.5)$$

Let $c_1 = (1/\tau_o - \zeta A)$ and $c_2 = \frac{K}{(\tau_o)^{1/2}}$

then the integral becomes

$$\int \exp(c_1 t + c_2 t^{1/2})dt \; . \qquad (I.6)$$

Let $s^2 = t$ then we have,

$$\int \exp(c_1 s^2 + c_2 s) 2sds \qquad (I.7)$$

which on completing the square becomes,

$$\exp(-c_2^2/4c_1) \int \exp\left(\sqrt{c_1}s + \frac{c_2}{2\sqrt{c_1}}\right)^2 2sds \ . \qquad (I.8)$$

Now let $z = c_1 s + \frac{c_2}{2\sqrt{c_1}}$, then

$$\exp(-c_2^2/4c_1) \int \exp(z^2)\, 2\left(\frac{z}{c_1} - \frac{c_2}{2\sqrt{c_1}}\right)\frac{dz}{\sqrt{c_1}}$$

$$= \exp(-c_2^2/4c_1)\left[\frac{2}{c_1}\int z\exp(z^2)dz - \frac{c_2}{c_1^{3/2}}\int \exp(z^2)dz\right]. \qquad (I.9)$$

Now,

$$\int z\exp(z^2)dz = \frac{1}{2}\exp(z^2) + a$$

where a is a constant, and

$$\int \exp(z^2)dz = \phi(z) = \phi(t)$$

is found from tables. The solution to the integral is then,

$$\frac{1}{1/\tau_o - \zeta A} \exp\left[-\zeta At + \frac{t}{\tau_o} + K\left(\frac{t}{\tau_o}\right)^{1/2}\right] - c_3\,\phi(t) + a$$

where $c_3 = \exp\left(\frac{-K^2}{4(1 - \zeta A\tau_o)}\right)\left(\tau_o \frac{K}{1/2(1/\tau_o - \zeta A)^{3/2}}\right)$.

The solution to the differential equation is then,

$$\frac{1}{1/\tau_o - \zeta A} \exp(-\zeta At) - c_3\phi(t)\exp-\left[\frac{t}{\tau_o} + K\left(\frac{t}{\tau_o}\right)^{1/2}\right] + a\exp-\left[\frac{t}{\tau_o} + K\left(\frac{t}{\tau_o}\right)^{1/2}\right]. \qquad (I.11)$$

REFERENCES.

[1] G.Destriau, J. Chim. Phys. 33, 587, (1936).

[2] W.W.Piper and F.E.Williams, Sol. Stat. Phys. 6, 95, (1958).

[3] D.Curie, Progr. in Semiconductors, 2, 249, (1957).

[4] W.W.Piper, J. Chem. Phys. 20, 1343, (1952).

[5] R.H.Bube, Phys. Rev. 83, 393, (1951).

[6] F.J.Studer and D.A.Cusano, J. Opt. Soc. Am., 45, 493, (1955).

[7] C.Feldman and M.O'Hara, J. Opt. Am., 47, 300, (1957).

[8] A.Vecht, J. Lum., 7, 213, (1973).

[9] A.Vecht, N.J.Werring, R.Ellis and P.J.F.Smith, Proc. I.E.E.E., 61, 902, (1973).

[10] I.T.Steinburger, V.Bar and E.Alexander, Phys. Rev., 121, 118, (1961).

[11] W.J.Biter, Indradev and F.Williams, J. Phys. Chem. Solids, 30, 503, (1969).

[12] W.A.Thorton, J. Appl. Phys., 33, 3045, (1962).

[13] N.A.Vlasenko and A.N.Gergell, Phys. Stat. Sol., 26, K77, (1968).

[14] T.Inoguchi, M.Takeda, Y.Kakihara, Y.Nakata and M.Yoshida, SID Intern. Symp. Dig., 86, (1974).

[15] M.Takeda, Y.Kakihara, M.Yoshida, M.Kawaguchi, H.Kishishita, Y.Yamauchi, T.Inoguchi and S.Mito, SID Intern. Symp. Dig. (1975).

[16] T.Suntola, J.Antson, A.Pakkala and S.Lindfors, SID Intern. Symp. Dig. 108, (1980).

[17] M.Fracowiak, E.Chimczak, M.Kozielski, J.Kruszgana and A.Kuleczka, J. Lum., 14, 243, (1976).

[18] E.Walentynowicz, E.Chimczak and W.Gordon, J. Lum., 17, 109, (1978).

[19] J.Benoit, P.Benalloul, R.Parrot and S.Mattler, J. Lum., 18-19, 739, (1979).

[20] J.Benoit and P.Benalloul, J. Lum., 23, 175, (1981).

[21] D.H.Smith, J. Lum., 23, 209, (1981).

[22] R.Turnquist and M.Ylilammi, J. Lum., 27, 285, (1982).

[23] S.Tanaka, H.Kobayashi, M.Shiiki, T.Kunou, V.Shanker and H.Sasakira, J. Lum., 31-32, 945, (1984).

[24] H.E.Gumlich, J. Lum., 23, 73, (1981).

[25] D.C.Krupka, J. Appl. Phys., 43, 476, (1972).

[26] E.Chimczak and J.W.Allen, J. Phys. D, 18, 951 (1985).

[27] E.Chimczak, W.S.Gordon and M-Bertrandt-Zytkowiak, Phys. Stat. Sol. (a), 82, 527, (1984)

[28] O.Goede, W.Heimbrodt, Dang-Dinh Thong, Phys. Stat. Sol. (b), 126, K159, (1984).

[29] W.Busse, H.E.Gumlich, B.Meissner, D.Theis, J. Lum., 12/13 693, (1978).

[30] N.A.Vlasenko, YuV.Kopytko and V.S.Pekar, Phys. Stat. Sol. (a), 81, 661, (1984).

[31] T.Forster, Zeitschrift fur naturforschung, 4a, 321, (1949).

[32] M.Yokota and O.Tanimoto, J. Phys. Soc. Jap., 22, 779, (1967).

[33] J.W.Allen, J. Lum., 31/32, 665, (1984).

[34] D.McClure, J. Chem. Phys., 39, 2850, (1963).

[35] B.Selle, Phys. Stat. Sol. 5, 649, (1964).

[36] S.G.Ayling and J.W.Allen, to be published.

[37] H.Roppischer and J.Jacobs, Phys. Stat. Sol. (a), 40, K117, (1977).

[38] J.M.Langer, J. Lum., 23, 141, (1981).

[39] H.Xiao-peng, L.Hong, J.Xue-yin, H.Ying, L.An-de, H.Shi-hua, Y.Jia-qi, Y.Bao-jun, D.Yu-min, Faguang Yu Xianshi, 16, (1983).

[40] N.T.Gordon and J.W.Allen, Sol. Stat. Comm., 37, 441, (1981).

[41] N.T.Gordon, Ph.D. thesis, St.Andrews, (1981).

[42] K.Turvey and J.W.Allen, J. Phys. C, 6, 2887, (1973).

[43] V.Marrello, L.Samuelson, A.Onton and W.Reater, J. Appl. Phys., 52, 3590, (1981).

[44] D.Hommel. H.Hartmann, M.Godlewski, J.M.Langer and A.Stapor, J. Cryst. Growth, 72, 346, (1985).

[45] D.Hommel, H.Hartmann and J.M.Langer, Phys. Stat. Sol. (a), 81, K199, (1984).

[46] D.Hommel, N.E.Rigby and J.W.Allen, Semi. Sci. Tech., 2, 112, (1987).

[47] K.Era, S.Shionoya, and Y.Washiwaza, J. Phys. Chem. Sol., 29, 1827, (1968).

[48] K.Era, S.Shionoya and Y.Washiwaza, J. Phys.Chem. Sol., 29, 1843, (1968).

[49] J.W.Allen, J. Phys. C, 19, 6287, (1986).

[50] F.J.Bryant, W.E.Hagston and A.Krier, Phys. Stat. Sol. (a), 94, 701, (1986).

[51] H.Kobayashi, S.Tanaka, T.Kunov, M.Siiki and H.Sasakura, 3rd intern. display research conf. Kobe, 5932, (1983).

[53] K.Okamoto and K.Watanabe, Appl. Phys. Lett., 49, 578, (1986).

[54] T.Tohda, Y.Fujita, T.Matsuoka and A.Abe, Appl. Phys.Lett., 48, 95, (1986).

[55] R.T.Tuenge, R.E.Coovert and W.A.Barrow, ECS 159th meeting, extended abstracts, 81-1, 425, (1981).

[56] R.Newman, Phys. Rev., 100, 700, (1955).

[57] L.W.Davies and A.R.Storm, Phys. Rev.,121, 381, (1961).

[58] A.G.Chynoweth and K.G.McKay, Phys. Rev., 102, 369, (1956).

[59] A.G.Chynoweth and H.K.Gummel, J. Phys. Chem. Sol., 16, 191, (1960).

[60] P.A.Wolff, J. Phys.Chem. Sol., 16, 184, (1960).

[61] M.Gershenzon and H.K.Mikulyak, J. Appl. Phys., 32, 1338, (1961).

[62] M.H.Pilkuhn, J. Appl. Phys., 40, 3162, (1969).

[63] G.F.Kholuyanov, Sov. Phys.-Sol. State, 3, 2405, (1962).

[64] T.Minami, H.Nanto and S.Takata, Phys. Stat. Sol. (a), 73, K293, (1982).

[65] R.C.Peebles, B.Sc. project, St.Andrews, (1972).

[66] M.S.Skolnick, J. Phys. D, 14, 301, (1981).

[67] H.Frohlich, Proc. Roy. Soc. A, 188, 532, (1947).

[68] R.Stratton, Proc. Roy. Soc. A, 246, 406, (1958).

[69] K.Turvey, Ph.D. thesis St.Andrews, (1973).

[70] F.J.Bryant, A.Krier and G.Z.Zhong, Sol. Stat. Elect., 28, 847, (1985).

[71] H.Kukimoto and S.Oda, J. Lum., 12/13, 923, (1976).

[72] T.D.Thompson and J.W.Allen, J. Phys. C, 20, L499, (1987).

[73] T.Figielski and A.Torun, Int. Conf. on Physics of Semiconductors, Exeter, 1962, 863, I.P.P.S.

[74] P.Eckelt, Phys. Stat. Sol. (a), 23, 307, (1967).

[75] D.J.Stukel, R.N.Euwema, T.C.Collins, F.Herman and R.L.Kortum, Phys. Rev., 179, 740, (1969).

[76] S.I.Kurganskii, O.V.Farberovich and E.P.Domashevskya, Sov. Phys.-Semicond., 14, 775, (1980).

[77] C.S.Wang and B.M.Klein, Phys. Rev. B, 24, 3393, (1981).

[78] M.Z.Huang and W.Y.Ching, J. Phys. Chem. Sol., 46, 977, (1985).

[79] F. Herman, R. L. Kortum, C. D. Kuglin and J. L. Shay, II-VI semicond. comp. 1967 conf. 503, Benjamin, N.Y. (1967).

[80] D. Miller and J. W. Allen, unpublished.

[81] D. J. DiMaria, M. V. Fischetti, E. Tierney and S. D. Brorson, Phys. Rev. Lett., 56, 1284, (1986).

[82] G. W. Ludwig and M. Aven, J. Appl. Phys., 38, 5327, (1967).

[83] N. Vagelatos, D. Wehe and J. S. King, J. Chem. Phys., 60, 3613, (1974).

[84] B. Henninon, F. Moussa, G. Pepy and K. Kunc, Phys. Lett., 36A, 376, (1971).

[85] R. Mach and G. O. Muller, Phys. Stat. Sol. (a), 69, 11, (1982).